SANDIA REPORT

SAND2009-0323
Unlimited Release
January, 2009

Joint Physical and Numerical Modeling of Water Distribution Networks

Amy Sun, Sean McKenna, Clifford K. Ho, Malynda Cappelle, Stephen W. Webb, Tim O'Hern, Leslie Orear Jr., Bart van Bloemen Waanders, Lucas McGrath, Jerome Wright, Benjamin Chwirka, Adam Zimmerman, Siri Khalsa, Joel Hartenberger, and Karen Kajder

Prepared by
Sandia National Laboratories
Albuquerque, New Mexico 87185 and Livermore, California 94550

Sandia is a multiprogram laboratory operated by Sandia Corporation,
a Lockheed Martin Company, for the United States Department of Energy's
National Nuclear Security Administration under Contract DE-AC04-94AL85000.

Issued by Sandia National Laboratories, operated for the United States Department of Energy by Sandia Corporation.

Available to DOE and DOE contractors from
U.S. Department of Energy
Office of Scientific and Technical Information
P.O. Box 62
Oak Ridge, TN 37831

Telephone: (865) 576-8401
Facsimile: (865) 576-5728
E-Mail: reports@adonis.osti.gov
Online ordering: http://www.osti.gov/bridge

Available to the public from
U.S. Department of Commerce
National Technical Information Service
5285 Port Royal Rd.
Springfield, VA 22161

Telephone: (800) 553-6847
Facsimile: (703) 605-6900
E-Mail: orders@ntis.fedworld.gov
Online order: http://www.ntis.gov/help/ordermethods.asp?loc=7-4-0#online

SAND2009-0323
Unlimited Release
January, 2009

Joint Physical and Numerical Modeling of Water Distribution Networks

Amy Sun, Sean McKenna, Clifford K. Ho, Malynda Cappelle, Stephen W. Webb, Leslie Orear Jr., Lucas McGrath, Jerome Wright, Benjamin Chwirka, Adam Zimmerman, Siri Khalsa, and Karen Kajder
Geosciences Center 6310

Tim O'Hern and Joel Hartenberger
Engineering Sciences Center 1510

Bart van Bloemen Waanders
Computer Science and Mathematics Center 1410

Sandia National Laboratories
P.O. Box 5800
Albuquerque, New Mexico 87185-MS0735

Abstract

This report summarizes the experimental and modeling effort undertaken to understand solute mixing in a water distribution network conducted during the last year of a 3-year project. The experimental effort involves measurement of extent of mixing within different configurations of pipe networks, measurement of dynamic mixing in a single mixing tank, and measurement of dynamic solute mixing in a combined network-tank configuration. High resolution analysis of turbulence mixing is carried out via high speed photography as well as 3D finite-volume based Large Eddy Simulation turbulence models. Macroscopic mixing rules based on flow momentum balance are also explored, and in some cases, implemented in EPANET. A new version EPANET code was developed to yield better mixing predictions. The impact of a storage tank on pipe mixing in a combined pipe-tank network during diurnal fill-and-drain cycles is assessed. Preliminary comparison between dynamic pilot data and EPANET-BAM is also reported.

ACKNOWLEDGMENTS

The Sandia Team thank Joe Chwirka, Walter Grayman, and Lewis Rossman for their valuable insight on experimental planning and areas of focus.

EXECUTIVE SUMMARY

This report summarizes the work conducted during the last year of a three-year LDRD project. While the first two years of this work focused on development and comparison of experimental and theoretical contaminant transport in a single junction and idealized network designs, this year's effort is further expanded into high-fidelity characterization of tracer-clear fluid interface, extension of solute mixing for bulk-advective model to include unequal pipe diameters, and dynamic mixing of scaled pipeline-tank systems in order to achieve greater understanding of solute mixing in water distribution systems.

With one exception in this report, *solute mixing at a single joint* refers to a condition where two pipes, perpendicular to one another, joining at a node with an initial known tracer inlet spiked with a given quantity of sodium chloride (i.e. contaminant) and a clear fluid inlet flowing adjacent to the tracer inlet. It is observed in experiments as well as in finite-volume based CFD results that there is incomplete solute mixing at the two outlet locations, which are downstream from either the tracer inlet or the clear inlet. (Austin et al., 2008; Romero-Gomez et al., 2008; Ho *et al*., 2006, 2007, 2008; Orear *et al*., 2005; van Bloemen Waanders et al., 2005; Webb and van Bloemen Waanders, 2006; Webb, 2007, and McKenna et al., 2007, 2008).

This year's experimental accomplishments on a single joint include characterization of turbulent mixing at the tracer-clear fluid interface and flow visualization of solute mixing with unequal pipe diameters and with 180 degree impinging mixing. All of experimental accomplishments are matched with theoretical studies in the same geometries. High fidelity, fine-grid turbulent mixing modeling based on Large Eddy Simulation (LES) is used to understand the instability around the tracer-clear interface. The instability characterized by periodicity of turbulence is compared between experimental and theoretical analysis. Analysis of 2-D images from high-speed photography near the thin mixing layer near the mid-point of the junction revealed either no distinct periodicity or a frequency that is lower than anticipated. Theoretical analysis from 3-D LES simulations showed a more distinct periodicity. One important aspect of the theoretical studies reveal a significant impact on the simulation results when the finite-volume mesh of the junction includes features of actual fittings and pipe disconnects. The outlet concentrations from the modeled turbulence mixing with finer features reveal an average of 64% and 36% salt concentrations, which match well to experimental observations of 58% and 42% respectively. Without the features, the simulation results yield incomplete mixing of around 96% and 4% at the tracer and clear pipe outlets respectively.

Incomplete solute mixing by way of bulk-phase analyses within a single joint is also carried out in this research. This accomplishment directly impacts the EPANET that is widely used in the current hydraulic engineering community. The bulk advective mixing modifications to EPANET, referred to as EPANET-BAM, are fully compatible with EPANET with an additional user-specified scaling factor that tunes the level of incomplete mixing (default is set at 0.5). The BAM analytical solution has been extended to include unequal pipe diameters in order to accommodate cases of asymmetric pipe junctions. The extent of mixing for junctions of dissimilar pipe diameters scales according to the difference in cross sectional areas. If the larger diameter pipe carries higher momentum, the solute mixing approaches the original BAM solutions, if the smaller diameter pipe carries higher momentum fluid, its concentration will be

modified by an additional contribution of differential area provided by the larger pipe. This modification shows agreement with experimental observations. Flow visualization of solute mixing at opposing tracer and clear inlets (180 degree impinging cross section) is also conducted in this work, and the observed outlet concentrations are equivalent to those obtained from complete solute mixing.

Complementary to the single-junction studies, much of the experimental effort this year has been devoted to dynamic mixing in scaled network and network-tank systems. These include 3x3 network, diamond network, tank mixing, and combined network-tank mixing systems. The 3x3 network refers to a network of nine single-joint junctions aligned in a tic-tac-toe fashion with tracer and clear fluid both introduced in one of four vertices of this checkerboard. Another idealized network geometry is also set up as a series of six diamonds, or six consecutive converging-diverging junctions. In both network configurations, steady-state mixing is reached before concentrations are recorded. Studies of incomplete mixing as a function of tracer outlet location and inlet conditions are carried out. The 3x3 network is a fine observation of incomplete mixing in network, as the concentrations at different pipe segments show varying concentrations downstream from the tracer and clear fluid inlets. No great variation in concentration is observed as outlet location changes.

The diamond network was set up to understand the physical extent of incomplete mixing based on observations from the 3x3 network. As tracer and clear fluids are introduced at the first converging single joint. As the concentrations are sampled at the outlets in subsequent divergent segments, they approach the fully-mixed limit. These experiments are run with different inlet flows. The experimental results show well-mixed asymptote appearing as early as past the third converging junction. The well-mixed limit is reached sooner in turbulent regime and relative insensitive to relative flow magnitude between the tracer and clear inlets.

Dynamic network mixing experiments with intermediate storage tank conclude the series of pilot-scaled experiments in this research. The dynamic mixing behavior of a 100-gallon storage tank is first characterized before it is used in conjunction with a 3x3 network. Injection of known tracer fluid into a tank holding known quantities of clear fluid is carried out to understand the time constant for which the tank becomes fully mixed. The experiments show the operating conditions are such that the tank reaches well-mixed limit quicker than theoretical correlations. The combined network-tank configuration consists of a 3x3 network; two supply tanks providing tracer and clear fluid in one vertex, a storage tank located in another vertex with flow control valves, and a demand tank at the outlet vertex of the network. A diurnal supply-demand pattern scaled after a municipal dynamic pattern is set up. In all of dynamic mixing experiments, comparison of experimental results with EPANET-BAM model is also carried out. Using a default of 0.5 scaled factor, results using EPANET-BAM qualitatively match the experimental data, but more data analysis is needed.

This year's work has provided key observations and critical advances towards experimental and theoretical research in contaminant transport in water distribution systems. The insight and expertise gained from this project should be leveraged and expanded into other areas of water security research. In particular, emphasis should be placed on the following topical areas for future research.

- Expansion of the experimental methodology towards enhancement of theoretical search algorithm for contaminant source detection. This work has validated incomplete mixing by forward deduction (i.e. source to detection points). These results are complementary to research to solve the inverse problem.
- Expansion of incomplete mixing assessment (numerical and experimental) for junctions of different geometries and configurations. Prevalence of different joint geometries exists in our current networks.
- Quantification of inaccuracies associated with a fully-mixed assumption in current hydraulic design codes and recommendations.
- Reactive solute transport.

TABLE OF CONTENTS

FIGURES

TABLES

NOMENCLATURE

C_s Smagorinski constant
d distance to the closet wall
D diffusivity
L_s length scale
p pressure
S Mean rate-of-strain tensor
Sc_t or Sc turbulent Schmidt number
t time
u fluid velocity, [L/T]
$\bar{u}$ filtered (resolved) fluid velocity
u' fluctuating (unresolved) fluid velocity
V computational cell volume
y distance of the first mesh point to the wall
Y tracer mass fraction

A_i Cross-sectional area of pipe *i* [L2]
C_i Solute concentration in pipe *i* [M/L3]
D_i Diameter of pipe *i* [L]
D_t Turbulent mass diffusivity [L2/T]
D_o Molecular mass diffusivity [L2/T]
Q_i Volumetric flow rate in pipe *i* [L3/T]
Q_{Tracer} Volumetric flow rate of tracer fluid [L3/T]
$Q_{ambient}$ Volumetric flow rate of clear fluid [L3/T]
Q_{supply} Volumetric flow rate of clear, ambient fluid [L3/T]
s Scaling parameter for combined complete-mixing and bulk-mixing models [-]
x Inlet flow ratio, Q1/Q2 [-]
y Outlet flow ratio, Q4/Q3 [-]

Greek
ρ fluid density, [M/L3]
μ fluid dynamic viscosity
μ_t Dynamic eddy viscosity [ML-1T-1]
ν fluid kinematic viscosity (= μ / ρ)
σ stress tensor
τ shear stress
δ delta function
κ von Karmen constant

Subscripts
i,j direction indice
l direction indice
t turbulent
w wall

Misc

filtered value

1. INTRODUCTION

Water distribution systems are comprised of complex networks of pipelines, pumps, tanks, water reclamation, and treatment stations. Threats to water distribution systems from accidental or intentional release of contaminants are poorly understood due to a lack of understanding of how these contaminants move through the distribution system. The source of contamination can be intractable or inaccurately determined; this is evident in recorded historical outbreaks (Clark, 1996).

Concurrent studies of network experiments and simulations at different scales are important to first understand the hydrodynamic behavior of mixed solutes moving through the system, to design detection points that minimize the impact of a contaminant event, and to deduce with confidence of the source of contamination.

This work has engaged in fundamental and engineering understanding of solute transport in water distribution systems. As the title of the project implies, a joint effort in physical experimentation and numerical modeling is required to enhance depth of knowledge in contaminant mixing. The physical modeling is comprised of experimental research that involves single-joint solute mixing measurements, idealized network designs and observations and small-scale dynamic mixing operations of combined network-tank set-up. The experiments have well prescribed inlet conditions in order to observe concentration profiles at various points downstream from the onset of mixing. The numerical modeling consists of high fidelity, finite-volume models as well as macroscopic mass and momentum balance.

The research conducted during the last year of this three-year LDRD project extends beyond the fundamental studies into solute mixing studies that have more realistic geometries and operating conditions. The studies are detailed from Chapter 2 to Chapter 5. Partial results from Chapter 2, 3, and 4 have been published in Proceedings of the 10th Annual Water Distribution System Analysis Symposium. An abstract based on results from Chapter 5 has been submitted for the 11th Annual Water Distribution System Analysis Symposium.

Chapter 2 gives a detailed description of the image analysis and CFD analysis for turbulent mixing at solute-fluid interface. The high fidelity analyses of a single joint explore the mechanisms for which the tracer fluid breaches the clear fluid at the point of mixing. The turbulence mixing event at the thin mixing boundary is simulated with the high-fidelity Large Eddy Simulation (LES) approach. The impact of varying pipe diameters, the ratio of inlet flows and small features in the junction are all studied and simulated. The data analysis for observed turbulent mixing event captured by high-speed photography is also described in the same chapter.

Chapter 3 describes solute mixing based on a bulk phase, macroscopic balance approach. In hydraulic engineering designs, macroscopic-level analysis is used to reach timely engineering decisions, and the work conducted here corrects for the fully-mixing assumptions in engineering analysis. This study is validated with experimental measurements and can be generalized to pipe joints of dissimilar pipe diameters.

Chapter 4 details small-scale network experiments involving 3x3 network and diamond network. The steady-state data of these mixing experiments are valuable in quantitatively assess the extent of incomplete solute mixing as fluids converge and diverge at different nodes. Observations of dependency on Reynolds numbers and ratio of inlet flows are also recorded.

The concluding chapter of experimental studies, Chapter 5, describes an important phase of this year's research. Dynamic mixing of a small-scale distribution system, comprised of source, storage and sink capacities in tank linked to a 3x3 network is described. Dynamic mixing experiments of standalone tank are first conducted. This is followed by combined network and tank system. More importantly, a dynamic supply-demand cycle mimicking the municipal diurnal cycle is conducted.

Finally, Chapter 6 summarizes the key findings of this year's research and lists recommendations.

2. HIGH FIDELITY CHARACTERIZATION OF SOLUTE MIXING IN A SINGLE JOINT

2.1. Detailed Investigation of Solute Mixing in Pipe Joints Through High Speed Photography

Investigation of turbulent mixing in pipe joints has been a topic of recent research interest. These investigations have relied on experimental results with downstream sensors to determine the bulk characteristics of mixing in pipe joints. High fidelity computational fluid dynamics models have also been employed to examine the fine scale physics of the mixing within the joint geometry. To date, high resolution imaging of experimental conditions within the pipe joint has not been reported. Here, we introduce high speed photography as a tool to accomplish this goal.

Cross joints with four pipes coming together in a single junction are the focus of this investigation. All pipes entering the junction are the same diameter and made of clear PVC. The cross joint was milled from clear acrylic material to allow for high resolution imaging of the mixing processes within the joint. Two pipes carry water into the joint, one with clear water and the other inlet with water containing dye and a salt tracer. Two outlet pipes carry water away from the joint. A high-speed digital camera was used to image mixing within the joint at an imaging rate of 30 Hz. Each grey-scale (8-bit) image is 1280 x 1024 pixels in a roughly 17.8 x 14.5 cm image containing the cross joint. The pixel size is approximately 0.13 x 0.14 mm.

Four experiments using the clear cross-joint have been visualized. The Reynolds number (Re) for the tracer inlet pipe is held constant at 1500, while a different Re in the clear inlet pipe is used for each experiment. The Re value in the outlets are held equal to each other at the average Re of the inlets. Re values in the clear inlet pipe values are: 500, 1000, 2000 and 5000. Visual examination of the images provides information on the mixing behavior including tracer transport along the walls of the pipe, transient variation in the amount of tracer entering each outlet, the sharpness of the clear-tracer interface and variation in the concentration of the tracer throughout the joint geometry. A sharp tracer-clear interface is visible for the clear inlet Re values of 500, 1000 and 2000, but decays to a broad gradual transition zone at a clear inlet Re of 5000. There are no visible instabilities in the clear-tracer interface at the lowest clear water Re (500), but regular periodic instabilities occur for the Re=1000 experiment and these become irregular, but still periodic at clear inlet Re = 2000 and then lose all regular structure in the Re = 5000 experiment.

2.1.1 Background

Accidental or malevolent contamination events within water distribution systems have motivated recent research on both the sensing and modeling of solute transport in water distribution systems. This work has included assessment of transport model based impacts on consumers (Watson et al., 2004; Bristow and Brumbelow, 2006; Khanal, et al., 2006) to different types of events, identification of the optimal sensor locations to mitigate those impacts (e.g., Berry, et al, 2006) and inverse modeling techniques to determine the location of the contamination source given sensor readings throughout the network (e.g., Laird et al., 2006). The underlying model of solute transport for these various security applications is that employed in EPANET (Rossman,

2000). This model considers mixing of a solute at a pipe network junction to be complete such that the outlet concentration of any junction is the flow weighted average of all inlet concentrations. This complete mixing model dictates that all outlets from the junction have the same concentration.

The applicability of the flow-weighted mixing model to solute transport studies has been called into question (van Bloemen Waanders, et al., 2005). Experimental work focused on cross-joints, where two inlets and two outlets, all at 90 degree angles to each other, meet has shown that for various flow conditions the concentrations, or mass fractions, in the two outlets can be quite different (McKenna et al., 2007; Austin, et al., 2008). In some cases, this difference can be such that 90% of the mass exits through a single outlet. These experimental observations have been studied with high fidelity computational fluid dynamics (CFD) models that elucidate the complex physics of the mixing processes occurring within the cross-joint (Webb and van Bloemen Waanders, 2006; Webb, 2007). Examination of the impact of incomplete mixing at an individual joint on solute transport at the full network scale has shown that dilution of contamination plumes within distribution networks containing cross joints may be less rapid than previously considered (Ho et al., 2006; Romero-Gomez, et al., 2008).

Two different approaches to examining mixing in cross-joints have been used in the publications discussed above. Experimental determination of mixing employs sensing of fully mixed, average concentrations well downstream of the joint. High fidelity numerical simulation with CFD models is able to resolve the fine-scale mixing processes occurring within the joint. In particular, CFD models using large-eddy simulation (LES) schemes have been able to demonstrate the formation of a sharp interface between the clear and tracer waters entering the joint, far from the model of complete mixing, along with transient instabilities that develop along this interface. The average concentrations in the outlet pipes and the simulated fine-scale mixing processes show good agreement, but to date, previous work has not reported direct experimental observation of transient mixing effects within a pipe joint.

The goals of this paper are to 1) Develop and apply relatively simplistic visualization tools (high speed photography) to identify and record the clear-tracer water interface and any transient instabilities along this interface as predicted by CFD models; 2) Previous experimental work (Mckenna et al., 2007) has shown that even when relatively large amounts of ambient water are introduced to the joint, it is still possible that a small fraction of tracer is able to "jump" this large clear water stream. Recent CFD work in 3-D (Webb, 2007) has demonstrated that laminar flow against the pipe walls (boundaries) is capable of transporting a significant fraction of the tracer across the ambient stream and into the pipe opposite of the tracer inlet. A goal of this current work is to experimentally verify this flow along the wall of the joint as a significant mode of mass transfer; and 3) Examine several image processing techniques that can be applied to better understand mixing processes in the cross joint and understand the limitations of these techniques given the two-dimensional imagery of a representation of a physically 3-D process.

2.1.2 Experimental Approach

Flow Apparatus and Concentration Measurements

The design of the mixing experiments was described previously by McKenna et al. (2007) and is briefly summarized here for completeness. The basic design of the cross-joint experiments is that of a large "+" sign. There are two inlets with the west (right hand) inlet providing clear ("tap" or "ambient") water with an ambient electrical conductivity and the south (lower) inlet providing the tracer water containing both a conductive solute and a colored dye. These two inlets are referred to as "clear" and "tracer", respectively. The two outlets are also referred to as "clear" and "tracer" with the outlet designation corresponding to that of the adjacent inlet. Here the ambient outlet is the north (upper) outlet and the tracer outlet is the west (left hand) outlet. The experimental apparatus is constructed from transparent PVC pipe. The cross-joint itself was milled from a single block of clear acrylic such that the 1" (2.54cm) pipes would fit together in the joint block. The upstream and downstream length of each arm of the cross joint was at least 70 pipe diameters to ensure that any tracer was completely mixed prior to entering the joint and then fully mixed again prior to reaching the downstream conductivity meters on the outlet legs. At the very end of each outlet leg, beyond the flow and conductivity sensors, a flow reducer was attached to facilitate flow and pressure adjustments within the pipe system.

Conductivity values for the ambient water used in the experiments ranged from 420 to 460 μS depending on the experiment. The tracer is produced by mixing food grade NaCl with tap water to produce a final conductivity of between 1700 and 1800μs, roughly 4.5 times that of the clear water. This amount of NaCl is not enough to create any significant density differences between the ambient and tracer fluids. Additionally, a blue food dye was added to the tracer for visualization in the cross-joint. Both the ambient water and the tracer solution are held in separate 0.455m^3 (100 gallon) tanks. The pressure within the two inlet pipes was kept equal upstream of the joint. The conductivity and the temperature of the fluids in the tanks are measured throughout the testing procedure. Two identical single-speed pumps are used to pump the fluids from each tank into the inlet pipes. A series of fittings and valves are used to control the flow rates entering the inlets. Excess flow from the pumps that is shunted away from the inlets is recirculated into the source tank from where it came to keep each tank well mixed.

Four experiments are examined in this paper. The flow conditions for these experiments are defined in **Table 1**. In all four experiments, the tracer inlet Re value is held constant at 1500 and the Re of the clear water inlet is varied from 500 to 5000. The Re values in the outlets are held equal to each other at the average Re value of the inlets. **Table 1** also contains the fraction of the tracer mass that leaves the joint through the tracer outlet (left side) as determined in experiments done prior to the visualization experiments. As noted in previous works, even when the amount of clear water entering the joint is greater than 3 times the amount of tracer water entering the joint (experiment R4), not all of the tracer mass leaves through the tracer outlet; 16 percent of the mass is able to cross the ambient stream to the opposite side of the joint (north) and exit there.

Table 1. Reynolds numbers (Re) of the clear and tracer water inlets and the fraction of the tracer mass exiting the joint through the tracer outlet leg for each of the four experiments.

	Experiment			
	R1	**R2**	**R3**	**R4**
Clear Inlet (Re)	500	1000	2000	5000
Tracer Inlet (Re)	1500	1500	1500	1500
Ratio (Tracer/Ambient)	3.0	1.5	0.75	0.3
Equal Outlet (Re)	1000	1250	1750	3250
Mass Fraction (Tracer Outlet)	0.46	0.72	0.86	0.86

High Speed Photography

The images acquired for this study were a first attempt at experimental capture of mixing conditions within the cross joint and, as such, the experimental procedure was developed to test the high speed photography approach. The cross-joint itself was machined into a solid block of acrylic in order to provide the best optical access and constrain the joint to known dimensions. Illumination with commercial photo flood lamps was set up to provide the best contrast between the clear and dyed streams. Images were acquired using two Redlake MotionPro cameras (1280 by 1024 spatial discretization, with 8 bit color), running at 30 frames per second. The pixel size is approximately 0.13 x 0.14 mm. Nearly 40 seconds of images were acquired for each experiment. We limit the analysis here to 1024 frames or 34.13 seconds for each of the four experiments. Each frame, or image, was saved to a tagged image format (tif) file of approximately 1.3 MB, or roughly 40MB of data per second. Two synchronized camera views were acquired, but images from the second (non-orthogonal) camera view proved to be less useful and are not examined here. The MotionPro cameras were controlled and the images acquired using Midas V. 2.1.8.1 image acquisition software.

Each image was processed prior to the analyses completed below. The first step in the image processing was to subtract the average background image from each experimental image. This subtraction eliminates any systematic color variation due to the camera and or lighting settings. As grey-scale images, the RGB values for each pixel are equal to each other (R=G=B) and are discretized into a range of 256 values (b-bit color). The images collected here tended to be rather dark and although variations in the amount of dye across the image space are easy to identify in the raw images, only about $1/5^{th}$ (50 color levels of 256 possible) of the full range of the color scale was utilized in the imaging. To enhance the visual aspect of the images, the color range of the raw images was expanded to the full 256 possible and a true RGB colormap was applied. This full color map is used in the static and dynamic visualizations discussed below; however, the quantitative analyses use only the color information in the original raw images, a range of roughly 50 levels translated from the raw values to run between 70 and 120.

The photographic images here are a 2-D representation of the 3-D mixing process within the joint. The color level in each pixel is an integrated value across the entire thickness of the joint at that location and the thickness of the joint varies from essentially zero at edge of the joint to the full 2.54cm at the center of the joint. The opacity of the dye used here is such that a high

concentration of dye, even in a thin section of the joint (near the edge) is enough to result in a full concentration reading in the photographic image.

2.1.3 Analysis Approach

Both qualitative and quantitative analyses are applied to the high resolution photography. The qualitative analyses are focused on the mixing behavior that occurs at the scale of the joint while the quantitative analyses focus on time series analysis of the color scale (concentration) data at each pixel in the image.

Qualitative Analysis

The qualitative analyses are based on examination of individual images as well as animations of all images collected over the full 34.13 second analysis period, which will be shown during the presentation of this paper. An example single frame for each experiment is shown in **Figure 1** and a number of interesting features of the tracer mixing can be elucidated from these images. Several observations are summarized below.

The interface between the clear (blue) and tracer (red) water domains is, as expected, sharpest for the two experiments with the lowest amount of ambient flow, R1 and R2 (top images, **Figure 1**). Areas of intermediate tracer concentration (light blue to orange) appear to be areas of tracer flow curling along the walls of the joint and are better examined in the movies presented in the oral presentation of this paper.

The R1 experiment (top left image, **Figure 1**) is a clear demonstration of what is essentially a steady state mixing process. The interface between the ambient and tracer waters is stable and constant. There is essentially no change in the concentration levels within the joint throughout the length of the experiment. Some minor fluctuations within the pipes downstream of the joint on both the ambient and tracer sides are visible. Interpretation of the color images suggests that mixing occurring within the outlet pipes downstream of the joint occurs due to tracer moving along the walls of the pipe.

For the R2, experiment, there is a continuous transfer of tracer into the opposite (north, or "clear") outlet leg at the downstream edge of the joint. This transfer is enhanced by transient instabilities moving along the tracer-clear interface. These instabilities are nearly periodic with a total of 24 instability events over the course of the experiment (rate of 0.71Hz).

The bottom two images of **Figure 1** have the largest amount of clear water entering the joint. Counter-intuitively, both of these images show clear evidence of tracer water migrating upstream into the clear water inlet such that mixing initiates upstream of the actual joint itself. This upstream migration of tracer appears to occur along the wall of the joint and is directly responsible for tracer being able to move across the ambient stream and into the opposite outlet of the joint.

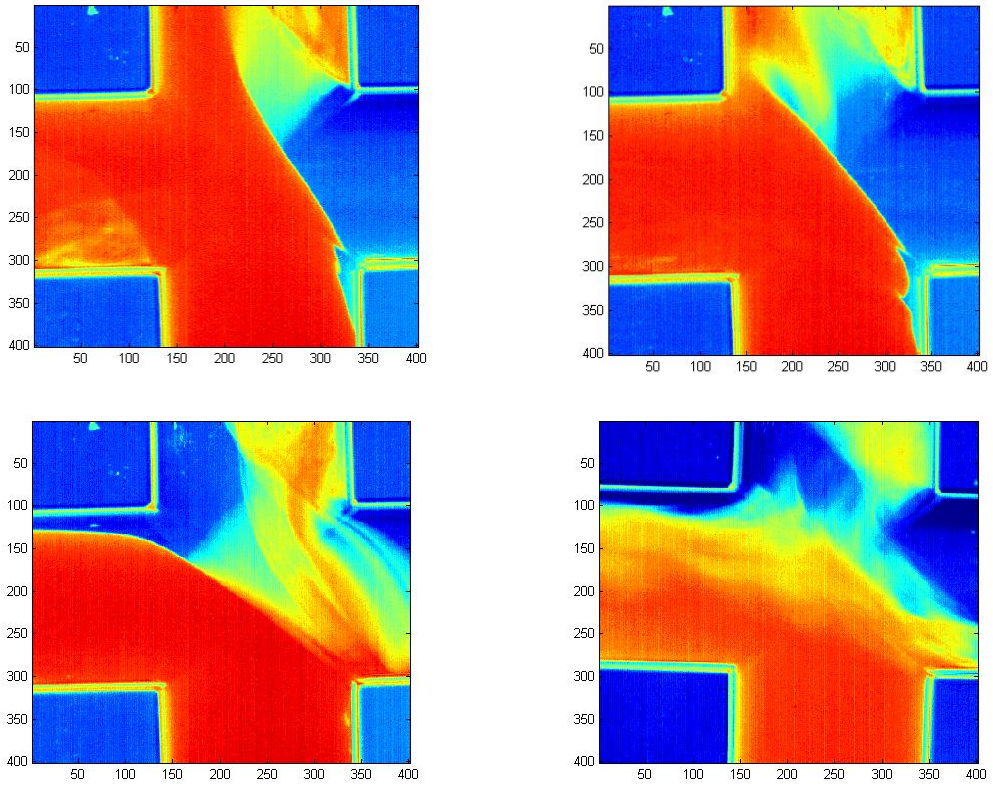

Figure 1. False color images of tracer mixing in the cross joint. Images are taken from experiments R1 (upper left), R2 (upper right), R3 (lower left) and R4 (lower right). The tracer enters the joint from the bottom and the clear water enters the joint from the right. X and Y axes units are in pixels.

For experiment R3, the tracer moves approximately 1.5 cm up into the clear water inlet and that position remains stable throughout the experiment; however, the width and amount of tracer material leaving that initial tracer migration are both time varying. The R3 experimental conditions create tracer transport into the opposite outlet leg through two mechanisms: 1) Steady-state mixing that occurs beginning upstream of the joint and appears to be facilitated by tracer flow along the pipe walls; and 2) Transient instabilities along the ambient/tracer interface. The frequency of these instabilities is not periodic. A total of 20 of these instabilities occur over the 34.1 sec experimental image (average occurrence rate of 0.59Hz).

The R4 experimental conditions also create mixing upstream of the joint itself with a stable region of tracer along the clear inlet pipe wall extending less than 1cm upstream of the joint (lower right image, **Figure 1**). There are no well-defined transient instabilities. All solute transport into the opposite leg appears to be due to unstable, non-periodic flow across the joint region itself. It is not possible to confirm from the 2-D imagery, but this transfer also appears to be facilitated by flow along the wall of the joint itself.

Quantitative Analysis

The high speed photography provides a 3-D matrix of data for each experiment that is 1280x1024 pixels by 1024 time steps, or over 1.3 billion color values for the approximately 34 seconds of imagery. The area of these images extends beyond the boundaries of the joint on all sides and is reduced here for analysis. The reduced data matrix for each experiment is 401x401 pixels by 1024 time steps (over 164 million color values). The reduced spatial extent of the images is focused on the joint area itself and is that shown in the images of **Figure 1**.

Several quantitative tools are applied to the photographic data matrix to examine the time series behavior of the tracer at each pixel location. For any location, the power spectrum density (PSD) is calculated across the 1024 time steps. The PSD is used to identify amount of energy, or power, within each band of the frequency range. The PSD of a pure sinusoidal wave with a frequency of 5Hz will clearly show that the majority of the energy in that signal is concentrated at 5Hz. As the signal is increasingly corrupted with noise, the energy will become increasingly spread throughout the frequency range and for a purely random signal, white noise, the energy will be uniformly spread through the frequency range with no dominant frequency value. The 30Hz sampling rate used for these images limits the maximum resolvable frequency to 15Hz (the Nyquist Frequency).

The PSD is calculated as the average of the magnitude of the Fourier transform squared. The Fourier transform is taken over the length of the time series recorded from the experiments. Integration of the PSD for a frequency interval provides the energy, or power, within that interval. The frequency interval containing the largest amount of the energy is the dominant frequency for that time series. The PSD was calculated for every point in the images across all 1024 time steps. The dominant frequency identified for every location was extremely long, on the order of 0.01Hz, or one cycle per 100 seconds, which may not be realistic given the 34 second length of the data. This result was also somewhat unexpected as clearly observable instabilities along the clear-tracer interface occur with what appears to be periodic regularity at a higher frequency, near 1Hz, in experiments R2 and R3.

Six example time series are shown in **Figure 2** for each of the four experiments. For each image in **Figure 2**, the time series of the tracer values are shown for six locations along a vertical line near the upstream side of the joint at an X coordinate of 300 pixels (see **Figure 1**) and at Y coordinates of 25, 75, 125, 175, 225 and 275 pixels moving from the top of the frame to the bottom. The 24 time series shown in **Figure 2** indicate a lack of a dominant frequency in the tracer concentrations. The R1 time series (upper left, **Figure 2**) show nearly constant values with the only changes being due to noise in the imaging system.

The bottom time series for R2 (location 300,275) displays significant drops in the concentration that occur roughly every 40 time steps. Closer examination of this time series shows that the intervals between these drops is variable. Additionally, the time interval between the sudden drops in concentration is considerably longer than the length of the drops themselves by a factor of 6-8 times. These variations make these time series non-sinusoidal and the PSD calculations do not identify a dominant frequency for the variations in the concentration values. Similar

results hold for the R3 and R4 time series with the R4 time series becoming less and less periodic in appearance (**Figure 2**, lower right image).

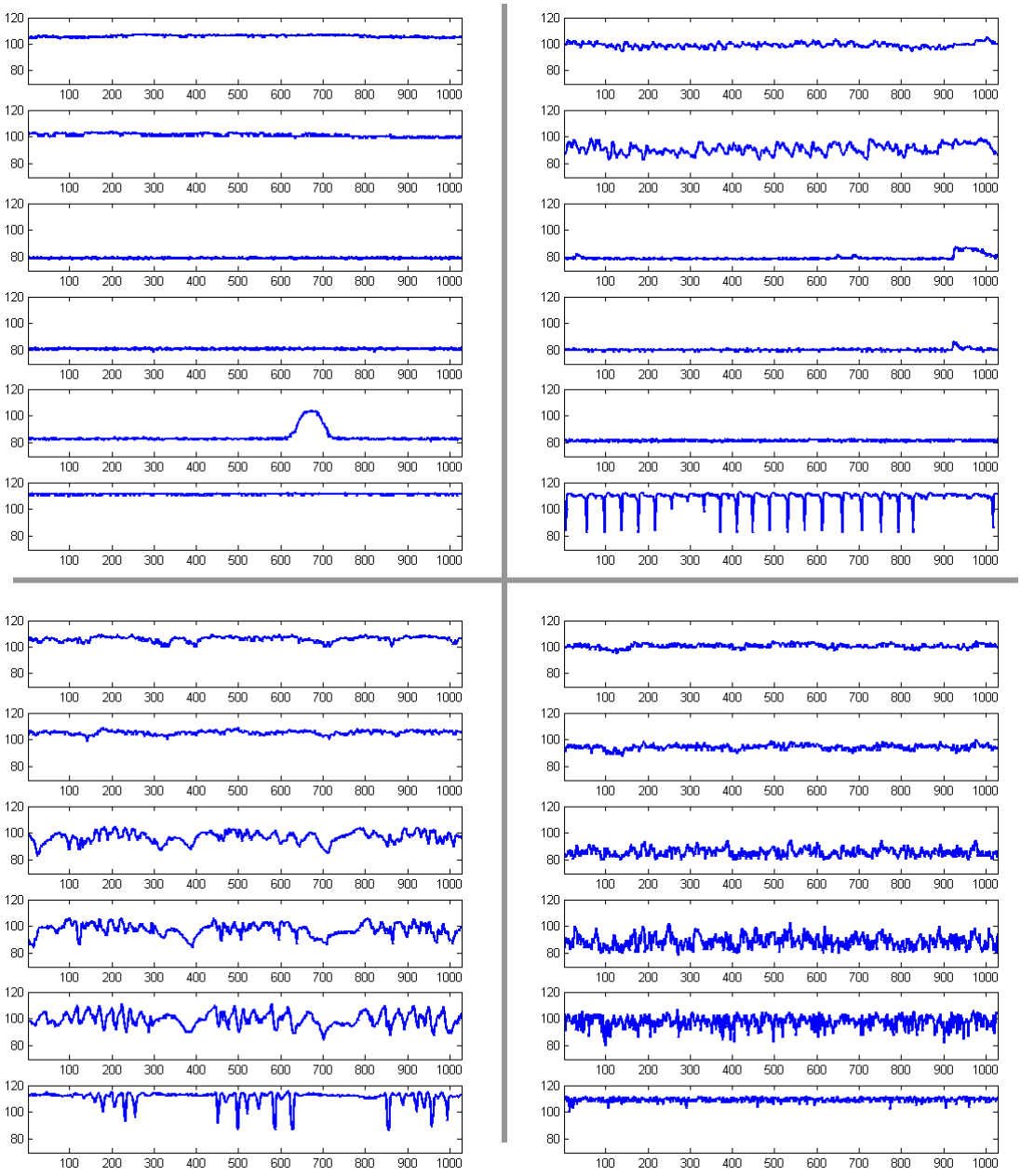

Figure 2. Time series of concentration (color) from the same six locations in each experiment (R1 upper left, R2 upper right, R3 lower left and R4 lower right). The X axis is the time step and the Y axis is the color level. The graphs in each image are arranged from row 25 (top) to row 275(bottom).

For non-periodic signals, a number of other time series analysis tools have been developed. Most of these measures focus on some aspect of the *information content* of the signal and include various measures of the signal complexity and entropy (see Wolf, 1999). Here, we calculate the entropy of the time series for each location within the image domain. The continuous time series is transformed to a binary (0/1) signal using the median value of the signal as a threshold and assigning all values above the threshold to "1" and those below to "0". This encoding can be thought of as using a two letter alphabet ($\lambda = 2$). The arrangement of the letters is then examined to determine the distribution of words of a given word length, *wL*. The number of possible words is λ^{wL}. For a random time series, the 0's and 1's will be evenly distributed and, for a relatively small *wL*, the frequency of occurrence for each word will be roughly equal. The entropy will be maximized if the probability of occurrence for each word is as likely as any other (maximum uncertainty). For a long sequence comprised of only a single letter, the next letter in the sequence is known (high predictability) and entropy and uncertainty are zero. As pointed out by Wolf (1999), for longer words, the binomial distribution defines the frequency of occurrence with words composed of a single letter, all 1's or all 0's, being the least common.

The frequency of occurrence across all words of length *wL* is summarized using the normalized entropy:

$$H(X) = -\frac{1}{wL}\sum_{i=1}^{\lambda^{wL}} P(L_i)\cdot \log_2(P(L_i))$$

where $P(L_i)$ is the probability of the L^{th} word occurring. For these calculations *wL* is set to 2 and therefore λ^{wL} equals 4 with the set of possible words being: (00,01,10,11). The $P(L_i)$ values for each word are approximated here using their relative frequencies of occurrence in each time series. The normalized entropy ranges from 0.0 to 1.0 with the maximum value being associated with a uniform, equally likely, distribution of all possible words. The resulting entropy maps for the imaged domain are shown in **Figure 3**.

The images in **Figure 3** show the entropy of each individual time series at each of the 410 x 401 locations. Areas of constant concentration as well as the background areas outside of the joint appear with speckled color patterns. The only change in the concentration in these areas is due to noise in the imaging system (e.g., the time series for the R1 experiment shown in **Figure 2**). Depending on the frequency of the random fluctuations about the median value, these pixels can result in low entropy, most values are the same with a few changes to other values, or high entropy where the values are oscillating about the median at nearly every time step. The noise in the imaging creates neighboring values of high and low entropy in areas of constant concentration leading to the speckled appearance of blue and red pixels. The entropy does not say anything about the actual value of the tracer concentration, high or low, at any location, only the frequency with which those values fluctuate.

The areas of tracer mixing are seen clearly in **Figure 3** as regions of constant, or smoothly varying, entropy values across space. In experiment R1 (upper left, **Figure 3**), the slowly varying interface between the tracer and the clear water is seen as a thin streak of low entropy values (blue). Other areas of low to medium entropy occur in the mixing zone in the downstream tracer outlet (left outlet) where the two waters continue to mix.

Increasing the amount of clear water entering the joint in experiment R2, pushes the interface between the tracer and the clear water further to the left (top right image, **Figure 3**) and makes that interface wider. A broad mixing zone with relatively high entropy develops in the clear outlet (top) and the area of the mixing zone in the tracer outlet (left) is reduced in size relative to the R1 experiment. Clear evidence for mixing upstream of the joint itself within the tracer inlet pipe is seen below the lower right corner of the joint.

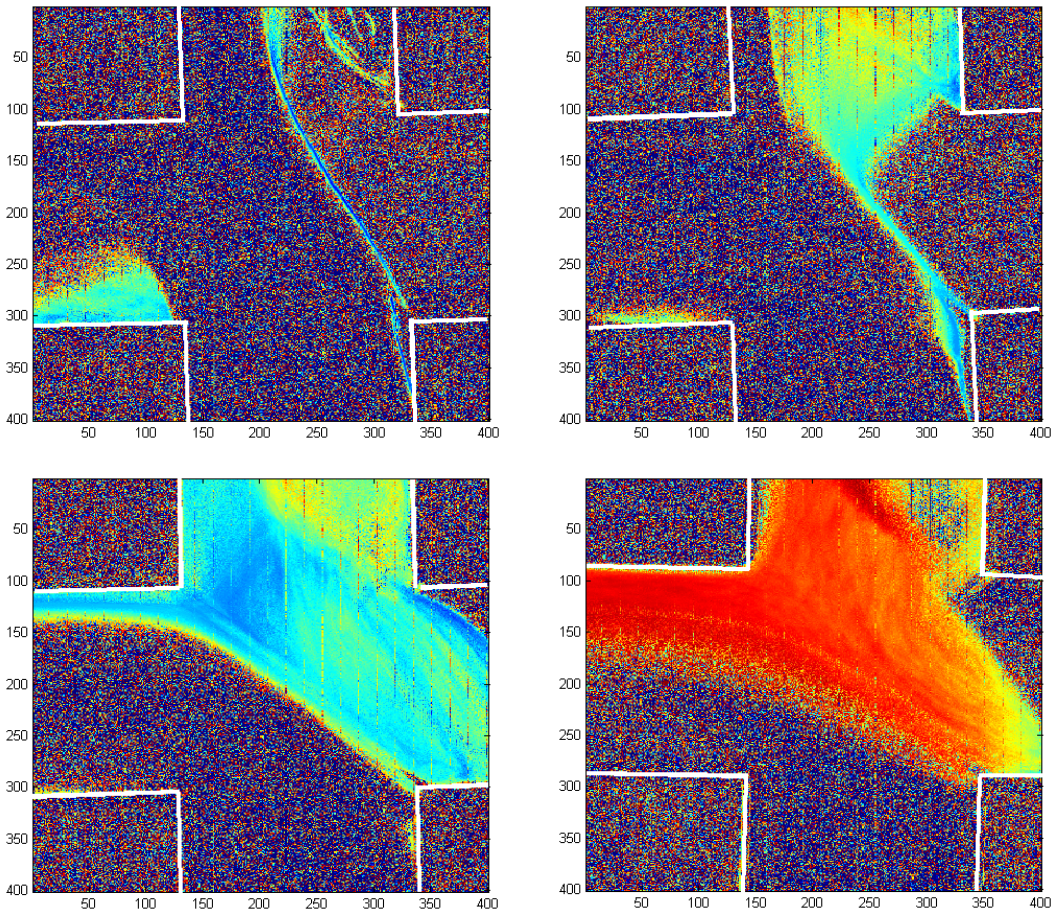

Figure 3. Maps of the normalized entropy as calculated across all time steps for experiments R1 (upper left), R2 (upper right), R3 (lower left) and R4 (lower right). The color scale ranges from 0.50 to 1.0 for all images. The white lines indicate the approximate boundaries of the cross-joint.

The R3 results (lower left image, **Figure 3**) show a mixing zone defined by a broad region of relatively low (light blue) entropy spread over half of the joint area. This area is characterized by slowly changing concentrations as non stationary regions of higher and lower tracer concentration move across this region and detach from the main zone of tracer. Similar to the R2 results, the areas of highest entropy occur downstream of the joint in the clear (top) outlet as well as along the clear-tracer water interface. The entropy image clearly shows the mixing zone extending well upstream of the joint into the clear water inlet. The interface between the tracer

and clear water is still relatively sharp and is pushed down and to the left, well into the tracer outlet leg, relative to the R2 results due to the larger amount of clear water entering the joint.

The entropy image for the R4 experiment (lower right, **Figure 3**) is strikingly different than the other 3 images with the broad mixing zone having a nearly constant entropy value close to 1.0. These results are due to the nearly random nature of the tracer fluctuations across the joint area and up into the clear water inlet pipe. The interface between the tracer concentration and the clear water is gradational as evidenced by the high entropy speckled zone. This interface is also pushed down and to the left into the tracer outlet leg as expected by the increased amount of clear water entering the joint.

2.1.4 Discussion

Visualization of the mixing processes in a cross joint is able to experimentally confirm a number of behaviors previously identified with CFD models. These include non-stationary instabilities in the clear-tracer water interface, the onset of mixing occurring upstream of the actual joint itself as well as tracer mixing facilitated by transport along the walls of the pipe. For all experiments, these visualizations clearly show the transfer of tracer across the joint to the opposite outlet leg. While the high speed photography used here provides conclusive evidence of these mixing behaviors, these are inherently qualitative results and can only provide 2-D images that integrate the results of a 3-D process. Quantitative values of the exact tracer concentration are not possible using this approach.

It is surprising that none of the locations within the joint area have a strongly sinusoidal behavior. The PSD analysis should be able to detect a dominant frequency between approximately 0.5 and 15Hz. Further analysis of the PSD with some simulated time series shows that the PSD calculated on the time series of the data may be indicative of a sinusoidal signal with a long period (near 0.01Hz) and a moderate amount of noise. For comparison, the PSD calculated for the time series at location (300,275) in experiment R2 (bottom plot, top right image of **Figure 2**) is shown in **Figure 4** and the PSD from a sinusoidal signal with a period of 0.01Hz and a moderate amount of noise is also shown. The similarities between these two PSD's include the dominant frequency very near to zero and a relatively uniform spread of the remaining energy across the frequency range. However, these similarities are not taken to be conclusive as a signal of 0.01Hz completes a full cycle in 100 seconds which is much longer than the full sample period of these experiments. Most likely, the data acquired here are not amenable to analysis with a PSD due to being non-stationary and/or representing non-periodic behavior indicative of chaotic systems.

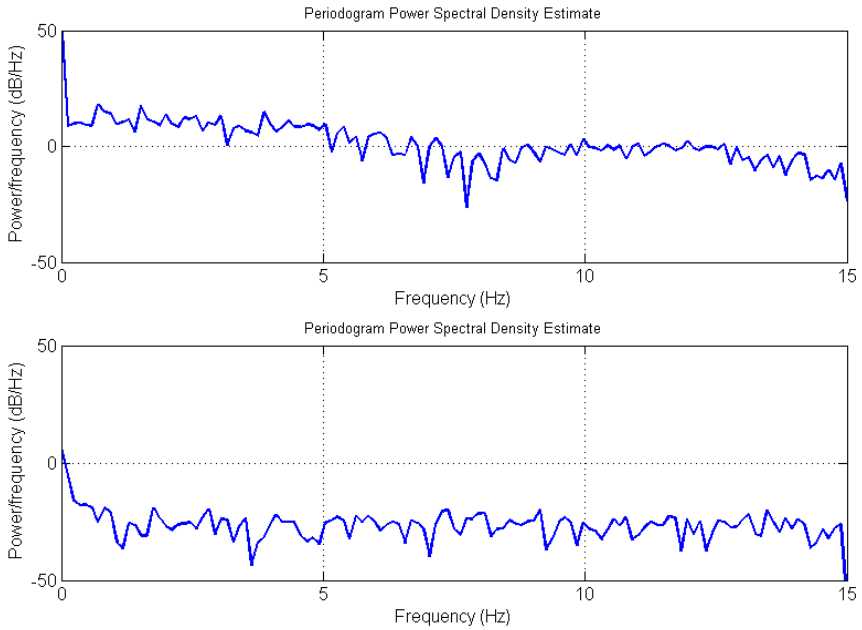

Figure 4. The PSD from location (300,275) in R2 (top image) and a PSD from a sinusoidal wave with a frequency of 0.01Hz and a small amount of noise (bottom image).

The lack of a dominant frequency in the time series data is at odds with the visual perception of non-stationary waves in R2 and R3 that travel along the clear-tracer interface in a relatively periodic manner. The reason these events are not seen in the time series analysis is that they occur in both space and time and the time series analysis done here considers each time series at each location to be independent and does not account for the event moving across the spatial domain. Additional analyses that take into account the changes in both space and time are being pursued.

2.1.5 Conclusions

Conclusions for the three major goals of this work are summarized as follows:

1) This work clearly demonstrates the utility of high speed photography as a relatively simple imaging tool to identify mixing phenomena within a joint. The high speed photography used here was able to clearly identify the sharp clear-tracer interface and record the transient instabilities along that interface as a process that contributes to the mixing of tracer within the joint area. These experimental results confirm previous predictions of this process as calculated through high resolution CFD modeling.
2) Additionally, the imaging completed here clearly shows that transport along the walls of the pipes within and even upstream of the joint can allow for tracer water to move across the ambient inflows and allow for tracer to exit the joint through the opposite outlet pipe. These experimental results confirm previous CFD simulations that demonstrated this type of annular flow around the stream of clear water.
3) The temporal behavior of the concentration at any location within the joint is not periodic. PSD calculations for every location were not able to identify a dominant frequency that could reasonably have come from these experiments. These time series may be representative of more complex, even chaotic, behavior. Entropy calculations for

each location provide maps of entropy across the joint domain that aid in identifying the location and style of mixing within the joint. These maps indicate that there is considerable structure in the mixing processes and that this structure varies considerably across the joint domain and across the different experiments.

2.2 High Fidelity Computational Fluid Dynamics for Mixing in Single Joints

In order to simulate the mixing in a cross and tees, a high-fidelity three-dimensional model has been developed using FLUENT, a commercial computational fluid dynamics (CFD) code (Fluent, Inc., 2005a, 2006). The code simulates fluid flow and heat transfer in fluids by solving the Navier-Stokes and energy conservation equations including turbulence. The selection of the turbulence approach is critical to fully resolving the fundamentals of the mixing behavior.

Much of the material included in this section is from Webb and van Bloemen Waanders (2006) and Webb (2007). Additional results are also included in this section.

2.2.1 Turbulence

There are numerous approaches to simulating turbulence (Pope, 2000). Traditional approaches such as steady Reynolds-Averaged Navier-Stokes (RANS) and unsteady RANS (URANS) solve for the time-averaged velocity by using two-equation (k-ε or k-ω) turbulence approaches. These approaches are computationally efficient but are limited in their ability to fully resolve all the appropriate details associated with turbulence. More recently, the Large Eddy Simulation (LES) approach has been gaining popularity. In this case, the Navier Stokes equations are spatially filtered so the fluid velocity is explicitly resolved down to the scale of the grid. In this way, large eddies are directly simulated. Small eddies, or eddies smaller than the mesh size, are modeled through a subgrid scale turbulence model. LES requires much more computational resources than steady RANS or URANS approaches due to the finer mesh required, but the results are much more realistic for complex situations and will be used for the present high-fidelity simulations.

All three approaches (RANS, URANS, LES) to calculating turbulence start with the instantaneous Navier-Stokes equations. However, the resulting turbulence equations are fundamentally different. In RANS and URANS, the instantaneous velocity is decomposed into a time-averaged velocity and a fluctuating velocity. Turbulence is modeled as a function of the fluctuating velocities, and the evolution of the time-averaged velocity is simulated. In steady RANS, the time-averaged velocity is simulated (resolved) and the velocity fluctuations are modeled (unresolved) through turbulence models. In URANS, the time-averaged velocity and some of the lower frequency unsteady behavior are simulated; the high frequency turbulent velocity fluctuations are modeled. In LES, the velocity is also decomposed. However, in this case, the decomposition is made through a spatial filter such that the velocity decomposition is the resolved velocity, or that which can be simulated down to the grid scale, and the residual, or unresolved velocity, which is modeled at the subgrid scale. The motion of the large eddies, relative to the grid, are simulated by the conservation equations. The rationale for LES is that momentum, mass, and passive scalars are mostly transported by large eddies, which are more problem dependent and are dictated by the geometry of the flow and boundary conditions. The smaller eddies are less dependent on problem specific conditions and are more isotropic, so they can be modeled through a defined relationship, or subgrid scale turbulence model, with more confidence. The entire frequency spectrum of the velocity fluctuations due to external events

and turbulence is directly simulated up to the frequency cutoff due to the size of the grid. As the grid is refined, the resolved frequency range becomes larger and the unresolved subgrid scale turbulence becomes smaller and smaller, eventually going to zero as all frequencies are simulated and Direct Numerical Simulation (DNS) is approached.

The Large Eddy Simulation (LES) approach is used in the high-fidelity computational fluid dynamics (CFD) simulations presented in this section. Other approaches to turbulence have been used to study mixing in single joints. Ho et al. (2006) used a 3-d steady-state RANS k-ε turbulence approach to investigate mixing in crosses and tees, while Romero-Gomez et al. (2006) used a 2-d steady-state k-ε turbulence model including some limited 3-d steady-state k-ε results. In both of these approaches, the model results were fit to the experimental data by varying the turbulent Schmidt number. In the case of Ho et al. (2006), the turbulent Schmidt number that fit the experimental data was between 0.001 and 0.01 for crosses and tees with 2.5D separation, and between 0.01 and 0.1 for tees with 5D separation. For Romero-Gomez et al. (2006), the turbulent Schmidt number that best fit their data was 0.135. Therefore, while the turbulent Schmidt number can be varied to fit the data, the value is not constant for a given model nor consistent between models. A more fundamental approach is needed and is developed here.

Preliminary results for mixing in a tee using an LES-type of approach were presented by van Bloemen Waanders et al., (2005) showed incomplete mixing. Although their numerical results compared favorably to preliminary experimental data, the results were considered qualitative because of a numerous few short-comings with the numerical model. Subsequently, Webb and van Bloemen Waanders (2006) performed three-dimensional simulations of crosses and tees, again for equal inlet and outlet flow rates, using the high-fidelity Large Eddy Simulation (LES) turbulence approach. Incomplete mixing was observed in the simulation results similar to the experimental data without the need to vary any turbulence parameter.

As mentioned above, all three approaches to turbulence decompose the actual fluid velocity. In LES, the velocity is decomposed into a filtered (resolved) velocity and a fluctuating (unresolved) component as follows:

$$u_i = \overline{u_i} + u_i'$$

The fundamental conservation equations for continuity and momentum are given below:

Continuity

$$\frac{\partial \rho}{\partial t} + \frac{\partial}{\partial x_i}\left(\rho \overline{u_i}\right) = 0$$

Momentum

$$\frac{\partial}{\partial t}\left(\rho\overline{u_i}\right)+\frac{\partial}{\partial x_j}\left(\rho\overline{u_i}\overline{u_j}\right)=\frac{\partial}{\partial x_i}\left(\mu\left(\frac{\partial\sigma_{ij}}{\partial x_j}\right)\right)-\frac{\partial\overline{p}}{\partial x_i}-\frac{\partial\tau_{ij}}{\partial x_j}$$

Stress tensor due to molecular viscosity

$$\sigma_{ij}=\left[\mu\left(\frac{\partial\overline{u_i}}{\partial x_j}+\frac{\partial\overline{u_j}}{\partial x_i}\right)\right]-\frac{2}{3}\mu\frac{\partial\overline{u_l}}{\partial x_l}\delta_{ij}$$

Turbulent stress

$$\tau_{ij}=\rho\overline{u_iu_j}-\rho\overline{u_i}\,\overline{u_j}$$

These equations are exactly the same as for RANS approaches except for the turbulent stress equation and the definition of the velocity. Rather than a time-averaged value that is used in RANS, LES resolves the fluid velocity down to the grid scale.

For LES, the subgrid scale model is:

$$\tau_{ij}-\frac{1}{3}\tau_{kk}\delta_{ij}=-2\mu_t\overline{S_{ij}}$$

$$\overline{S_{ij}}=\frac{1}{2}\left(\frac{\partial\overline{u_i}}{\partial x_j}+\frac{\partial\overline{u_j}}{\partial x_i}\right)$$

The Smagorinski model (Smagorinski, 1963) is the most widely-used LES subgrid scale model

$$\mu_t=\rho L_s^2\left|\overline{S}\right|$$

$$\left|\overline{S}\right|=\sqrt{2\overline{S_{ij}}\,\overline{S_{ij}}}$$

L_s is a length scale. Fluent calculates the value as follows:

$$L_s=\min\left(\kappa d, C_sV^{1/3}\right)$$

where κ is the von Karman constant, d is the distance to the closest wall, C_s is the Smagorinski constant, and V is the computational cell volume. The present simulations use the dynamic Smagorinski model, where the constant C_s is based on local conditions as detailed in Kim (2004).

The equations for species transport without reactions or sources terms are:

$$\frac{\partial}{\partial t}(\rho Y) + \frac{\partial}{\partial x_i}\left(\rho \overline{u_i} Y\right) = -\frac{\partial J_i}{\partial x_i}$$

$$J_i = -\left(\rho D + \frac{\mu_t}{Sc_t}\right)\frac{\partial Y}{\partial x_i}$$

The turbulent Schmidt number, Sc_t, calculated by the dynamic approach similar to the Smagorinski constant, C_s, or is a constant user-specified value.

The influence of the turbulent Schmidt number, Sc_t, is significantly different for RANS models (including URANS) and for LES. In RANS, most of the turbulence is modeled rather than simulated, so the ratio of μ_t / Sc_t will be large and will often overwhelm the laminar contribution. In LES, the ratio of μ_t / Sc_t will be much smaller than in RANS and will be a function of the grid size as can be seen from the Smagorinski subgrid scale model equations above through the length scale. In fact, as the grid gets smaller and smaller and goes toward Direct Numerical Simulation (DNS), the turbulent viscosity goes to zero, all the mixing is explicitly resolved by the simulations, and there is no effect of the turbulent Schmidt number. Therefore, values of the turbulent Schmidt number are not transferable between RANS and LES approaches.

The FLUENT CFD code has been validated for LES for a number of situations. Successful data-model comparisons have been conducted for fully-developed channel flow, flow over a square cylinder, flow over a sphere, flow and heat transfer over isolated circular cylinders, and flow in tube bundles (Kim, 2004, Kim and Mohan, 2005, Kim, 2006, Kim and Nakamura, 2006, Webb and Cook, 2006).

2.2.2 Simulation Model

In the laboratory experiments (Ho et al., 2006), a cross or double-sided tee is used with long upstream and downstream pipe runs. One inlet branch has a salt tracer, and the tracer distribution in the two outlet braches is measured to evaluate the mixing in the cross or tee. The long inlet pipe runs result in fully-developed inlet flow conditions. Rather than simulating the long upstream pipe runs or specifying an arbitrary inlet boundary condition, a small periodic model of pipe flow is used to calculate fully-developed LES conditions for the inlets. The geometric setup of the CFD model is shown in **Figure 5** including the periodic inlet pipe sections.

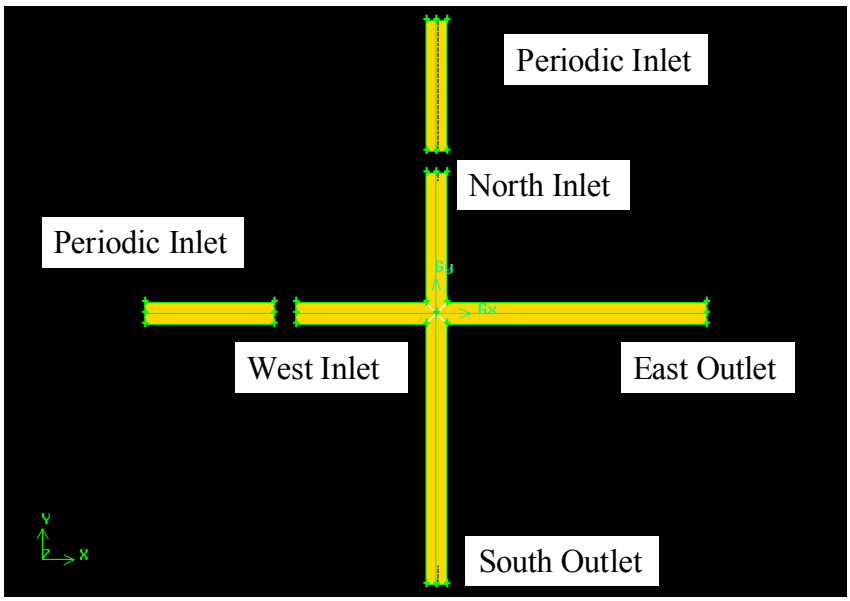

Figure 5. Fluent Model Setup for Crosses.

The periodic inlets are run independently of the full model. This setup is much more efficient than including them in the full model because fully-developed LES conditions, which can take some time to develop, are calculated without the need to simulate the entire cross model. Once these fully-developed LES conditions are established, they are fed directly into the cross model, thereby providing appropriate turbulence characteristics to the critical intersecting fluid interfaces.

A User Defined Function (UDF) was written for Fluent to take the results from the periodic inlet model after fully-developed conditions were established and write them to a file at every time step for every grid point on the inlet periodic mesh. These files are then used as input boundary conditions for the full model. Separate models/files were used for the two inlets to the cross to permit independent inlet variations. The meshes and the time steps in the periodic inlet models and the cross inlets are required to be identical.

The fluid density and fluid viscosity are assumed to be 998.2 kg/m^3 and 0.001003 Pa-s, respectively. The molecular diffusivity for the tracer-water mixture is 10^{-9} m^2/s. The general behavior of the flow field, such as the velocity profile, velocity fluctuations, and shear stress, in these periodic inlet models compare favorably to literature data for pipe flow as given in AGARD (1998) and associated test cases for pipes and channels. Separate validation simulations for test case PCH03 for a Reynolds number of about 24,600 have been performed and show very good results.

The spatial discretization methods used are PRESTO! for pressure, bounded central differencing or central differencing for momentum, and second order upwind for energy and species. SIMPLEC was used for pressure-velocity coupling. A second-order temporal discretization scheme was used for all simulations. For the outlet boundary conditions, the flow rate fractions from the experimental data are specified boundary conditions.

This general approach has been used in all the simulation results presented in this chapter. Results for specific cases are presented in the next section.

For a cross, a number of cases have been simulated including

1. 2-in diameter cross where the Reynolds number is 40,000 in both inlets (from Webb and van Bloemen Waanders, 2006);
2. 1-in, 2-in, 4-in, and 8-in crosses where the Reynolds number is 40,000 in both inlets to study the pipe diameter effect;
3. 1-in diameter cross for comparison to the clear cross experimental data; and
4. 1-in diameter cross including the effect of local geometry on mixing behavior (from Webb, 2007).

Some limited results are also given for 2-in diameter tees (from Webb and van Bloemen Waanders, 2006).

2.2.3 Crosses

1 2-inch Diameter Cross

The first set of simulation results are for a 2 inch diameter cross with inlet mass flow rates corresponding to a Reynolds number of 40,000 in both inlets. Two meshes were developed for these simulations to assess the mesh sensitivity. The geometry is simply that of two intersection pipes. These simulation results have been presented in Webb and van Bloemen Waanders (2006) but are repeated here for completeness.

Two separate meshes were developed for the simulations. A coarse mesh was developed for preliminary simulations, while a fine mesh was made to resolve many of the details of the flow and to check for mesh convergence. The coarse mesh is shown in **Figures 6 and 7**. **Figure 6** shows the cross/pipe intersection details on the mid-plane. The pipe cross model is broken up into 4 volumes based on the middle of the cross, so the mesh is symmetrical in all directions. The pipe and cross faces were paved and extruded to the inlets/outlets to complete the volume mesh. **Figure 7** shows the mesh on the inlet face, which consists of a boundary layer mesh on the pipe walls and a paved mesh in the middle. The total number of cells in the cross section of the model is 128,900. **Figures 8 and 9** show the details of the finer mesh with a total of 1,742,400 cells.

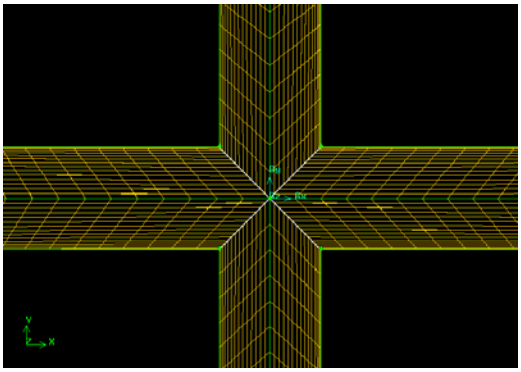

Figure 6. Fluent Coarse Mid-Plane Mesh.

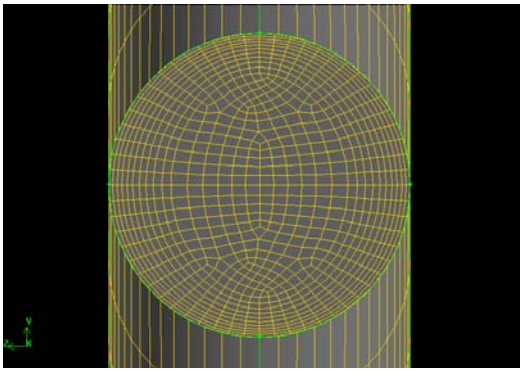

Figure 7. Fluent Coarse Inlet Face Mesh.

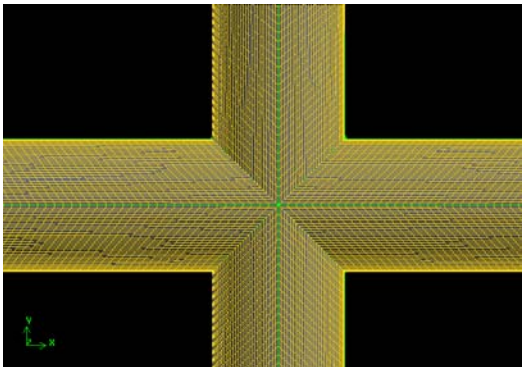

Figure 8. Fluent Fine Mid-Plane Mesh.

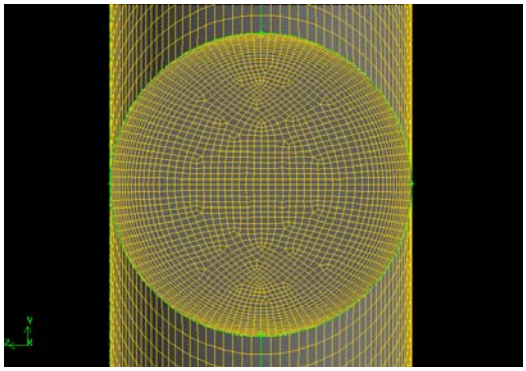

Figure 9. Fluent Fine Inlet Face Mesh.

One measure of mesh quality for turbulent flow is the y^+ value, or the dimensionless distance of the first mesh point away from the wall

$$y^+ = \frac{y\sqrt{\tau_w / \rho}}{\nu}$$

where y is the physical distance of the first mesh point from the wall, τ_w is the wall shear stress, ρ is the fluid density, and ν is the fluid viscosity. For LES simulations, the y^+ values should be about 1.0 (Fluent, 2005b). For the present meshes, the y^+ values range between 4 and 10 for the coarse model, and between 2 and 6 for the fine model.

Fine Mesh Results

The fine mesh results will be discussed first because they demonstrate the detailed flow and mixing characteristic of the flow. The coarse results will be cited to confirm mesh convergence for the predicted mixing behavior.

Mixing in a cross is incomplete. Clean fluid enters the north inlet, while contaminated fluid enters the west inlet. The two streams seem to "bounce" off each other with a limited amount of mixing. The north inlet stream is generally deflected to the east outlet, while the west inlet

stream is deflected to the south outlet. This behavior is qualitatively similar to that seen by Ashgriz et al. (2001) for two impinging jets at low flow rates. While the details of the flow and behavior after impingement are quite different, the fact that the two fluid streams seem to bounce off each other with limited mixing is similar.

The mass-averaged concentrations in the east and south outlets for the nominal flow rates are shown in **Figure 10** as a function of time. For complete mixing, the mass fractions for both outlets would be 50%, or 0.5. The results show that about 91% of the contaminated water from the west inlet goes out the south outlet, while only about 9% goes out the east outlet. The oscillatory behavior of the outlet concentrations is due to unsteady mixing in the cross that is captured by the LES turbulence approach.

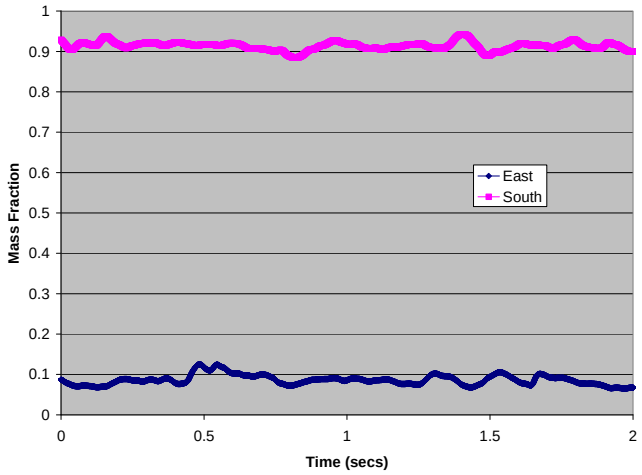

Figure 10. Time-Dependent Outlet Normalized Concentrations for Nominal Flow Rates.

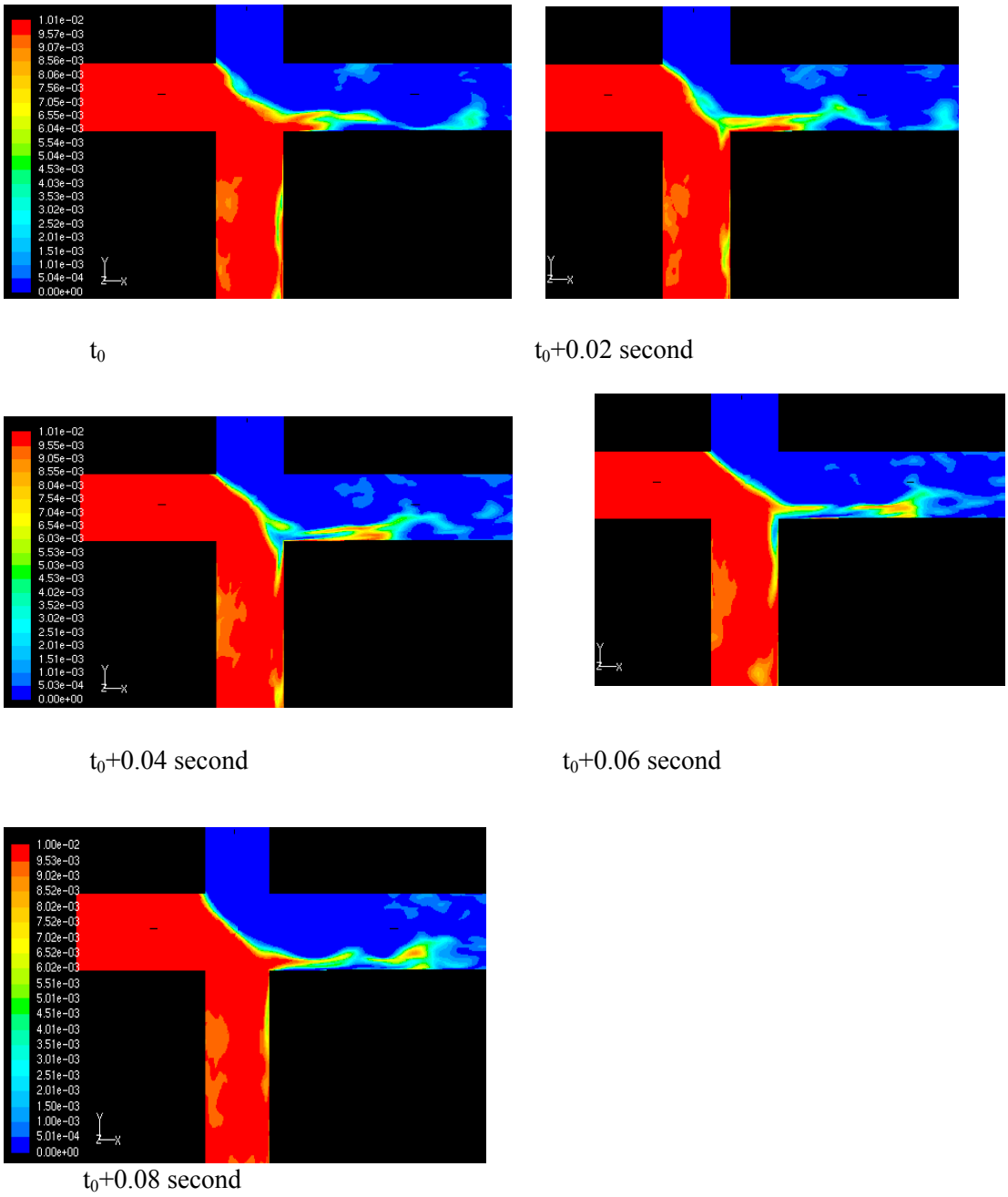

Figure 11. Unsteady Behavior of Mixing Interface.

The behavior of the mixing interface between the clean and contaminated fluid is highly transient and is shown in **Figure 11**, where discrete snapshots of concentration contours on the center plane are shown. Each picture represents a time slice 0.02 seconds greater than the previous one. In the first picture, some of the contaminated fluid entering the west inlet goes into the east outlet leg. In the next two snapshots, the unsteady interface cuts off this fluid parcel, and essentially all of the contaminated fluid goes into the south leg. The following two pictures re-establish some

contaminated fluid passing through to the east leg. The behavior of the interface then recycles back to the beginning of the sequence. The fluid crossing over (north to south; west to east) is not continuous but is divided into discrete parcels due to the unsteady behavior of the interface. The behavior is similar to the interface between two shear layers. The interface oscillates at about 10 to 12 Hz based on these results.

The mixing split of 0.91-0.09 is slightly higher than the preliminary data which gave a 0.87-0.13 mixing split. The preliminary data were scoping experiments using the experimental setup described in Ho et al. (2006). One possibility is that the actual flow rates, which are different than the nominal values, may cause some of the difference. As mentioned earlier, the nominal (desired) flow rate is 1.6 kg/s through each inlet/outlet. The actual inlet flow rates in the north and west legs of the experiment were 1.57 and 1.594 kg/s, respectively. Because of experimental uncertainties, the outlet mass flow rate was a few percent larger than the inlet flow rate. The east flow rate was 1.507 kg/s, while the east value was 1.646 kg/s. The flow split between the east and south outlet legs was unequal due to differences in flow resistance caused by downstream fittings. Therefore, the inlet flow rates were honored, and the outlet flow rate fractions were specified so mass in and mass out are equal.

The effect of using the actual flow rates on the mixing behavior is minimal. Rather than a 0.91-0.09 split based on the nominal flow rates, the split was 0.90-0.10 using the actual flow rates. As discussed earlier, the experimental split was 0.87-0.13.

Coarse Mesh Results

The results from the coarse mesh simulations agree very well with the fine mesh results indicating mesh convergence. The coarse mesh split for the nominal flow rates is 0.91-0.09, while the actual flow rate values are 0.90-0.10, or the same as the fine mesh to two decimal places. Therefore, the coarse mesh simulations can be used to estimate the mixing ratios in crosses and tees.

Pipe Diameter Effect

The simple geometry of intersecting pipes has been extended to look at the possible influence of pipe diameter on the mixing characteristics. As mentioned by McKenna et al. (2007), “At higher Reynolds numbers there is a possible trend in MF with increasing pipe diameter….There are not enough data at all pipe diameters and Reynolds numbers to confirm this trend…”.

The model consists of a 1-in nominal pipe intersecting tee (ID=1.029 in) with a Reynolds number of 40,000 in each of the inlet legs similar to the 2-in cross described above. The resulting mesh for the 1-in intersecting pipes is 760,500 cells, which in between the coarse and fine meshes discussed earlier. The mesh was simply scaled linearly to get the model for the 2-in, 4-in, and 8-in pipe diameters. The Reynolds numbers for the inlets was kept at a constant value of 40,000, which results in a decreasing average inlet velocity with increasing pipe diameter.

The results are summarized in **Figures 12 to 15** below.

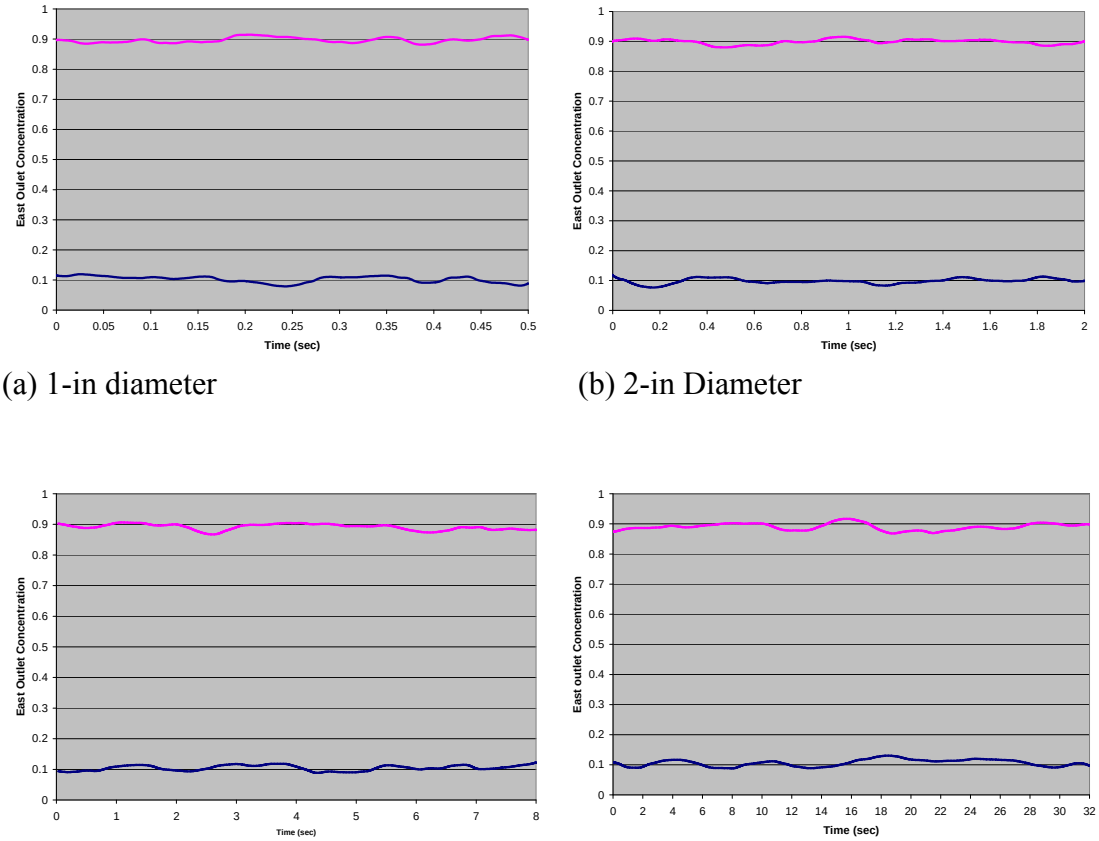

(a) 1-in diameter (b) 2-in Diameter

(c) 4-in diameter (d) 8-in diameter

Figure 12. Tracer Outlet Mass Fractions for South Outlet (Pink) and East Outlet (Blue).

The results are remarkably consistent for the various pipe sizes with a mixing ratio of 0.90 to 0.10 for all cases. These results only apply to the case of constant Reynolds number. The effect of changing Reynolds numbers, such as if the velocity were kept constant, has not been investigated.

The time dependence of the outlet concentrations vary with pipe diameter. The scaling used in the above figures is based on a first order estimate of the eddy turnover time. The size of the eddies will scale approximately linearly with the pipe diameter. In addition, the fluid velocity in the eddies is proportional to the fluid velocity, which decreases with increasing pipe diameter. The effect of an increasing eddy scale and a decreasing velocity is to change the eddy turnover time by a factor of 4 for each factor of 2 change in pipe diameter, which is used in the above figures. The variability of the outlet concentrations looks very similar for all the pipe sizes when this scaling is used.

1-inch diameter Clear Cross, Comparison against Image Analysis

In order to try to understand the mixing dynamics in crosses and to validate high-fidelity CFD models, experiments in clear crosses have been conducted as summarized by McKenna et al. (2008). The clear cross was milled from a solid piece of acrylic to provide optical viewing including movies. The diameter in the cross and in the connecting pipes was essentially constant at 1.00 inches.

In the experiments, clean fluid flowed into the cross through the west inlet, while the tracer came into the cross through the south inlet. The outlet designation is the based on the adjacent inlet designation. Therefore, the north outlet is the clean outlet while the east outlet is the tracer outlet.

Table 2 summarizes the flow conditions and results from the four experiments conducted with the clear cross. In each case, the Reynolds number of the tracer inlet was 1500. The Reynolds number of the clear fluid ranged from 500 for experiment R1 to 5000 for experiment R4. The CFD results for each experiment are discussed individually below.

Pictures of the mixing in the cross from McKenna et al. (2008) are shown in **Figure 13** for all four experiments. Comparable pictures at the midplane of the cross are shown in **Figure 14** from the CFD simulations. The experimental images are an integration of all concentration across the full diameter of the joint. The images from the models are iso-plane concentration. Hence, while there are qualitative match, the difference in dimensionality must be noted.

R1 – McKenna et al. (2008) note that mixing in this case is essentially a steady process with minor fluctuations. The CFD results show this same characteristic. The flow velocity in the center of the cross is practically constant with oscillations of about 0.1% around the mean value. The mass fraction of the tracer going through the tracer outlet is about 0.55 from the CFD simulations compared to a value of 0.46 from the experiments.

R2 – According to McKenna et al. (2008), mixing in this case includes transient instabilities at the tracer-clear interface at a rate of about 0.7 Hz. The CFD simulations show a similar instability of the tracer-clear interface. The total variation in the fluid velocity (min to max) at the center of the cross is about 12% of the mean value, and the instabilities have a frequency of about 0.65 Hz based on visual observation. The tracer outlet mass fraction from the experiments is 0.72 compared to 0.76 from the CFD simulations.

R3 – McKenna et al. (2008) note that for this experiment, the tracer moves up into the clear inlet leg, which is also seen in the CFD results. They also state that the frequency of instabilities in the cross is not periodic and has an average rate of 0.59 Hz. The CFD simulations show significant instabilities in the cross such that the total variation in fluid velocity at the center of the cross is about 50% of the mean value. The instabilities of the tracer-clean interface as measured by the variability of the velocity and tracer concentration at the center of the cross are periodic with a frequency of about 0.8 Hz. The tracer outlet mass fraction is 0.86 from the experiments and 0.89 from the CFD simulations.

R4 – The behavior of the R4 experiment is similar to that of R3 as discussed by McKenna et al. (2008), and there are no "well-defined periodic instabilities". The frequency of the instabilities is not given. The CFD results show fluid instabilities characterized by a total variation of 44% of the mean value at the center of the cross. The instabilities noted in the CFD simulations have different frequencies with an average occurrence rate of between 4-5 Hz for the major variations. There are many more minor fluctuations in the results. The tracer outlet from the tests is about 0.86, or the same as for R3. The results from then CFD simulations are significantly different at 0.67.

Note that R1 and R2 are definitely in the laminar flow regime, while R3 is more laminar than turbulent. However, R4 is laminar in the tracer inlet and turbulent in the clear inlet. The outlets have a nominal Reynolds number of 3250. As is well known, CFD codes have difficulty predicting the laminar-turbulent transition. Perhaps this deficiency is part of the reason for the large discrepancy in the tracer out mass fraction for the R4 experiment.

Results from the CFD simulations indicate that the approach to steady-state mixing mass fractions is long in these cases. The model in these simulations has about 1 foot upstream of the cross and about 2 feet downstream. In this case, the time to steady-state conditions for these experiments is 3 minutes or more according to the outlet mass fractions. For the actual experiments, McKenna et al (2008) note that the upstream and downstream legs are each 70 pipe diameters or more, or at least 6 ft upstream and downstream. Based on the simulation results, steady-state mass fractions may not be reached until 12 minutes or more after introduction of the tracer.

As mentioned by McKenna et al. (2008), these experiments have confirmed many of the results from the high fidelity CFD simulations including the transient instabilities of the tracer-clear interface (Webb and van Bloemen Waanders, 2006) as well as annular flow along the cross (Webb, 2007).

Table 2 - Clear Cross Experimental Conditions and Results Including CFD Predictions

	Experiment			
	R1	**R2**	**R3**	**R4**
Clear Inlet (Re)	500	1000	2000	5000
Tracer Inlet (Re)	1500	1500	1500	1500
Ratio (Tracer/Ambient)	3.0	1.5	0.75	0.3
Mass Fraction (Tracer Outlet)				
Experimental Data (2 Tests)	0.46 to 0.52	0.68 to 0.75	0.83 to 0.85	0.83 to 0.85
CFD Simulation Results	0.55	0.76	0.89	0.67

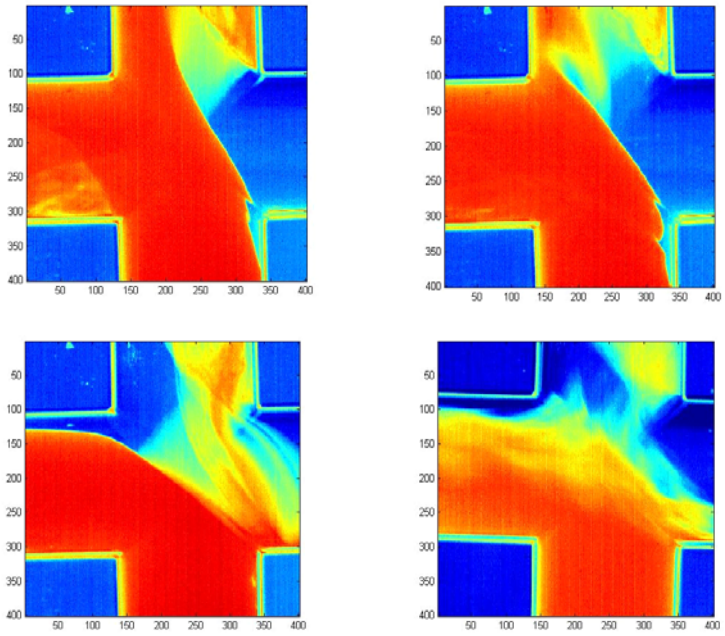

Figure 13. False color images of tracer mixing in the cross joint. Images are taken from experiments R1 (upper left), R2 (upper right), R3 (lower left) and R4 (lower right). The tracer enters the joint from the bottom and the clear water enters the joint from the right.

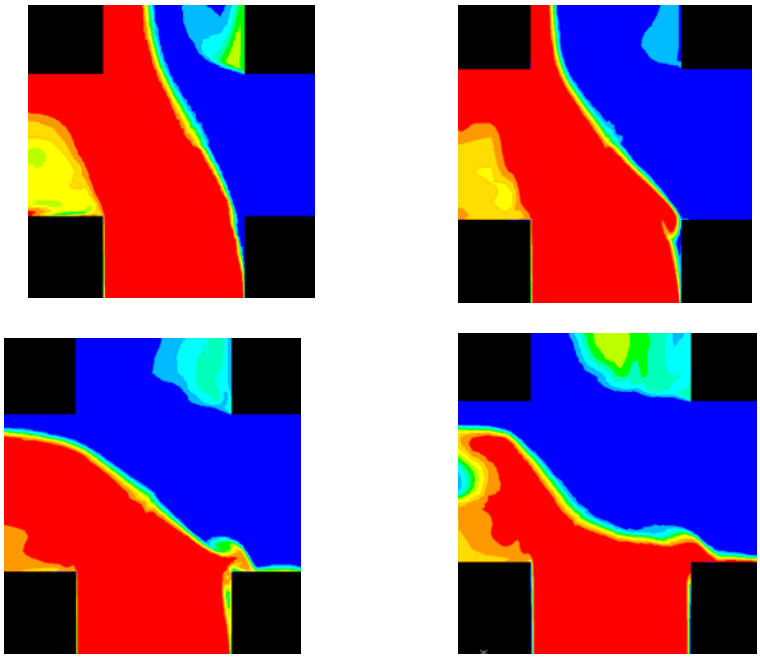

Figure 14. CFD Results for experiments R1 (upper left), R2 (upper right), R3 (lower left) and R4 (lower right).

1-inch Diameter Cross Including Local Geometry Effects

Simulations have been performed for a cross with unequal flow rates. There results have been presented in Webb (2007) and are included here for completeness.

For unequal inlet flow rates in a cross, a consistent trend in the experimental data of McKenna et al. (2007) is that the mixing becomes more complete as the ratio of the inlet mass flow rates (tracer/clean) decreases. This trend was also seen in the experimental data of Romero-Gomez et al. (2006). However, Romero-Gomez et al. (2006) did not believe their results and attributed this trend to errors in the sensors.

Romero-Gomez et al. (2006) also performed numerical simulations of mixing at pipe junctions for unequal inlet and outlet flow rates. Similar to Ho et al. (2006), they used a Reynolds-Averaged Navier Stokes (RANS) turbulence model to predict the mixing in the pipe junctions and fit the turbulent Schmidt number to the data. Unlike Ho et al. (2006), they used a two-dimensional numerical model. In general, their CFD simulations are in agreement with the experimental data. However, for unequal inlet flow rates, their CFD results show different trends than their experimental data. Their numerical results show decreased mixing as the ratio of the inlet mass flow rates (tracer/clean) decreases, while the data show the opposite trend. As mentioned above, Romero-Gomez et al. (2006) attributed the difference to experimental error.

A consistent trend in the experimental data of McKenna et al. (2007) and Romero-Gomez et al. (2006) is that for unequal inlet flow rates and equal outlet flow rates, the mixing in a cross becomes more complete as the ratio of the inlet mass flow rates (tracer/clean) decreases. In contrast, the CFD results of Romero-Gomez et al. (2006) show the opposite trend. The details of the mixing in crosses with unequal inlet flow rates and equal outlet flow rates are examined in the present study to understand the phenomena involved and to resolve this discrepancy.

A model for a 1-inch cross based on the simple intersecting pipes geometry has been developed similar to earlier models. Simulations were performed for a 1-inch cross with the smallest ratio of inlet mass flow rates (tracer/clean) in the experimental data set. The Reynolds number of the tracer inlet is nominally 1500, while the Reynolds number of the clean inlet is nominally 40,000. Thus, the fluid with the tracer entering the west inlet (refer to **Figure 13**) is laminar, while the clean fluid entering the north inlet is fully turbulent. The simulation results are highly transient.

The contours of tracer concentration along the centerline of the model at a certain time are shown in **Figure 15**. **Figure 15a** shows the results on a linear scale, while **Figure 15b** uses a log scale. As shown in **Figure 15a**, the significantly larger clean mass flow rate coming in the north inlet overwhelms the tracer mass flow rate introduced in the west inlet, diverting almost all of the tracer to the south outlet. **Figure 15b** shows that some of the tracer does "jump" across the fitting from the west inlet to the east outlet, although the east outlet leg tracer concentration is small.

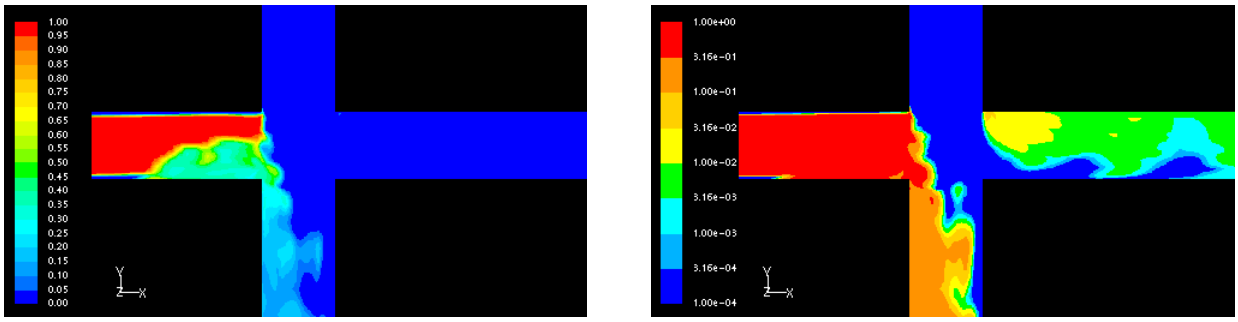

(a) (b)

Figure 15. Concentration Contours On Model Centerline.

To understand how the tracer "jumps" across the fitting, iso-contours of concentration at the same time are plotted in **Figure 15**. **Figures 15a** (side view) and **15b** (top view) show different views of the iso-contours that indicate that some of the tracer is flowing near the wall and around the central portion of the flow. This limited amount of tracer does not mix with the clean water in the fitting but rather flows around the clean flow.

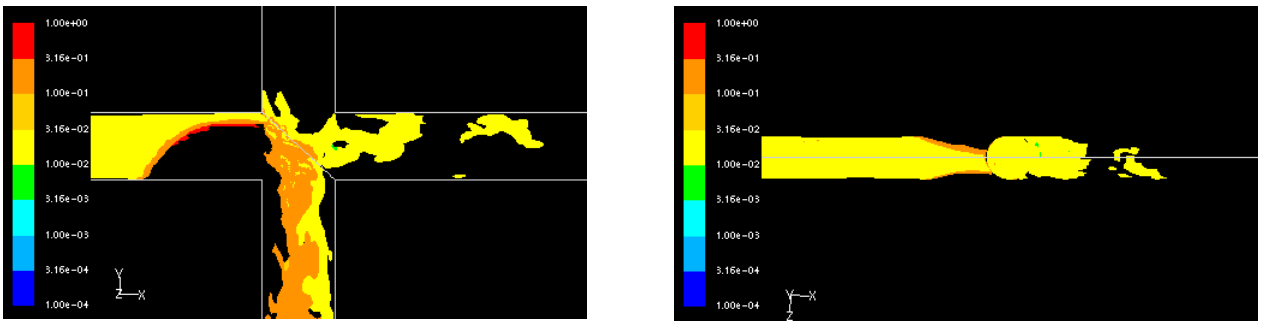

(a) Side View (b) Top View

Figure 16. Tracer Iso-Contours.

The mass-averaged concentrations in the east and south outlets for the nominal flow rates are shown in **Figure 17** as a function of time. For complete mixing, the mass fractions for both outlets would be 50%, or 0.5. The results show that about 96% of the contaminated water from the west inlet goes out the south outlet, while only about 4% goes out the east outlet. The oscillatory behavior of the outlet concentrations is due to unsteady mixing in the cross that is captured by the LES turbulence approach.

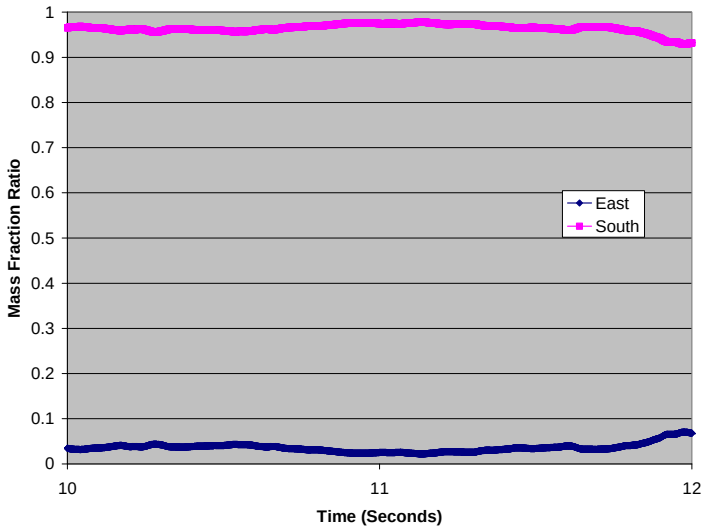

Figure 17. Time-Dependent Outlet Normalized Concentrations for Nominal Flow Rates.

In contrast to these numerical results, the experimental data of McKenna et al. (2007) indicate that approximately 58% of the tracer exits the south outlet, while 42% goes out the east outlet. Note that the experimental results of Romero-Gomez et al. (2006) show a similar trend.

The dramatic difference between the experimental data and the simulations is a major concern. A high fidelity turbulence model has been used, and the mesh is reasonable. Little change is expected if the mesh were further refined. A clue to the resolution of the mixing behavior was seen in **Figures 16a and 16b**, which shows that some of the tracer "jumps" across the fitting by flowing along the wall. The flow area around the wall of the pipe intersection is important for the ability of the tracer to "jump" across the fitting.

Upon further examination, the geometry used in the initial simulations, which simply consisted of two intersecting pipes, is overly simplified. **Figure 18a** shows the geometry of an actual 1-inch PVC cross through the centerline. The stops for the inlet and outlet pipes at the corners of the fitting are clearly seen. **Figure 18b** adds the pipe geometry for the 1-inch fitting. There are significant gaps in the fitting where the pipes come together. In contrast, **Figure 18c** shows the geometry for the initial simulations with the intersecting pipe geometry. For the 1-inch cross, the corner flow area in the cross is significant. There is a significant flow area around the fitting for the tracer fluid to "jump" across the fitting.

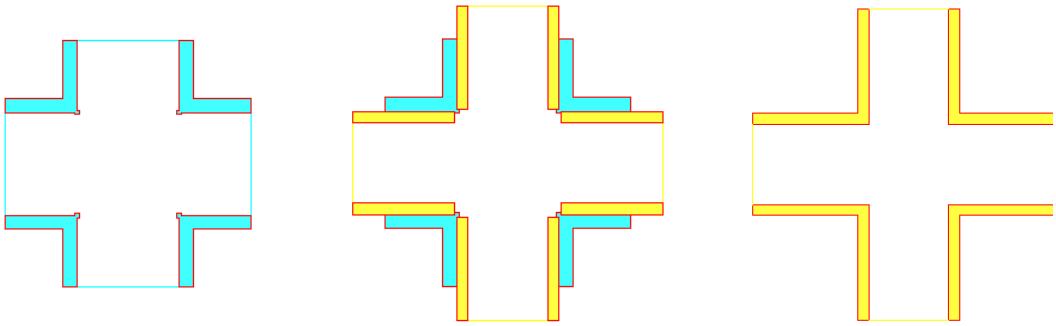

(a) Fitting Only (b) Fitting and Pipes (c) Intersecting Pipes

Figure 18. Geometry of Cross and Pipes.

The mixing simulations have been redone using this modified fluid region geometry. The mesh is exactly the same as before except for additional volume in the cross due to the change in geometry. The contours of the tracer mass fraction along the centerline are shown in **Figure 19**. **Figure 19a** is on a linear scale, while **Figure 19b** has the same results on a log scale. The general behavior is similar to that shown earlier in **Figure 15** for the original geometry except that substantially more of the tracer "jumps" across the fitting. Note the presence of the tracer in the upper right corner of the fitting.

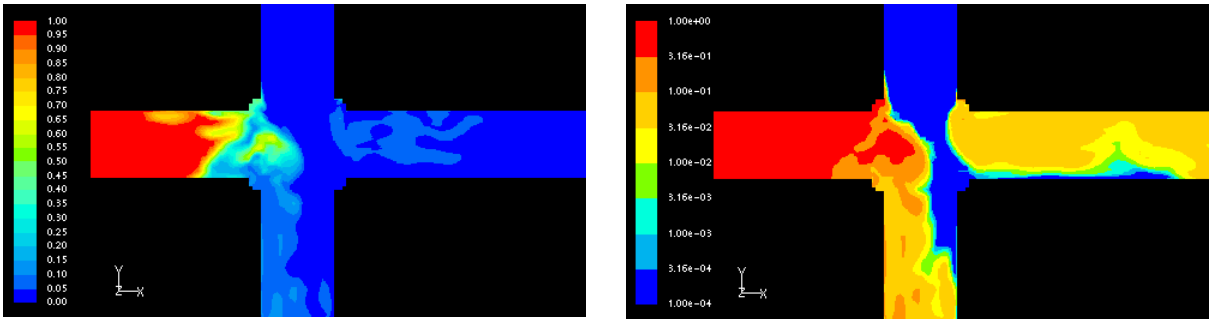

(a) (b)

Figure 19. Concentration Contours On Model Centerline For Revised Geometry.

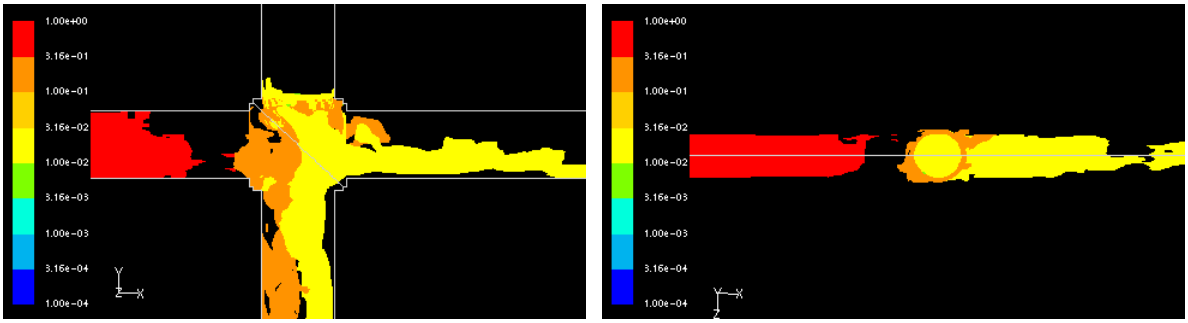

(a) Side View (b) Top View

Figure 20. Tracer Iso-Contours for Revised Geometry.

Figure 20 shows iso-contours of concentration similar to **Figure 16** for the original geometry. **Figures 20a** (side view) and **20b** (top view) show different views of the iso-contours that indicate that some of the tracer is flowing near the wall and around the central portion of the flow. In contrast to the limited amount of tracer jumping across the fitting, the amount for the revised geometry is much larger.

The mass-averaged concentrations in the east and south outlets for the nominal flow rates are shown in **Figure 21** as a function of time similar to **Figure 17** for the original geometry. The results show that about 64% of the contaminated water from the west inlet goes out the south outlet, while about 36% of the tracer "jumps" the fitting and goes out the east outlet. The frequency and magnitude of the oscillations are much larger then for the original model. These results compare favorably with the experimental data of 58% and 42%, respectively as discussed earlier.

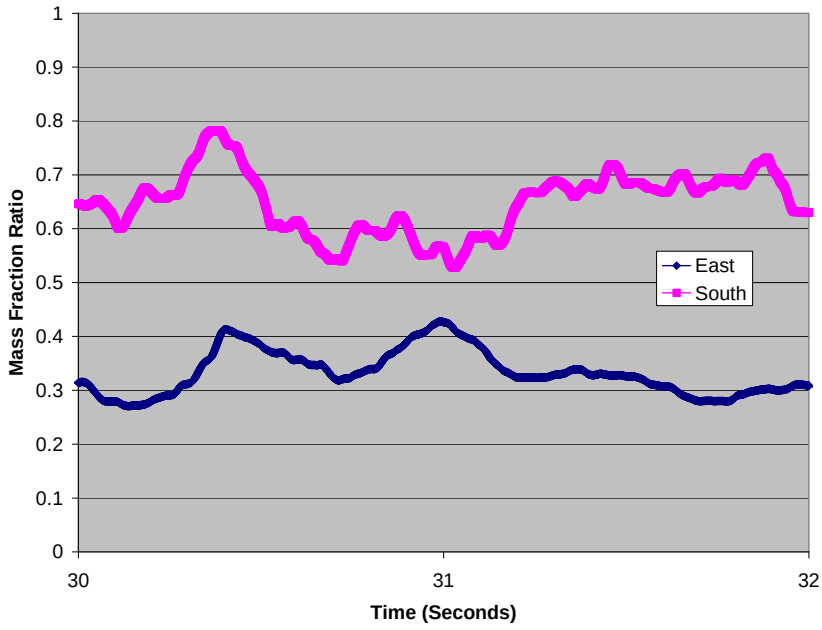

Figure 21. Time-Dependent Outlet Normalized Concentrations for Nominal Flow Rates for Revised Geometry.

The simulations have been extended for different values of the ratio of tracer to ambient Reynolds numbers for both the simple geometry on intersecting pipes and for the detailed geometry given above. For small values of the Reynolds number ratio, the difference in the mixing results is significant, and the details of the cross are important in resolving the mixing in the cross. The simple intersecting pipe model does not agree with the data (McKenna, et al.,2007) at these low ratios, while the model including the details of the fitting show good agreement with the experiments. As the ratio increases, the influence of the detailed geometry becomes less important.

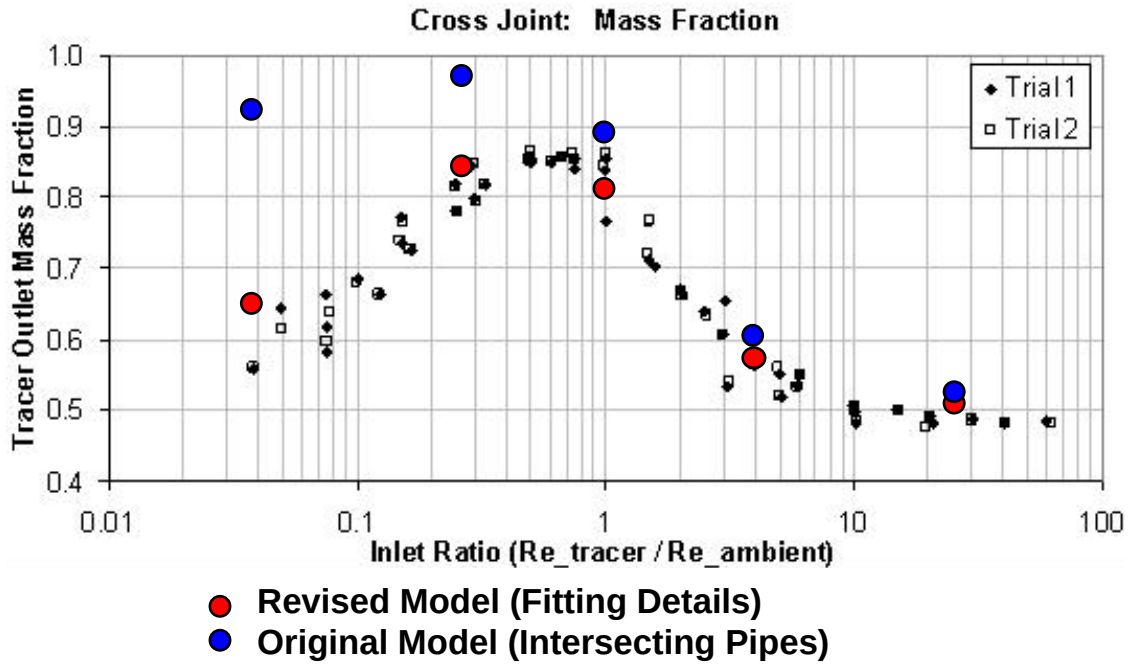

Figure 22. Effect of Inclusion of Fitting Details on Mixing in a Cross.

Tees

In addition to the crosses, preliminary simulations for double-sided tees at different separation distances have been performed using the coarse mesh. The two tees are on opposite sides. The primary reason for conducting laboratory and numerical experiments on tees was to evaluate the effects of retention time on mixing. The model for a separation distance (centerline to centerline) of 2.5 diameters is shown in **Figure 23**. These results are from Webb and van Bloemen Waanders (2006) are included here for completeness.

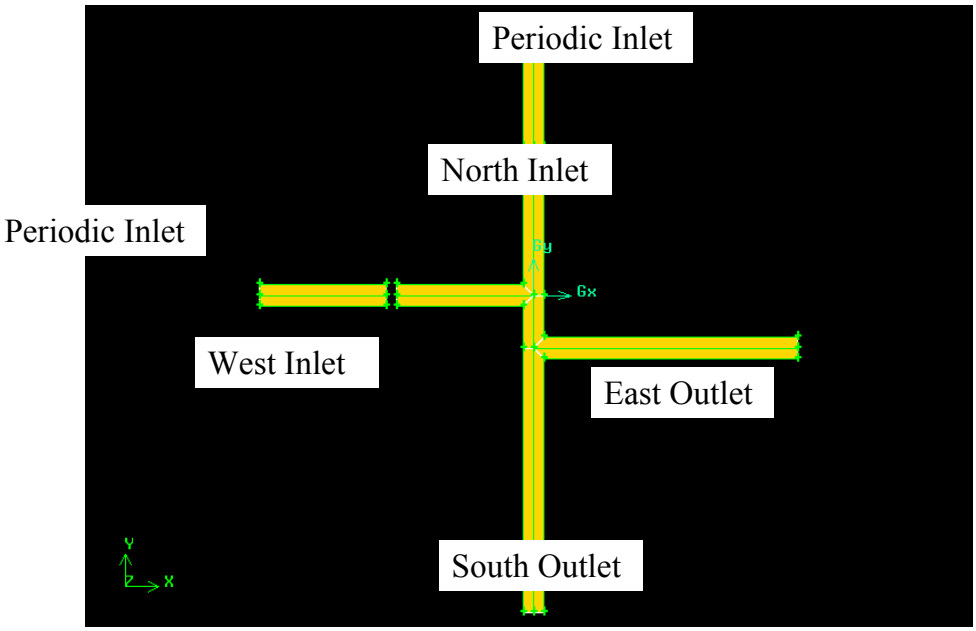

Figure 23. Fluent Model Setup for Tees With 2.5D Separation.

For the 2.5 diameter separation distance, a snapshot of the concentration contours is shown in **Figure 24**. The contaminated water coming in the west leg seems to hug the west side of the connecting leg, indicating that the orientation of the two tees may be important. The calculated flow split from these simulations is 0.59-0.41. The preliminary experimental data show a flow split of 0.68-0.26, which can be normalized to a 0.72-0.28 split.

Concentration contours are shown in **Figure 25** for the 10 diameter separation distance model. While the contaminated water still tends to hug the west side of the connecting pipe, there is more mixing between the tees. The calculated flow split is 0.55-0.45 for this model. Experimental data are not available for this configuration.

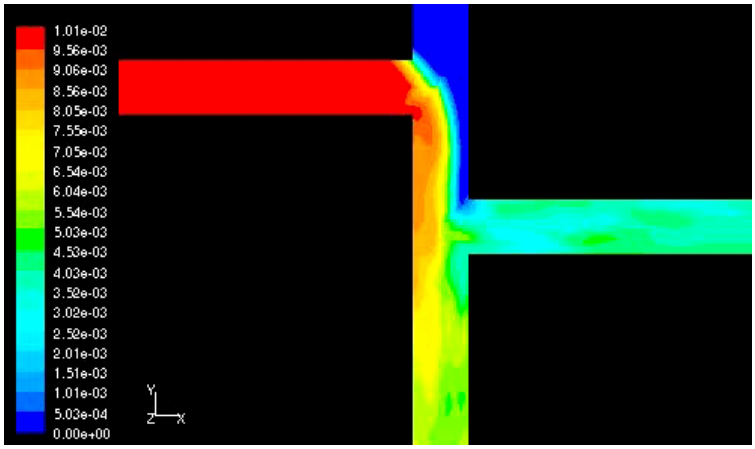

Figure 24. Concentration Contours for 2.5D Separation Tee.

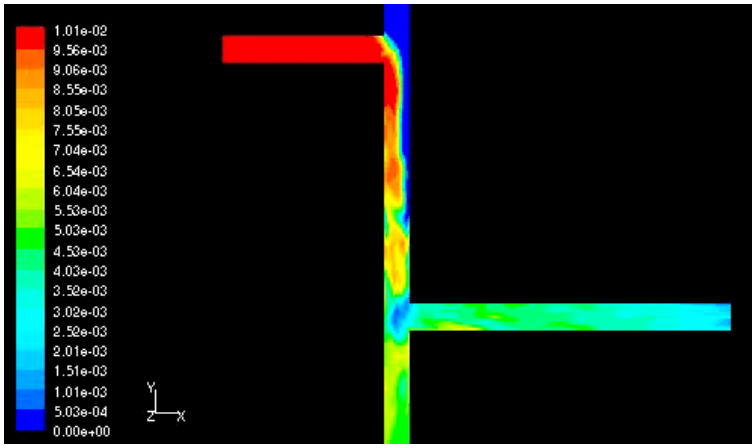

Figure 25. Concentration Contours for 10D Separation Tee.

2.2.4 Discussion and Conclusions

High-fidelity LES simulations have been performed for crosses and tees. The mixing results from the high-fidelity approach, in general, agree well with the experimental data. In some instances, the details of the local cross geometry significantly influence the mixing results as confirmed by high-fidelity simulations. Unlike models that use the RANS turbulence model and rely on fitting the turbulent Schmidt number to the data, the high-fidelity model has no fitting parameters. Note that while the RANS models can be made to fit the data, the value of the turbulent Schmidt number is not constant for a given model nor consistent between models.

- Mixing in crosses and tees is due to unstable interfacial behavior similar to shear layer instability, which is successfully captured in the high-fidelity model developed in this section. This behavior has been validated by the clear cross experiments summarized in McKenna (2008).

- The mixing across the shear layer interface is highly unsteady. Part of the unsteadiness is due to the turbulent velocity fluctuations in the inlet flow, which is naturally modeled using LES. For example, van Toonder etc. axial rms velocity fluctuations are approximately constant with Reynolds number and vary from about 38% of the local velocity near the wall to about 4% at the centerline (AGARD, 1998). These turbulent fluctuations are probably a significant contributor to the transient behavior of the mixing interface.

- In some instances, mixing in a cross is partially due to the tracer "jumping" across the fitting by flowing around the pipe intersection walls as shown in the clear cross experiments. Note that this behaviour was predicted by the high-fidelity model results given by Webb (2007) before the experiments were conducted.

The high-fidelity approach is not the cure all. The approach takes significant amounts of computer time, sometimes weeks on an 8-CPU machine due to the small time steps of around 0.001 seconds and the long simulation times in many cases. In addition, there are discrepancies between the model results and the experimental data that have not been resolved. In any event, the high-fidelity CFD approach developed here is an important tool in understanding the mixing phenomena in fittings.

3. SOLUTE MIXING MODIFICATIONS IN EPANET

The spreading of solutes or contaminants through water-distribution pipe networks is controlled largely by mixing at pipe junctions where varying flow rates and concentrations can enter the junction. Rigorous computational-fluid-dynamics (CFD) models based on turbulent Navier-Stokes equations are presented in Section 2.2. Alternative models of solute mixing within these pipe junctions are presented in this chapter. In particular, a new model that describes the bulk mixing behavior resulting from different flow rates entering and leaving the junction is described here. Comparisons with experimental data have confirmed that this bulk-mixing model provides a lower bound to the amount of mixing that can occur within a pipe junction, while the complete-mixing model yields an upper bound. In addition, a simple scaling parameter is used to estimate the actual (intermediate) mixing behavior based on the bounding predictions of the complete-mixing and bulk-mixing models. These simple analytical models can be readily implemented into network-scale models to develop predictions and bounding scenarios of solute transport and water quality in water-distribution systems.

3.1. INTRODUCTION

Solute transport in water distribution systems is a growing concern because of the potential for accidental or intentional contamination events. Understanding how solutes move and mix through a network of pipes and junctions is critical for developing mitigation plans should a contamination event occur. The software EPANET (Rossman, 2000), sponsored by the U.S. Environmental Protection Agency, is a standard for modeling hydraulic and water-quality behavior in water distribution piping systems. However, mixing of solutes within pipe junctions is assumed to be complete and instantaneous, contrary to recent studies that showed that mixing in individual pipe junctions was incomplete (Orear *et al*., 2005; van Bloemen Waanders, 2005; Ho *et al*., 2006; Webb and van Bloemen Waanders, 2006; Romero-Gomez *et al*., 2006; and McKenna *et al.*, 2007). Impinging flows within a cross junction or a T-junction (**Figure 26**) tended to bifurcate rather than mix completely. Other models of flow and transport in pipe networks have also assumed complete mixing at pipe junctions (e.g., Islam and Chaudhry, 1998).

Solute mixing *within the junction* is therefore limited to the impinging interface where the flows converge (**Figure 26**). Because the flow in water distribution systems is typically turbulent (velocity = 0.91-1.5 m/s (3-5 ft/s); pipe diameter = 0.2-0.3 m (8-12 in); Re~10^5 (Clark *et al*., 1977)), instabilities can form at the impinging interface that enhance mixing (see Webb and van Bloemen Waanders, 2006). However, a dominant factor controlling the mixing behavior and concentrations is the relative bulk flow rates entering and/or leaving the junction (Romero-Gomez *et al*., 2006). In cross junctions, the incoming flow streams will bifurcate to varying degrees through the outlet pipes depending on the relative flow rates through each leg of the junction. Thus, the amount of mixing that occurs within the junction depends on the relative momentum that carries constituents from one stream into another stream and, to a lesser degree, on the turbulent instabilities and diffusive mass transfer that occur along the impinging interface.

The purpose of this study is to provide a review and evaluation of alternative mixing models that have been developed to predict solute mixing in pipe junctions, with a focus on a new analytical

bulk-mixing model that estimates the minimum amount of mixing that can occur based on the relative flow rates in the junction. Mixing of solutes within the junction is assumed to be conservative and non-reacting. However, processes involving wall-reactions, bulk-flow reactions, and decay have been incorporated in previous models of flow and transport within pipes (e.g., Rossman, 2000; Islam and Chaudhry, 1998).

First, a complete-mixing model that is implemented in EPANET and many other network-scale models is discussed. These models assume complete and instantaneous mixing of constituents within a junction. Then, the new bulk-mixing model is presented. Comparisons to previous experimental data are made to show that the complete-mixing and bulk-mixing models bound the actual mixing behavior. Therefore, these simple analytical models can be used in network-scale models to evaluate physically bounding scenarios of solute mixing and transport through a water-distribution network.

3.2. MACROSCOPIC MIXING MODELS

Complete Mixing Model

The complete mixing model is employed by EPANET and other water-distribution network models that assume complete and instantaneous mixing within pipe junctions. Discretized numerical models are not needed, and the formulation can be readily implemented as a closed-form analytical equation in the network models for fast and efficient calculations.
In the complete-mixing model, the concentration in the fluid leaving the junction is uniform (equal in all outlet pipes) and dependent on the flow-weighted concentrations entering the pipe. A solute mass balance yields the following equation for the concentration leaving the junction in any outlet pipe, C_{out} [M/L^3], based on prescribed flow rates entering the junction:

$$C_{out} = \frac{\sum_{i=1}^{n} Q_i C_i}{Q_{out}} = \frac{\sum_{i=1}^{n} Q_i C_i}{\sum_{i=1}^{n} Q_i} \qquad (3.1)$$

where Q_i is the flow rate [L^3/T] entering the junction from pipe or source i, n is the number of pipes or flow sources entering the junction, and C_i is the concentration [M/L^3] in each pipe or source entering the junction. No storage is assumed to exist in the junction, so the total flow rate out of the junction, Q_{out}, is equal to the total flow rate into the junction.

The disadvantage of the complete-mixing model is that it does not accurately capture the physical mixing processes that have been observed in experiments and simulations using CFD models for many flow configurations. The complete-mixing model predicts the greatest possible mixing that can physically occur within a junction. As shown in Ho *et al*. (2006) and Romero-Gomez *et al*. (2006), this assumption can yield concentrations that are significantly different than actual concentrations for many junction configurations and boundary conditions.

Bulk Mixing Model – Equal pipe sizes

The bulk-mixing model is intended to complement the complete-mixing model by providing a physically based lower limit for mixing in junctions. The bulk-mixing model is based on knowledge of the relative flow rates entering and leaving a junction, and the concentrations entering the junction.

As shown in **Figure 26**, unequal momentum from different fluid streams will cause a bulk transfer of fluid and constituents between the incoming and outgoing flows. With unequal flow rates, CFD models show that the extra momentum carried by one stream may be sufficient to cross over the junction into the opposite stream. **Figure 26** illustrates this situation in which the flow rate of the clean-water inlet is ~80% greater than the flow rate of the tracer inlet (outlet flow rates are equal).

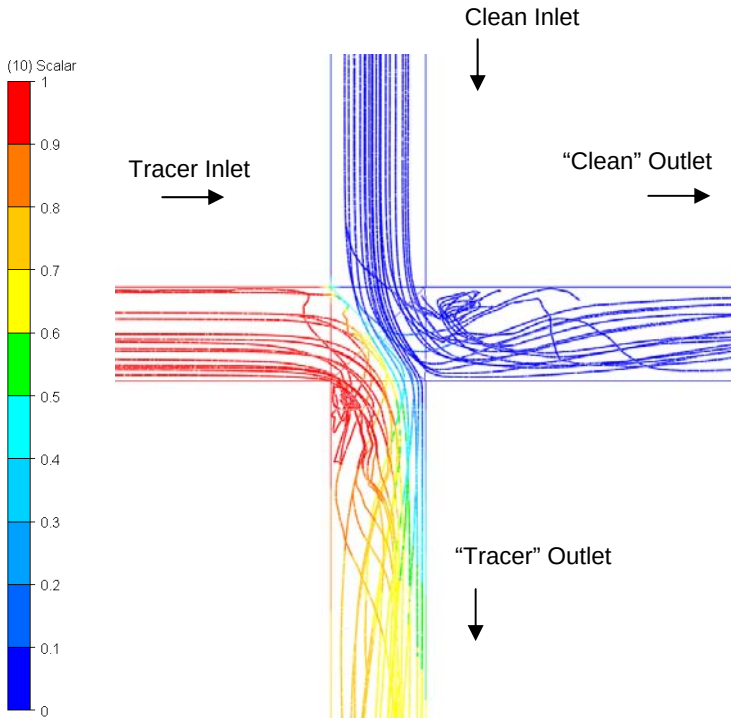

Figure 26. CFD-simulated three-dimensional flow lines colored by the normalized scalar (tracer) concentration. The flow rate in the clean inlet is about 80% greater than the flow rate in the tracer inlet (adapted from Ho et al., 2006).

As a result, the additional momentum of the clean water causes some of the clean water to push across the junction into the opposing outlet pipe. This bulk-fluid mixing behavior will dilute the concentration in the "tracer" outlet pipe while reducing the amount of tracer that can migrate into the "clean" outlet. Similar (but opposite) behavior will occur if the flow rate in the tracer inlet is greater than the flow rate in the clean inlet with equal outlet flow rates. These different flow patterns are illustrated in **Figure 27**.

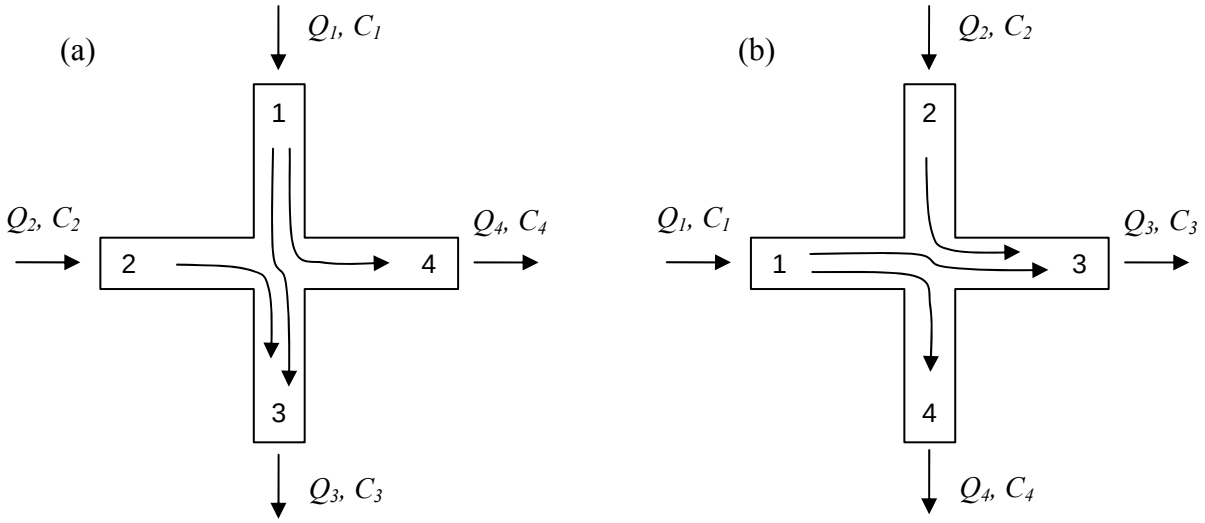

Figure 27 Numbering assignment in the bulk-mixing model for different flow configurations: a) the greatest momentum is in the vertical direction; b) the greatest momentum is in the horizontal direction. Flow rate is denoted by Q [L3/T], and concentration is denoted by C [M/L3].

The bulk-mixing model assumes that mixing occurs only via interaction of the bulk fluid. Mixing caused by diffusion and instabilities at the impinging interface are neglected. So, for the confined cross junction shown in **Figure 27** with equal pipe sizes, mixing will only occur if different flow rates exist in adjacent inlet/outlet pipes. If all flow rates are equal, or if the flow rates in adjacent inlet/outlet pipes are equal, the flow is assumed to bifurcate completely and no mixing will occur from the bulk fluid flow. Therefore, the bulk-mixing model provides a physically based lower bound to the amount of mixing that can occur within junctions. The bulk mixing model is derived below assuming the flow rates are known (or calculated) in each pipe. First, the pipes are numbered so that the nomenclature used in the solution is consistent for all flow configurations:

1. Calculate the total fluid momentum rate ($\sum Q_i^2/A_i$) in pairs of opposing legs (i.e., inlet and outlet pipes situated 180° from each other), where A_i is the cross-sectional area of the pipe.
2. For the pipe pair with the largest combined fluid momentum rate, assign "1" to the inlet and "3" to the outlet.
3. Assign "2" to the remaining inlet and "4" to the remaining outlet.

Assuming constant water density, the momentum criteria for the pipe nomenclature defined above is as follows:

$$\frac{Q_1^2}{A_1}+\frac{Q_3^2}{A_3}>\frac{Q_2^2}{A_2}+\frac{Q_4^2}{A_4} \qquad (3.2)$$

In the experiments and analyses evaluated in this paper, the pipes connected by a single junction are all assumed to be equal in cross-sectional area. Mixing in junctions with unequal pipe sizes is considered later.

Two examples of the prescribed numbering scheme associated with different flow patterns are shown in **Figure 27**. In the examples, different flow rates in the individual pipes cause a dominant momentum in one of the opposing pipe pairs. In **Figure 27a**, the dominant momentum is from top to bottom, whereas in **Figure 27b** the dominant momentum is from left to right. Because of the numbering scheme imposed above, pipes 1 and 3 always correspond to the inlet and outlet, respectively, of the pipe with the largest momentum. Thus, with this numbering scheme, the bulk-mixing model assumes that all of the flow from inlet pipe 2 flows into outlet pipe 3 since the dominant momentum from pipe 1 to pipe 3 is assumed to prevent any "cross-over" flow from pipe 2 to pipe 4. Flow from inlet pipe 1 flows into both outlet pipes 3 and 4. Therefore, the concentration in outlet pipe 3 is a mixture of the fluid concentrations from inlet pipes 1 and 2. The concentration in outlet pipe 4 is the same as the concentration in inlet pipe 1, which is the sole source of flow for outlet pipe 4.

With the prescribed numbering scheme shown in **Figure 27**, a rigorous derivation of the concentrations in each of the outlet pipes can be made, assuming that the flow rate in each pipe is known along with the inlet concentrations (C_1 and C_2). In this model, we assume that the constituents are well mixed before entering and after leaving the junction. Previous studies have shown that constituents are well mixed within ~10 pipe diameters downstream of the junction (Plesniak and Cusano, 2005; Ho *et al*., 2006). The following expression results from a mass balance on the solute leaving outlet pipe 4:

$$Q_4 C_4 = Q_{1\to 4} C_1 = Q_4 C_1 \qquad (3.3)$$

where $Q_{1\to 4}$ is the portion of the flow from inlet pipe 1 that flows into outlet pipe 4. Since none of the flow from inlet pipe 2 is assumed to cross over into outlet pipe 4, all of the flow leaving outlet pipe 4 is from inlet pipe 1 (i.e., $Q_{1\to 4} = Q_4$). Therefore, Equation (3.3) states that the solute concentration in outlet pipe 4 is equal to the solute concentration in inlet pipe 1:

$$C_4 = C_1 \qquad (3.4)$$

The concentration in outlet pipe 3 is derived by performing a solute mass balance on the entire cross junction:

$$Q_1 C_1 + Q_2 C_2 = Q_3 C_3 + Q_4 C_4 \qquad (3.5)$$

Using Equation (3.4) in Equation (3.5) results in the following equation for the solute concentration in outlet pipe 3:

$$C_3 = \frac{Q_2 C_2 + (Q_1 - Q_4) C_1}{Q_3} \qquad (3.6)$$

Equations (3.4) and (3.6) describe the bulk-mixing analytical solutions for the outlet concentrations assuming the flow rates and inlet concentrations are known. In a network model, these solutions can be applied sequentially to each downstream junction starting with the upstream-most junction where the concentration boundary conditions are prescribed. The flow rate in each pipe is typically calculated beforehand in network or CFD models based on prescribed boundary conditions of pressure and/or flow rates. In transient simulations, the bulk-mixing model solution can be applied at each time step with updated flow rates at each junction.

The solution for the concentration in outlet pipe 3 can also be rewritten in terms of the ratios of the inlet and outlet flow rates. Previous studies have expressed mixing-test results in terms of these ratios (Romero-Gomez *et al*., 2006), defined here as x and y:

$$x = \frac{Q_1}{Q_2}, \quad y = \frac{Q_4}{Q_3} \qquad (3.7)$$

The flow ratios, Q_2/Q_3 and Q_1/Q_3, expressed in Equation (3.6) can be derived using the definitions in Equation (3.7) and conservation of water mass flowing through the cross junction:

$$Q_1 + Q_2 = Q_3 + Q_4 \qquad (3.8)$$

Using Equation (3.7) in Equation (3.8) to define individual flow rates in terms of x and y yields the following expressions for the flow ratios, Q_2/Q_3 and Q_1/Q_3, in Equation (3.6):

$$\frac{Q_2}{Q_3} = \frac{y+1}{x+1} \qquad (3.9)$$

$$\frac{Q_1}{Q_3} = \frac{y+1}{1/x+1} \qquad (3.10)$$

Equations **Error! Reference source not found.** and **Error! Reference source not found.**, together with the definition for y, are used to rewrite Equation (3.6) in terms of the inlet and outlet flow ratios:

$$C_3 = \left(\frac{y+1}{x+1}\right) C_2 + \left(\frac{x-y}{x+1}\right) C_1 \qquad (3.11)$$

Finally, if the pipe diameters are all equal, the inlet and outlet flow ratios can also be equivalently expressed as the ratio of the Reynolds number for each pipe, i:

$$\mathrm{Re}_i = \frac{V_i D_i}{\nu} \qquad (3.12)$$

where V_i is the fluid velocity [L/T] in pipe i, D_i is the diameter [L] of pipe i, and ν is the kinematic viscosity of the water [L^2/T]. If the pipe diameters are all equal, Equation (3.6) can be written as a function of the Reynolds number for each pipe:

$$C_3 = \frac{\mathrm{Re}_2 C_2 + (\mathrm{Re}_1 - \mathrm{Re}_4) C_1}{\mathrm{Re}_3} \qquad (3.13)$$

Scaling Parameter for Combined Complete-Mixing and Bulk-Mixing Models

Because the complete-mixing model and the bulk-mixing model provide upper and lower bounds, respectively, for the mixing behavior in junctions, the actual amount of mixing will fall in between these two bounds. Therefore, a scaling parameter, $0 \leq s \leq 1$, can be defined to estimate a combined (intermediate) concentration, $C_{combined}$, in an outlet pipe based on the physically bounding concentrations calculated from the complete ($C_{complete}$) and bulk (C_{bulk}) mixing models described earlier:

$$C_{combined} = C_{bulk} + s\,(C_{complete} - C_{bulk}) \quad (3.14)$$

The value of the scaling parameter, s, may depend on fluid properties, flow conditions, and the geometric configuration of the pipe junction, all of which can contribute to local instabilities at the impinging interface and turbulent mixing within the junction that are not captured by the bulk-mixing model. More rigorous evaluations of the scaling parameter and its correlation to various parameters, flow conditions, and system features is beyond the scope of the current study. Therefore, in this study, we treat the scaling parameter as a fitting parameter. For s values close to 1, the predicted behavior resembles the complete-mixing model. For s values close to 0, the predicted behavior is closer to the bulk-mixing model.

Evaluation of Complete-Mixing and Bulk-Mixing Models to Experimental Data

In this section, the results of the complete-mixing and bulk-mixing models are compared to the experimental results presented in Romero-Gomez *et al*. (2006) and McKenna *et al*. (2007). Experiments performed by Romero-Gomez *et al*. (2006) investigated different ratios of inlet and outlet flow rates. In one set of experiments, the flow rates at the inlets (tracer inlet and clean-water inlet) were varied while the outlet flow rates were held equal. In a second set of experiments, the flow rates at the outlets were varied while the inlet flow rates were held equal. In the study presented by McKenna *et al.* (2007), only the inlet flow rates were varied while the outlet flow rates were held equal. In the following discussion, the outlet adjacent (90°) to the tracer inlet is denoted the "tracer outlet," and the outlet adjacent to the clean-water inlet is denoted the "clean outlet." The relative orientation of the tracer and clean-water inlets and

outlets used in the experiments follow the same orientation shown in **Figure 26**. In the models, the concentration at the tracer and clean-water inlets were prescribed to be 1 and 0, respectively. **Figure 28 and Figure 29** show the analytical and experimental normalized tracer concentrations at the tracer outlet for different flow configurations. In **Figure 28**, the inlet flow ratios (tracer/clean) were varied while the outlet flow rates were held equal. In **Figure 29**, the outlet flow ratios (tracer/clean) were varied while the inlet flow rates were held equal. Results show that the complete-mixing model and the bulk-mixing model bound the data for all values of the inlet and outlet flow ratios. Greater mixing (or dilution) is indicated by lower values of normalized concentration at the tracer outlet. As discussed previously, the complete-mixing model assumes that the concentrations in the outlet pipes are equal, caused by complete and instantaneous mixing within the junction. Therefore, the complete-mixing model yields the lowest values for the tracer-outlet normalized concentrations for all cases. The bulk-mixing model predicts higher normalized concentrations at the tracer outlet for all inlet flow ratios because mixing of the tracer is caused by mixing of the bulk fluids only (no diffusion or turbulent mixing).

In **Figure 28**, tracer/clean inlet flow ratios less than one indicate that a greater amount of clean water was introduced into the cross junction than tracer water. For tracer/clean inlet flow ratios greater than one, more tracer water was introduced into the cross junction than clean water. The experimental data shown in **Figure 28** are bounded by the results of the bulk-mixing and complete-mixing models, and the trends are similar to those of the models. As more flow is introduced through the tracer inlet relative to the clean-water inlet, less dilution from the clean water occurs and the normalized concentration in the tracer outlet increases towards a value of 1. However, because of transient instabilities caused by turbulent flow (and perhaps external instabilities such as oscillations from the mechanical pumps), a small amount of dilution persists, even with inlet flow ratios (tracer/clean) greater than one. For inlet flow ratios between approximately 0.3 and 3, the data can be predicted using the combined model with a scaling parameter between 0.2 and 0.5. For inlet flow ratios less than 0.3 or greater than 3, the data are more accurately predicted using the combined model with a scaling parameter between 0.5 and 0.8. This implies that mixing was enhanced when there was a significant discrepancy in the flow rates (more than a factor of three).

As stated earlier, the pipe diameters used in the two data sets **Figure 28** (Romero-Gomez et al., 2006, and McKenna et al., 2007) were different. Also, the PVC pipe junctions used in the two data sets were made from different manufacturers. The NIBCO fittings used in Romero-Gomez et al. (2006) created a more flush connection between the inner diameter of the pipes and the inner diameter of the junction compared to the Spears fittings used in McKenna et al. (2007). Therefore, the Spears fittings allowed for more expansion of the fluid when it entered the junction, and one would expect more mixing to occur in the experiments performed by McKenna et al. (2007). This behavior is somewhat reflected in the data shown in **Figure 28**, although the trends are quite comparable for the range of inlet flow ratios that overlapped the two sets of data.

Figure 29 shows the model and experimental results for different outlet flow ratios (tracer/clean) and equal inlet flow ratios. Only the data of Romero-Gomez et al. (2006) were used; McKenna et al. (2007) did not consider different outlet flow ratios. When the outlet flow ratio (tracer/clean) is less than 1, a greater amount of water is being pulled into the clean outlet

relative to the tracer outlet. When the outlet flow ratio is greater than 1, a greater amount of water is being pulled into the tracer outlet relative to the clean outlet. In **Figure 29**, the tracer and clean-water inlet flow rates are equal. Therefore, the complete-mixing model predicts that the outlet concentrations will be 0.5 (half the normalized concentration of the tracer inlet), even though the outlet flow rates are unequal. However, the experimental data and the bulk-mixing model show significant deviations from the complete-mixing model. In cases where the outlet flow ratios (tracer/clean) were greater than one, the larger flow through the tracer outlet was supplemented by the water from the clean-water inlet, diluting the tracer concentration (**Figure 27(a)**). At very large outlet flow ratios (tracer/clean), nearly all of the water entering the junction from both the tracer and clean-water inlet will exit through the tracer outlet, and the tracer-outlet concentration will asymptotically approach 0.5 to reflect the equal inlet flows.

Below an outlet flow ratio of one, **Figure 29** shows that the experimental tracer-outlet concentrations tend toward 1 since the water leaving the tracer outlet is comprised primarily of the water from the tracer inlet. The bulk-mixing model predicts normalized tracer-outlet concentrations of 1 for these conditions because it assumes that the predominant flow from the tracer inlet to the clean outlet (horizontal pipe in **Figure 27**(b)) prevents any clean water from crossing over the junction to dilute the water leaving the tracer outlet. Overall, the trends in the experimental data are well matched by the predictions of the bulk-mixing model, especially for outlet flow ratios greater than a factor of two or three. For outlet flow ratios less than two, the combined model with a scaling parameter of approximately 0.1 to 0.2 appear to match the data quite well.

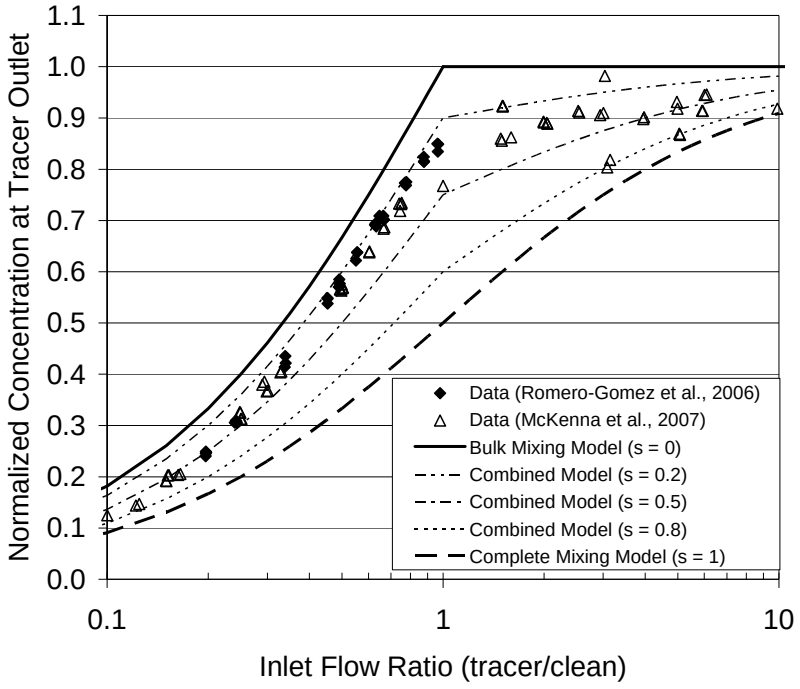

Figure 28. Comparison of experimental and modeled normalized concentrations at the tracer outlet (outlet adjacent to the tracer inlet) for different inlet flow rates and equal outlet flow rates.

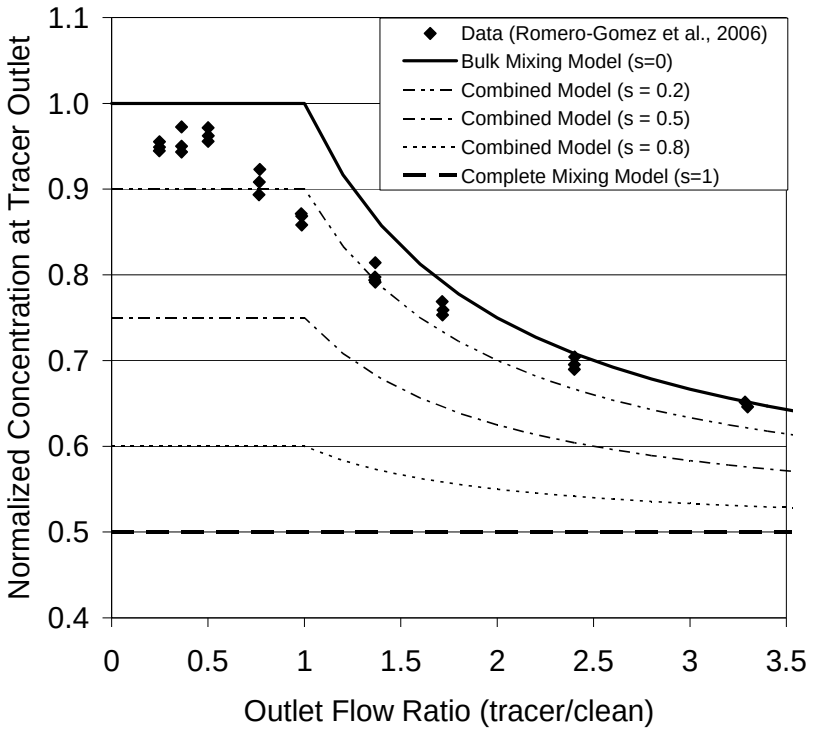

Figure 29. Comparison of experimental and modeled normalized concentrations at the tracer outlet (outlet adjacent to the tracer inlet) for equal inlet flow rates and different outlet flow rates.

3.3 EPA-BAM Modifications

In a network model such as those implemented in EPANET (Rossman, 2000), the solution described in the previous section can be applied sequentially to each downstream junction starting with the upstream-most junction where the concentration boundary conditions are prescribed. The flow rate in each pipe is calculated based on prescribed boundary conditions of pressure and/or flow rates, and the bulk-advective mixing model solution can be applied at each time step using updated flow rates at each junction.

The new bulk advective mixing (BAM) model has been implemented in EPANET (Rossman, 2000) and is being distributed as an open-source software known as EPANET-BAM (Khalsa and Ho, 2007). EPANET-BAM allows the user to select a mixing parameter, s (between 0 and 1) for each junction in the network, that linearly scales the mixing results between the lower-bound results of the bulk advective mixing model ($s = 0$) and the upper-bound results of the complete-mixing model ($s = 1$):

For mixing parameter values less than one, the model is referred to generally as the bulk advective mixing model (BAM) throughout the remainder of this paper; for mixing parameter values equal to one, the model is referred to as the complete-mixing model. Comparisons between the BAM model and experiments have been performed for single-joint tests (Ho, 2008) and small-scale network tests (Ho and Khalsa, 2008). Results showed that a mixing parameter between 0.2 and 0.5 yielded good matches with the experimental data.

User Interface

All features and functions of EPANET-BAM are compatible with EPANET 2.0. **Figure 30** shows a screen image from a sample network model in EPANET-BAM. The only change in EPANET-BAM is the addition of the mixing parameter, which appears as a new field in the junction property editor (**Figure 30**). A value of 1 for the mixing parameter indicates that the junction will use the complete mixing model, and a value less than 1 indicates that the junction will implement BAM (Equation (3.14)). A default mixing parameter value of 0.5 is initially assigned to all junctions based on the results of experimental comparisons (Ho, 2008; Ho and Khalsa, 2008).

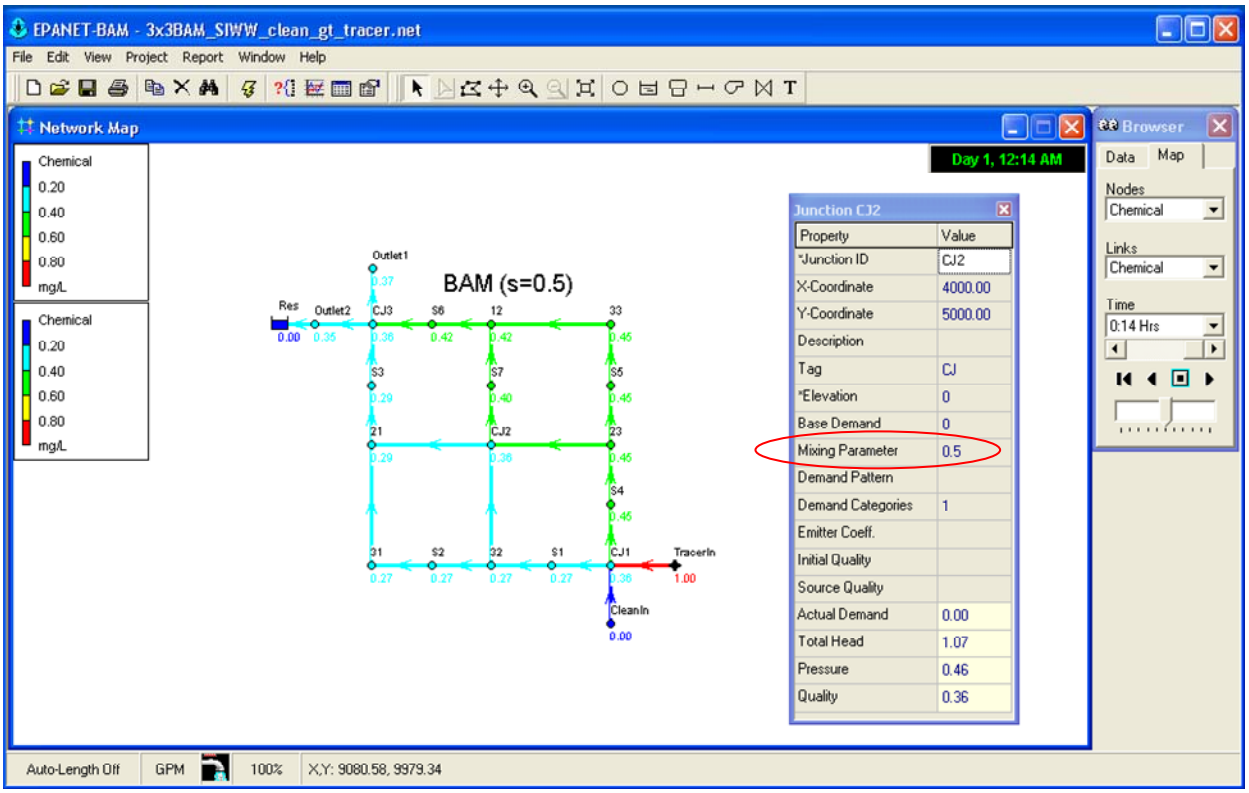

Figure 30. Screen image of EPANET-BAM with new Mixing Parameter field circled.

Junction Configurations

Even though a mixing parameter is assigned to each junction, the BAM model will only be applied in EPANET-BAM for valid cross junctions. Valid cross junctions consist of junctions with four pipes with two adjacent inlet flows and two adjacent outlet flows. These criteria hold for any angle of pipe intersection at a junction; junction configurations that meet these criteria but defined by non-orthogonal intersecting pipes are also considered valid cross junctions. For all other junction configurations, the complete mixing model ($s = 1$) is applied (see **Figure 31**). Because the junction configuration can change in time due to transient flow rates and boundary conditions, EPANET-BAM checks each junction configuration at each time step and applies the user-prescribed mixing parameter for a junction if it meets the valid cross-junction criteria.

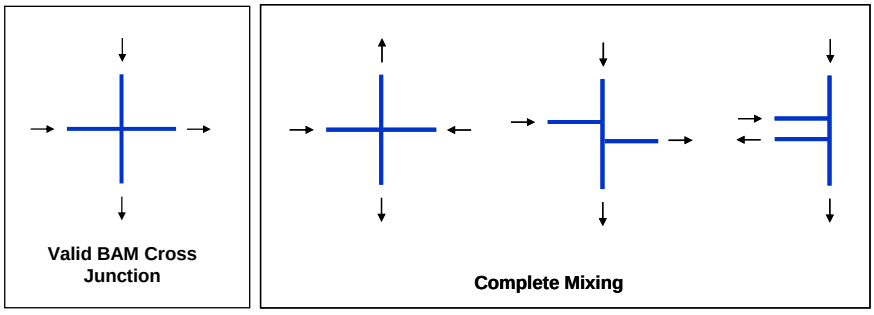

Figure 31. Example of a valid cross junction for implementation of the BAM model (left) and examples of other junction configurations that automatically use the complete mixing model (right).

Transferring Files from EPANET to EPANET-BAM

Existing files that were created in EPANET 2.0 are not directly compatible with EPANET-BAM, but they can be converted to EPANET-BAM readable files. The graphical user interface and solver in EPANET-BAM require that an additional column titled 'MixParam' be added to the input file under [JUNCTIONS] between the 'Demand' and 'Pattern' columns:

```
[JUNCTIONS]
;ID   Elev   Demand      MixParam    Pattern
 J1   0      0           0.5         P1      ;
 J2   0      0           0.5         P2      ;
```

If the existing file is in a *.NET format, the file can be read into EPANET 2.0 and then exported into a *.INP text file (File menu -> Export -> Network). The 'MixParam' column can then be added to the text file using a word processor or spreadsheet (e.g., Excel). EPANET-BAM can then read the revised text file with the additional column.

Code Modifications

Code modifications to EPANET 2.0 that enabled the implementation of the BAM model in EPANET-BAM are summarized below.

epanet.c

[Modified Functions]

geterrmsg():	return error message for new error ERR252, which occurs when not all nodes have coordinates defined.

input2.c

[Modified Functions]

readdata():	ensure all nodes have coordinates defined.
newline():	when COORDINATES or VERTICES section is encountered, call coordsdata() or verticesdata() (input3.c) instead of ignoring.

input3.c

[Modified Functions]

juncdata():	read value from additional MixParam column under [JUNCTIONS].

[New Functions]

coordsdata():	processes node coordinates under [COORDINATES].
verticesdata():	processes vertex coordinates under [VERTICES].

quality.c

[Modified Functions]

openqual():	allocate memory for cross junctions array.
closequal():	free memory for cross junctions array.
transport():	call findcrossjuncs() to collect cross junction data before calling accumulate().
accumulate():	after upstream concentrations are transported downstream, store in cross junction array the concentrations of link segments that are inlets of valid cross junctions.
release():	call bmfastoutconc() and bmslowoutconc() to set concentrations of outlet segments of valid cross junctions using the BAM model.

[New Functions]

findcrossjuncs():	fills cross junctions array by determining which junctions are cross junctions valid for BAM model.
bmfastoutconc():	uses BAM model to calculate concentration at the outlet of a valid cross junction corresponding to the larger inlet + outlet flow rate sum.
bmslowoutconc():	uses BAM model to calculate concentration at the outlet of a valid cross junction corresponding to the smaller inlet + outlet flow rate sum.
angle():	calculates angle of the position vector of a point counter-clockwise above the horizontal axis, with specified origin coordinates. Used by nonadjlink().
getlinkcoords():	determines the coordinates of the node or vertex responsible for the angular orientation of a specified link about a specified node.
nonadjlink():	for a specified link connected to a cross junction, determines which of the three other links connected to the cross junction is not adjacent to the specified link.

funcs.h

Added prototypes for new functions:

input3.c: coordsdata(), verticesdata().

quality.c: findcrossjuncs(), bmfastoutconc(), bmslowoutconc(), angle(), getlinkcoords(), nonadjlink().

types.h

- New Coordinate Object (Coord) stores a pair of coordinates.
- Modified Node Object (Snode) to store BAM scaling parameter and coordinates.
- New Cross Junction Object stores flow rates for BAM calculations.
- Modified Link Object (Slink) to store coordinates of the two vertices closest to the connected nodes when such vertices exist.

text.h

- Added error message for new error ERR252, which occurs when not all nodes have coordinates defined.

3.4. Single-Joint Flow Visualization Experiments

Visualization of Physical Mixing Processes

A number of experiments have been performed to characterize the mixing behavior within individual pipe joints (Orear *et al*., 2005; and McKenna et al., 2007; Austin et al., 2008). Pumps were used to supply water through pipes joined by a cross junction. The flow rates were controlled at both the inlets and outlets of the pipes using valves, and flow meters were used to monitor the flow rate through each pipe. The pipes were constructed of PVC with prescribed diameters, and the inlet and outlet pipe lengths were sufficiently long (20-100 pipe diameters) to ensure the water was well mixed within each pipe section before entering the junction and before being monitored by the electrical conductivity sensors in the effluent pipes. Water entering the system was pumped from two supply tanks (a well-mixed tracer supply tank and a clean-water supply tank), and water leaving the system was emptied into two effluent tanks. **Figure 32** shows a photograph and sketch of the test apparatus used by Orear et al. (2005) and McKenna et al. (2007).

For all experiments, NaCl was mixed with water in the tracer supply tank. The amount of NaCl added was enough to raise the electrical conductivity of the tracer solution to two to four times above that of the "clean" water. The NaCl tracer was monitored in the effluent pipes using electrical conductivity sensors, and normalized concentrations of the tracer were calculated using the maximum value of the conductivity of the NaCl solution and the minimum value of the conductivity of the clean water. Thus, the normalized concentration of the tracer water was 1, and the normalized concentration of the clean tap water was 0.

For the visualization experiments presented in this study, the cross junction connecting the inlet and outlet pipes was fabricated from a clear block of acrylic. The PVC pipes were then fitted into the acrylic block such that the inner diameter of the pipes was flush with the inner diameter of the junction openings. For the equal pipe-size tests, the inner diameter of the pipes and junction openings was 2.6 cm (~1 inch). For the unequal pipe-size tests, the inner diameters of the pipes and junction openings were 2.6 cm (~1 inch) and 5.2 cm (~2 inches). Blue food coloring was added to the NaCl tracer, and a digital video camera was used to record images of the mixing and distribution of the dyed tracer within the clear junction.

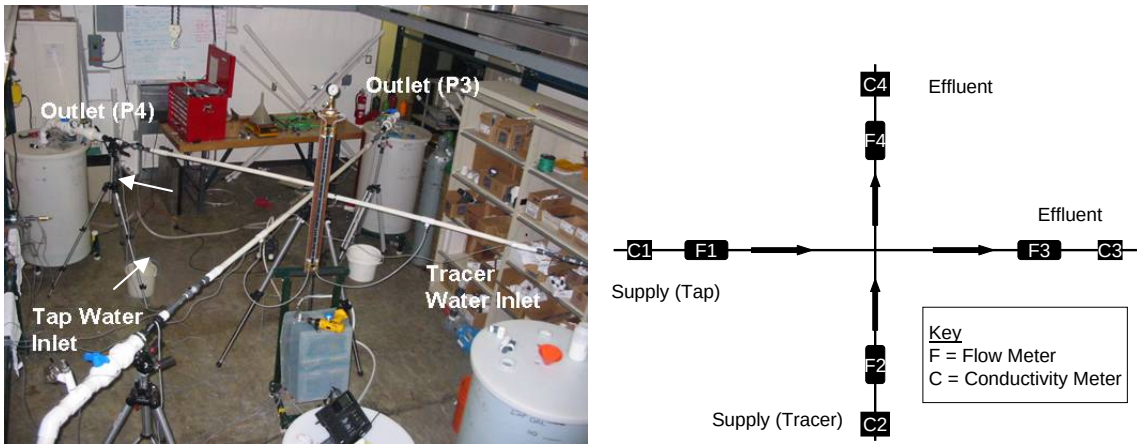

Figure 32. Photograph and sketch of single-joint apparatus used in experiments (Orear et al., 2005 and McKenna et al., 2007).

Adjacent inlets – equal pipe sizes

Figure 33 shows video images of solute mixing in a cross junction with adjacent inlets and equal pipe sizes (2.6 cm). The Reynolds number for the flow rates ranged from approximately 4,000 to 13,000, indicating that the flow was turbulent in all pipes. Tracer was introduced in the pipe on the right, and clean water was introduced in the pipe at the bottom. The top image was taken when the flow rates in all the pipes were nearly equal. The middle image was taken when the tracer inlet flow was approximately three times greater than the clean inlet flow (outlet flow rates were equal). The bottom image was taken when the clean inlet flow was approximately three times greater than the tracer inlet flow (outlet flow rates were equal).

The images in **Figure 33** show that the incoming fluid streams reflect off one another and, depending on the relative momentum flux of each stream, may cross over the junction into the opposing outlet pipe. In the top image, the flow rates are approximately equal in each pipe, and the incoming tracer and clean water streams reflect off one another and exit through the adjacent outlet pipes. The averaged normalized concentration of the top outlet pipe adjacent to the tracer inlet was measured to be approximately 0.9, while the averaged normalized concentration of the left outlet pipe adjacent to the clean inlet was only ~0.1. Turbulent and transient instabilities along the impinging interface (where the two incoming fluid streams meet in the junction) causes some of the fluid to mix (Webb and van Bloemen Waanders, 2006), but the majority of the incoming flows stay separated.

In the middle image of **Figure 33**, the larger momentum flux of the incoming tracer water on the right causes some of the flow to cross over the junction into the opposing outlet pipe on the left. This effectively blocks the incoming clean water from the bottom, forcing the clean water to exit through the adjacent outlet pipe on the left. The effluent exiting the top outlet pipe is composed entirely of the tracer water, and the measured normalized concentration was approximately 1. The normalized concentration of the effluent in the left outlet pipe was approximately 0.55. The bottom image of **Figure 33** shows a similar but opposite effect when the clean water inlet flow rate is approximately three times greater than the tracer inlet flow rate. The higher momentum clean water now flows across the junction from the bottom inlet to the top outlet and

effectively diverts the incoming tracer water from the right into the top outlet as well. In this case, the measured average normalized concentration in the left outlet is 0, and the measured average normalized concentration in the top outlet is ~0.5.

Table 2. Summary of tests with adjacent inlets and equal pipe sizes.

Pipe	Average Flow Rate (m3/s)	Velocity (m/s)	Reynolds Number	Normalized Concentration
Case 1: Equal Flow Rates				
Tracer in (right)	7.9E-05	0.15	4,300	1.0
Clean in (bottom)	7.5E-05	0.14	4,100	0.0
Effluent (left)	7.6E-05	0.14	4,100	0.12
Effluent (top)	8.3E-05	0.15	4,500	0.91
Case 2: Tracer Inlet > Clean Inlet				
Tracer in (right)	2.3E-04	0.43	12,000	1.00
Clean in (bottom)	7.4E-05	0.14	4,000	0.00
Effluent (left)	1.5E-04	0.28	8,300	0.55
Effluent (top)	1.5E-04	0.29	8,400	1.0
Case 3: Clean Inlet > Tracer Inlet				
Tracer in (right)	7.4E-05	0.14	4,100	1.0
Clean in (bottom)	2.4E-04	0.45	13,000	0.00
Effluent (left)	1.6E-04	0.29	8,600	0.02
Effluent (top)	1.6E-04	0.30	8,700	0.47

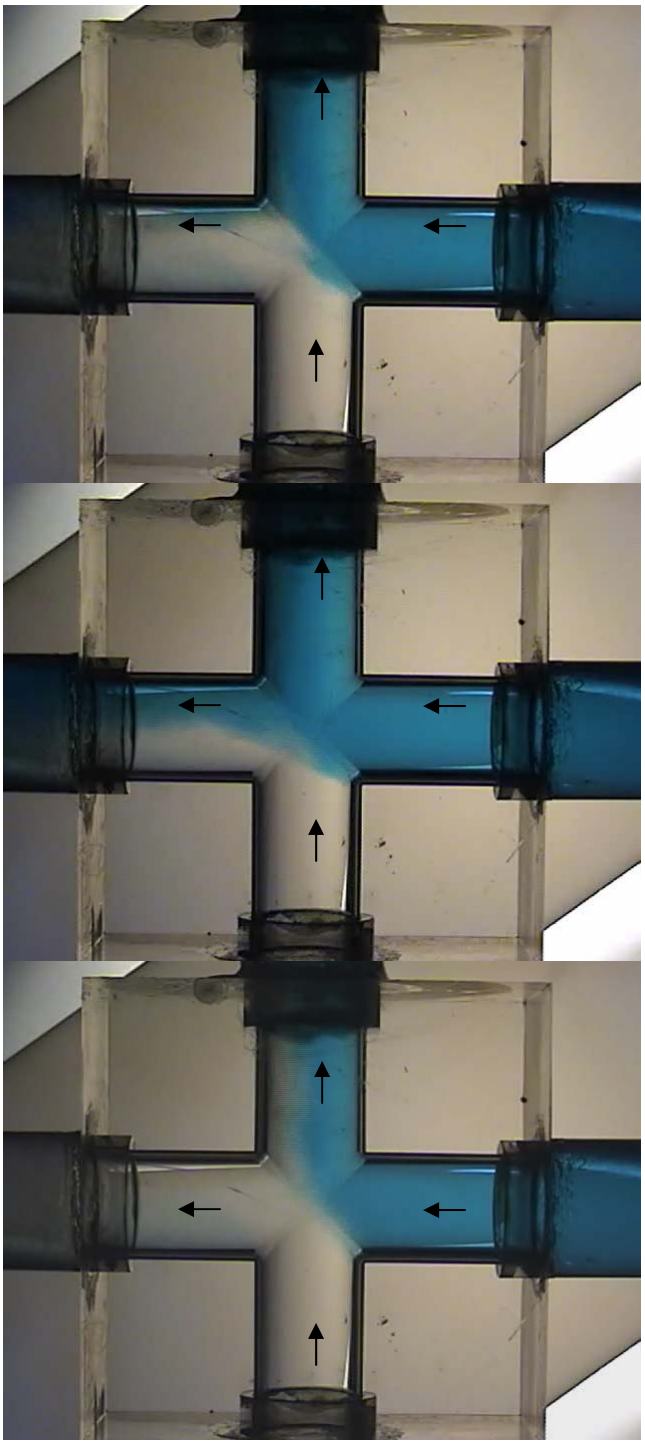

Figure 33. Video images of solute mixing in a pipe junction with adjacent inlets (tracer inlet is on the right, clean inlet is at the bottom). Top: 1:1 tracer/clean inlet flow rates, Middle: 3:1 tracer/clean inlet flow rates, Bottom: 1:3 tracer/clean inlet flow rates**.**

Adjacent inlets – unequal pipe sizes

Figure 34 shows video images from experiments of mixing in a cross junction with adjacent inlets and unequal pipe sizes. The diameter of the larger vertical pipe (~2.6 cm) is twice the diameter of the smaller horizontal pipe (~5.2 cm). Tracer is introduced in the small pipe on the right, and clean water is introduced in the larger pipe on the bottom.

The top image in **Figure 34** shows the mixing behavior when the flow rate in the larger pipe has a momentum that is 14 times greater than the momentum in the small pipe; the flow rate ratio between the larger pipe and the smaller pipe is ~7.6 to 1. The greater momentum causes the flow in the larger pipe to push across the junction, effectively blocking the incoming flow from the smaller pipe. Thus, the flow at the left outlet pipe is composed primarily of the fluid from the adjacent inlet at the bottom, and the flow at the top outlet pipe is composed of a mixture of fluid coming from both the bottom and right inlets.

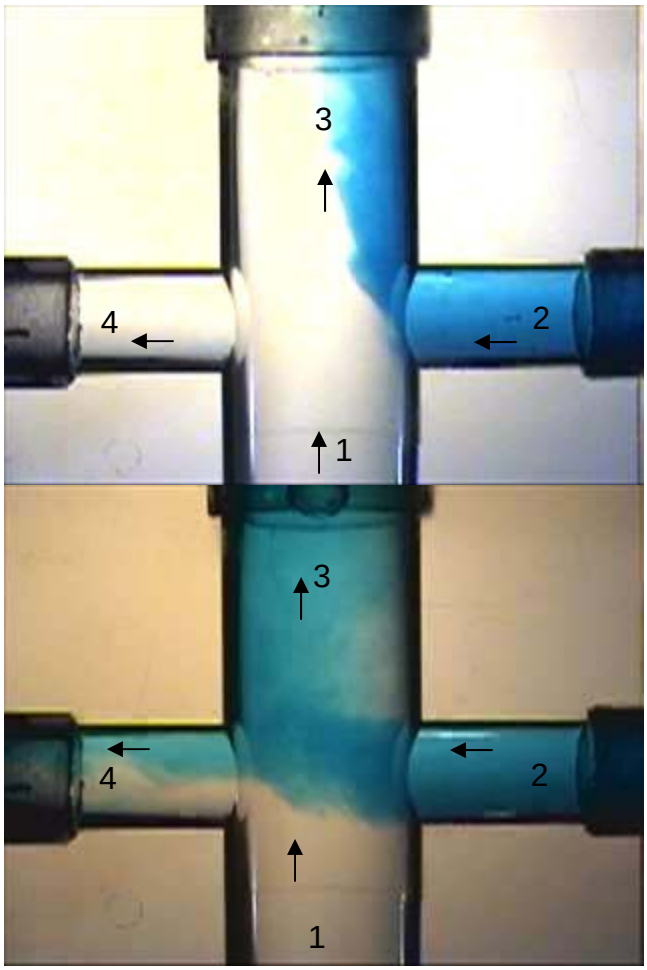

Figure 34. Video images of solute mixing in a pipe junction with adjacent inlets and unequal pipe diameters (tracer inlet is on the right, clean inlet is at the bottom). Top: 1:14 momentum ratio (small pipe/large pipe), Bottom: 4:1 momentum ratio (small pipe/large pipe).

The bottom image in **Figure 34** shows the mixing behavior when the momentum in the smaller pipe is four times greater than the momentum in the larger pipe; the flow rate ratio is nearly equal to one. In this case, the tracer from the smaller pipe inlet is seen to penetrate through the junction into the opposing outlet. However, rather than deflecting all of the clean water from the adjacent inlet, some of the clean water wraps around the flow emanating from the smaller pipe and also propagates through the junction to the opposing outlet, as indicated by the outlet concentrations summarized in Table 3 for these tests. In Table 3, pipes 1 and 2 denote the clean (larger pipe) and tracer (smaller pipe) inlets, respectively, and pipes 3 and 4 denote the outlets opposing the clean and tracer inlets, respectively. The results in Table 3 confirm the cross-over behavior described for the equal-pipe sizes, but it also shows that flow in the larger pipe can wrap around the flow from the smaller pipe when the momentum in the smaller pipe is greater than in the larger pipe. For example, for Cases 2, 4, and 5, the momentum in the larger pipe (1 and 3) is greater than in the smaller pipe (2 and 4). Therefore, the flow from the larger pipe completely deflects the incoming flow from the inlet of the smaller pipe, and the outlet concentration in pipe 4 is composed entirely of clean water (normalized concentration equals 0). For cases 1, 3, and 6, the momentum is greater in the smaller pipe, and although it penetrates across the junction, some of the clean water entering from the large pipe inlet wraps around and dilutes the outlet concentration in pipe 4, reducing the normalized concentration to a value less than one.

Table 3. Summary of experiments with adjacent inlets and unequal pipe sizes.

Case	Flow Pipe 1 (m^3/s)	Flow Pipe 2 (m^3/s)	Flow Pipe 3 (m^3/s)	Flow Pipe 4 (m^3/s)	Momentum Ratio (2+4)/(1+3)	Flow Ratio (2+4)/(1+3)	Normalized Concentration in Outlet Pipe 3	Normalized Concentration in Outlet Pipe 4
1	0.000245	0.000191	0.000253	0.000184	2.27	0.75	0.64	0.16
2	0.000239	6.65E-05	0.000244	6.29E-05	0.29	0.27	0.30	0.00
3	1.22E-04	1.81E-04	1.25E-04	1.78E-04	8.43	1.45	0.61	0.60
4	2.36E-04	1.17E-04	2.40E-04	1.14E-04	0.94	0.48	0.51	0.01
5	4.82E-04	6.59E-05	4.88E-04	6.22E-05	0.07	0.13	0.15	0.00
6	1.19E-04	1.22E-04	1.20E-04	1.20E-04	4.10	1.01	0.65	0.40

Opposing inlets – equal pipe sizes

Figure 35 shows a video image of solute mixing in a cross junction with opposing (180º) inlets. The tracer enters the junction on the right, and clean water enters on the left. The incoming flows collide in the junction and then exit through the top and bottom outlet pipes. Different combinations of flow rates in each of the inlet and outlet pipes were investigated as summarized in Table 4. The Reynolds number ranged from ~6,000 to 30,000 to maintain turbulent flow conditions within each pipe. **Figure 35** shows an extreme combination of flow rates where the flow ratios in the tracer inlet, clean inlet, top outlet, and bottom outlet were 5.5, 3.1, 7.6, and 1.0 relative to the lowest flow rate, respectively. Even under these extreme flow ratios (and in all of the cases summarized in Table 4), the measured tracer concentrations in the top and bottom outlets were nearly equal, indicating complete mixing within the junction. Section 0 provides additional discussion regarding the processes and assumptions that lead to a derivation of the complete mixing model for mixing in a cross junction with opposing inlets.

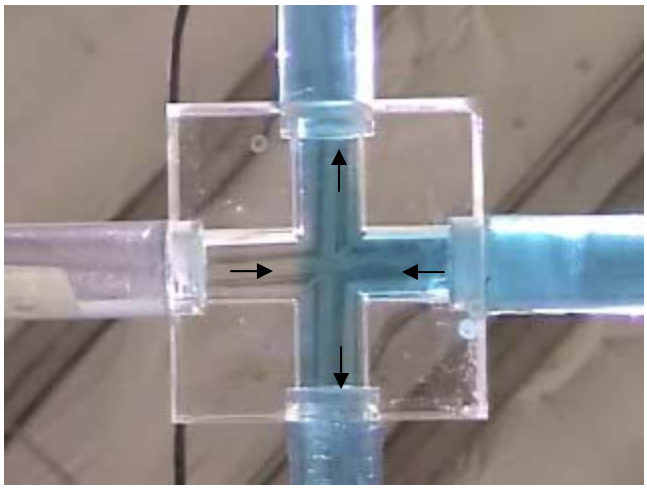

Figure 35. Video images of solute mixing in a pipe junction with opposing (180º) inlets (tracer inlet is on the right, clean inlet is on the left).

Table 4. Summary of tests with opposing inlets (180º) and equal pipe sizes.

Case	Average Velocity (m/s)				Normalized Outlet Concentration	
	Tracer in (right)	Clean in (left)	Effluent (top)	Effluent (bottom)	Top	Bottom
1	0.24	0.23	0.24	0.23	0.52	0.52
2	0.23	0.44	0.34	0.34	0.36	0.36
3	0.23	0.45	0.22	0.46	0.35	0.35
4	0.22	0.92	0.58	0.59	0.20	0.20
5	0.22	0.88	0.44	0.68	0.19	0.21
6	0.24	0.89	0.23	0.92	0.22	0.22
7	0.22	0.94	0.93	0.24	0.18	0.16
8	0.23	0.44	0.27	0.40	0.35	0.37

3.5 EPA-BAM Comparison to Experiments – Alternative Junction Configurations

Models of Mixing in Alternative Junction Configurations

In earlier bulk-mixing analysis, only a single joint of equal pipe sizes has been considered, modeled. Based on the observed physical mixing processes discussed above, models are derived to describe the salient processes of solute mixing in the alternative pipe-junction configurations

Impact of Different Pipe Sizes

Pipes of different sizes may be connected by a single cross joint. In these situations, the amount of mixing may be enhanced or diminished depending on the relative fluid momentum flux in the different sized pipes. For example, imagine a cross junction comprised of a larger diameter pipe in one direction and a smaller diameter pipe in the perpendicular direction. If the momentum flux is predominant along the larger pipe, flow from the smaller diameter pipe will become nearly entirely entrained within the flow from the larger diameter pipe (i.e., the momentum from the flow in the larger diameter pipe will prevent flow from the incoming smaller pipe from passing across the junction), minimizing the apparent mixing within the junction. This behavior is more consistent with the bulk-mixing model. However, if the momentum flux is predominant along the smaller pipe, greater mixing may be possible as the incoming fluid from the smaller pipe spreads out into the larger diameter junction. This is similar to a jet spraying into a larger bulk fluid medium. Additional studies are still needed to better understand mixing in junctions with different pipe sizes and to determine how well the complete-mixing and bulk-mixing models predict the actual behavior.

Bulk Mixing Model – Adjacent inlets – unequal pipe sizes

Derive model for unequal pipe sizes. Show sketches. Provide Excel chart comparing data to model predictions. Discuss why no mixing parameter is needed here (turbulent mixing within core region enhanced mixing, but turbulent mixing in wrap-around region has opposing effect). The previous section derived the BAM model for adjacent inlets with equal pipe sizes. In this section, we derive a model that accommodates mixing in unequal pipe sizes. Many different combinations of pipe sizes can exist at a junction, but we focus on the case when a larger pipe is intersected by a smaller pipe (e.g., a pipe main intersected by smaller pipes). **Figure 36** and **Figure 37** show a sketch of a cross junction with adjacent inlets and two different pipe sizes.

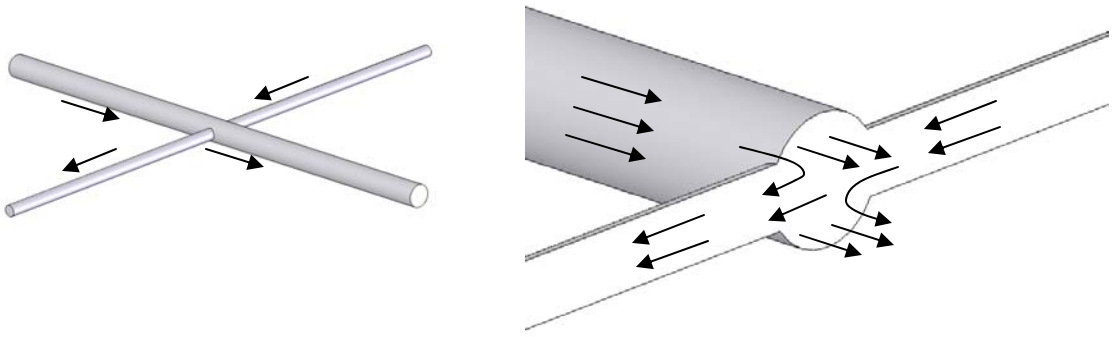

Figure 36. Cross junction with adjacent inlets and two different pipe sizes.

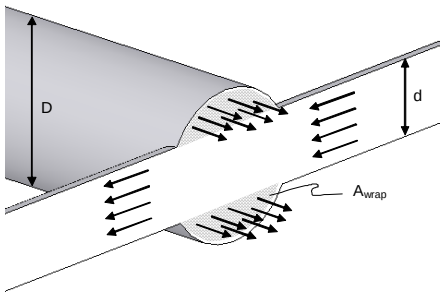

Figure 37. Close-up of cross-junction with unequal pipe diameters.

As described in the experiments of unequal pipe diameters, the mixing behavior depends on whether the momentum is greater in the larger or smaller pipe. If the momentum is greater in the larger pipe, it will cross over the junction and effectively deflect all of the flow from the incoming smaller pipe into the its adjacent outlet pipe. This behavior is similar to the BAM model described in the previous section for equal pipe sizes. Therefore, the BAM model can be applied to this configuration with unequal pipe sizes when the momentum is greater in the larger pipe.

If the momentum is greater in the smaller pipe, the experiments indicate that the flow in the smaller pipe will cross over the junction, but the flow in the larger pipe can wrap around the flow "penetrating" through the junction in the smaller pipe. As a result, the flow in both outlet pipes will be composed of a mixture of flow from both inlet pipes. A model of this wrap-around flow and mixing can be derived assuming that the flow and transport through the "core" and "wrap-around" regions within the junction is proportional to the geometric areas of the different pipe sizes. The core region is defined by the size of the smaller pipe, and mixing in the core region is assumed to behave similarly to the processes described by the BAM model. The wrap-around region is the area outside of the core region that is available for wrap-around flow due to the extra volume of the larger pipe (see **Figure 36).** This model, denoted as BAM-WRAP, is derived as follows:

$$A_{wrap} = \left(\frac{D}{2}\right)^2 \left(\theta - \sin\theta\right)$$

where $$\theta = 2\cos^{-1}\left(\frac{d}{D}\right)$$

$$Q_{i,wrap} = \left(\frac{A_{wrap}}{\pi D^2 / 4}\right) Q_i$$

Flow rate in smaller diameter section calculated as difference between total flow in a pipe and wrap-around flow:

$$Q_{i,BAM} = Q_i - Q_{i,wrap}$$

$C_{i,BAM}$ calculated using BAM model and appropriate flow rates ($Q_{i,BAM}$)
Calculate mass flow in smaller diameter section using BAM-calculated concentrations and flow rates:

$$\dot{m}_{i,BAM} = Q_{i,BAM} C_{i,BAM}$$

Calculate mass flow from wrap-around in pipe *i*:

$$\dot{m}_{i,wrap} = Q_{i,wrap} C_i$$

Calculate total concentration in pipe *i* by dividing total mass flow rate by the total flow rate in that pipe:

$$C_i = \frac{\dot{m}_{i,BAM} + \dot{m}_{i,wrap}}{Q_i}$$

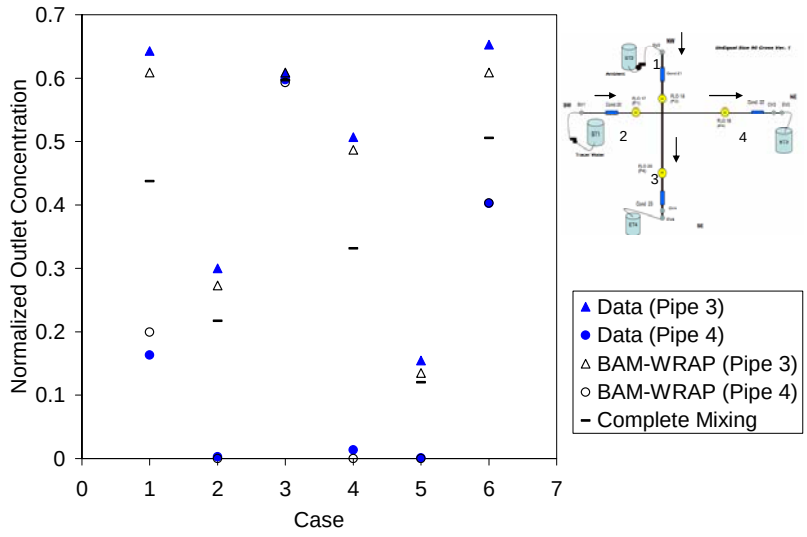

Figure 38. Plot of measured and predicted normalized outlet concentrations for mixing in a cross junction with adjacent inlet flows and different pipe sizes.

Bulk Mixing Model – 180 Degree Mixing of Opposite Inlets with *equal pipe sizes*

Provide model for complete mixing and compare to data for different runs.
Section 0 showed empirically that mixing in cross junctions with opposing inlets yielded nearly equal outlet concentrations for different combinations of inlet and outlet flow rates. In this section, a model is derived that demonstrates this junction configuration yields results that are

equivalent to complete mixing. **Figure 39** shows the configuration and numbering scheme for the model.

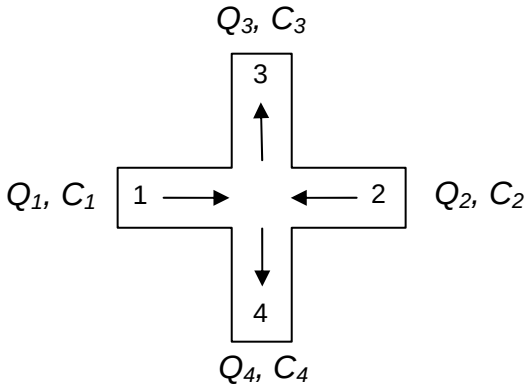

Figure 39. Configuration and numbering scheme for model of mixing with opposing inlets.

We assume that the fraction of flow from an inlet pipe that exits a particular outlet pipe is equal to the ratio of flow in that outlet pipe to the total outflow. For example, if 30% of the outflow is through pipe 3 and 70% of the outflow is through pipe 4, then 30% of the inlet flow from each of pipes 1 and 2 will exit pipe 3, and 70% of the inlet flow from each of pipes 1 and 2 will exit pipe 4. This condition ensures conservation of fluid mass and can be expressed as follows:

$$\frac{Q_{1\to3}}{Q_1} = \frac{Q_{2\to3}}{Q_2} = \frac{Q_3}{Q_3 + Q_4} \qquad (1)$$

$$\frac{Q_{1\to4}}{Q_1} = \frac{Q_{2\to4}}{Q_2} = \frac{Q_4}{Q_3 + Q_4} \qquad (2)$$

where $Q_{i\to j}$ denotes the flow rate from pipe *i* to pipe *j*. Summing **Equations (1) and (2)** demonstrates that fluid mass is conserved in the system. The concentrations at the outlet pipes can be expressed as a function of the flow rates and inlet concentrations as follows:

$$C_3 = \frac{Q_{1\to3}C_1 + Q_{2\to3}C_2}{Q_3} \qquad (3)$$

$$C_4 = \frac{Q_{1\to4}C_1 + Q_{2\to4}C_2}{Q_4} \qquad (4)$$

Plugging **Equations (1) and (2) into (3) and (4)** yields the following expression for the outlet concentrations:

$$C_3 = C_4 = \frac{Q_1 C_1 + Q_2 C_2}{Q_3 + Q_4} \qquad (5)$$

Equation (5) is equivalent to the results of the complete mixing model and demonstrates that the outlet concentrations are equal. The key assumption is that the fraction of flow from any inlet pipe that leaves a particular outlet pipe is equal to the fraction of flow in that outlet pipe to the total outflow.

Figure 40 shows the measured normalized outlet concentrations from the experiments summarized in Table 4 along with the results of the complete mixing model. These results demonstrate that mixing in cross junctions with opposing inlets yields equal outlet concentrations, with different combinations of inlet and outlet flow rates. The assumption used to derive **Equation (5)** is not dependent on pipe sizes, so this conclusion should be valid for cross junctions with opposing inlets and different pipes sizes as well.

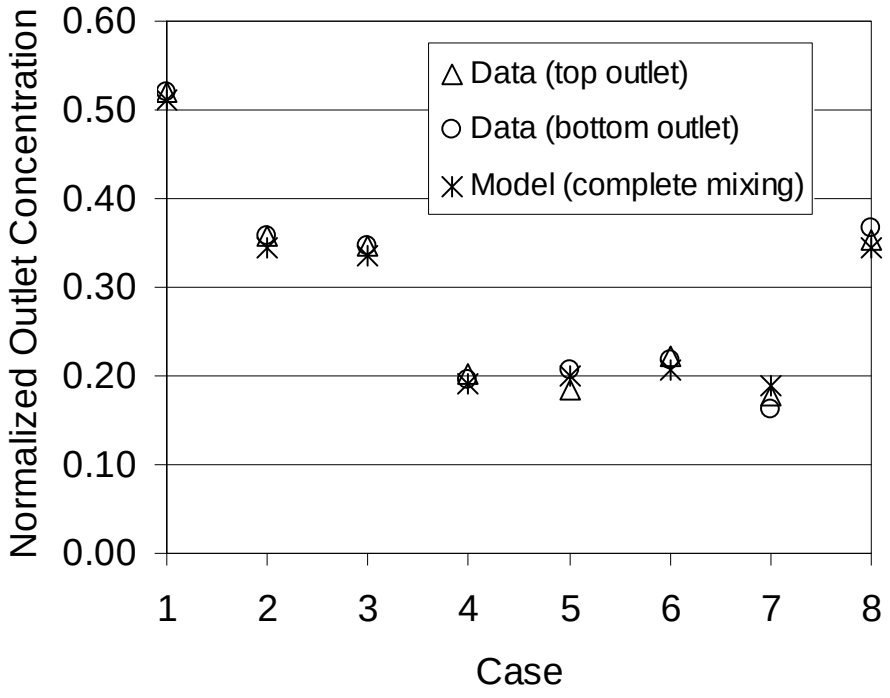

Figure 40. Comparison between measured and predicted normalized outlet concentrations for mixing in a cross junction with opposing (180º) inlets.

3.6 Summary and Conclusions

This chapter has described alternative modeling approaches for estimating solute mixing in pipe junctions for water-distribution systems. Because CFD models are not readily implemented in network-scale models such as EPANET, closed-form analytical models that can be implemented in network-scale models were introduced.

- A new bulk-mixing model was derived that assumes mixing of constituents only occurs from the bulk transfer and mixing of fluid streams caused by unequal flow rates entering and leaving the junction. The two analytical models, the complete-mixing and bulk-mixing models, provide an upper and lower bound, respectively, to the amount of mixing that can physically occur in pipe junctions. A scaling (or mixing) parameter, s, was used to combine the results of the two bounding analytical models. Furthermore, the bulk mixing model was developed for mixing in joints with unequal pipe sizes. The additional considerations are derived from the areal differences in the two pipes. Comparisons with experimental data have confirmed the applicability of these models.

- A bulk advective mixing (BAM) model has been implemented into the EPANET 2.0 software. The augmented version, EPANET-BAM, allows predictions of water quality and solute transport that are based on either complete or incomplete mixing at cross junctions. The features and applications of EPANET-BAM are identical to EPANET 2.0. The only change is the addition of a mixing parameter that linearly scales the predicted results between complete ($s = 1$) and incomplete ($s = 0$) mixing.

4. STEADY-STATE NETWORK MIXING STUDIES

Chapters 2 and 3 summarize the results for mixing studies in a single joint. The subsequent chapters of this report are devoted to multi-joint studies. Earlier effort in this project was devoted to simple and idealized geometries, the 3x3 network is one which illustrates the propagation on incomplete mixing in network of converging and diverging junctions. Prior study of a 3x3 network had been captured in SAND2005-6776 as well as in publications [refs].

This chapter summarizes the steady-state, multi-joint experiments that were conducted in 2007 and 2008. Some of experiments that were performed earlier are repeated due to add-on data acquisition features. More importantly, the earlier findings are further enhanced with new insights and additional sensitivity runs. The recent 3x3 network experiments have focused on the effect of the final effluent concentrations by modifying of the location of the outlets.

A set of experiments consisting of 22-node diamond network are also conducted in this study and presented in this chapter. These are important as this configuration measures the spatial decay of incomplete solute mixing in a consistent manner.

Some of the recent experimental data have been applied as validation data for EPANET-BAM code and the data-model comparison shows consistent improvement using bulk advective mixing modifications as seen in the single-joint runs.

4.1. EXPERIMENTAL SET-UP

The 3x3 network set up is only briefly described in this section for consistency. A more detailed description can be found in earlier SAND report [SAND2005-6776, Ho (2006) and Orear (2005)?]. The earlier and recent 3x3 network studies all have physical set up identical to the picture shown in **Figure 41**. Nine mixing joints are laid out in a checkerboard fashion.

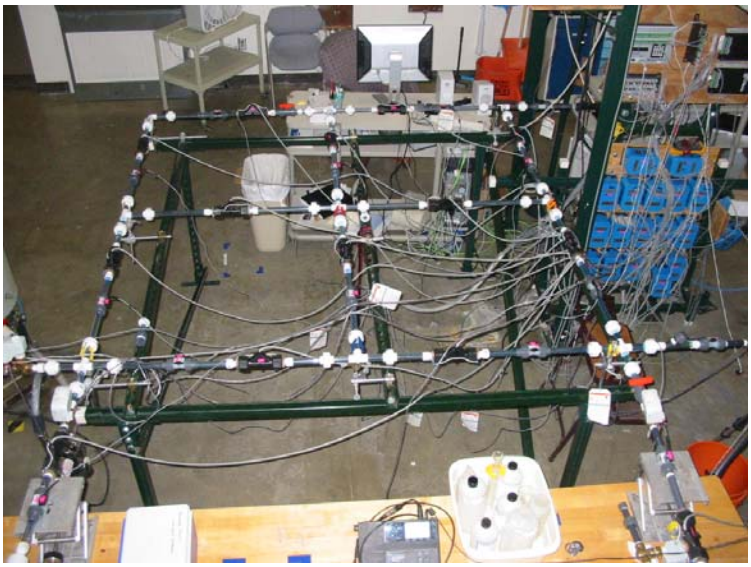

Figure 41. Physical set-up of the 3x3 network study.

Figure 42 shows a schematic of the layout and the locations of inlets and outlets. The clear fluid entering the system is often referred to as the ambient inlet flow. The more recent 3x3 network studies are fitted with additional water meters and conductivity probes, but probes are placed in identical locations. **Figure 42** and **Figure 42b** differs only in the numbering convention for probe identifications.

A 20:1 ratio (based on pipe diameter) was utilized for the experiments. A new model was built that had interchangeable segments. Both types of network experimental set-ups utilize 0.5 inch diameter clear PVC pipe segments. Each segment is three feet in length and contains either pipe only, pipe and a flow meter, or pipe and a conductivity meter. These variations supported quick modifications and calibration of meters. Measurements of salt concentration are inferred by the conductivity of fluid at segments throughout the network.

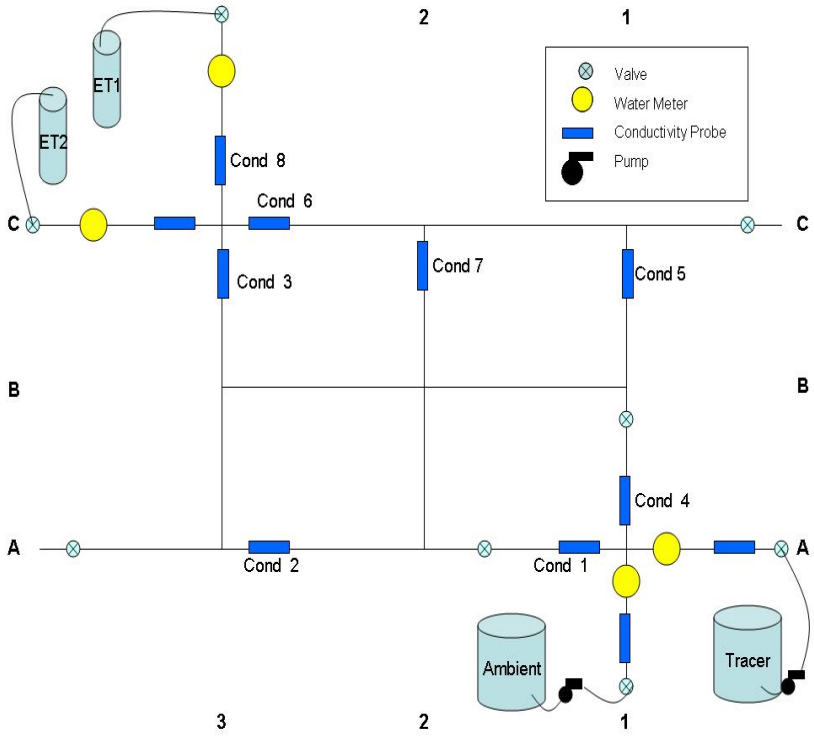

Figure 42a. 3x3 Network Sensor placement conducted in 2005 and 2006.

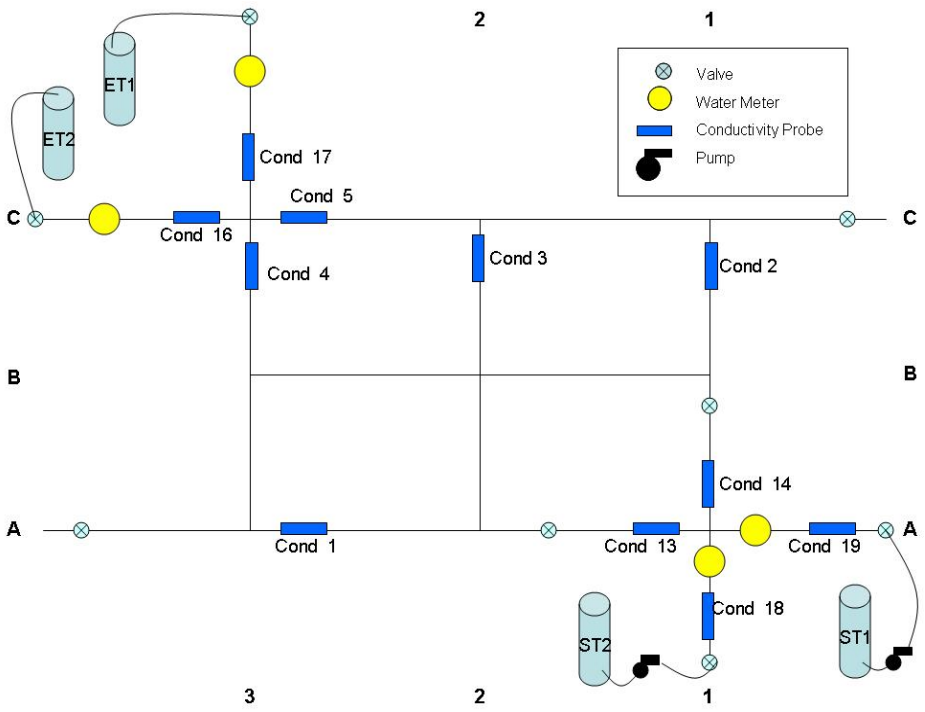

Figure 42b. 3x3 Flow Diagram and Labeling in 2007 and 2008 (ST1 and ST2 are supply tanks, ET1 and ET2 are effluent tanks).

Table 5 lists the conditions of tracer and ambient (clear fluid) inlets. Scenario 1 refers to the conditions at which the tracer inlet flow rate being greater than the ambient inlet flow while the opposite holds for Scenario 2.

Table 5. Summary of 3x3 Network Experimental Conditions

	Flow Rates (gpm)				Average Run Conditions			
Scenario Description	$Q_{A,IN}$	$Q_{T,IN}$	$Q_{A,OUT}$	$Q_{T,OUT}$	Reynolds Number			
					A-in	T-in	A-Out	T-out
Scenario 1	0.99	1.21	1.15	1.02	14,100	17,100	16,300	14,500
Scenario 2	1.58	0.86	1.21	1.21	22,400	12,200	17,300	17,200

4.2 Calibration & Experimental Procedures

Prior to running each experiment the network conductivity probes' calibration was verified by filling the system with ambient water and comparing the readings to a calibrated handheld conductivity meter. If any meter was off by more than 10%, it was recalibrated. Next, the system was filled with "tracer" water, which was water with a salt solution. Again, the network conductivity probes' calibration was verified by filling the system with ambient water and comparing the readings to a calibrated handheld conductivity meter. If any meter was off by more than 10%, it was recalibrated. Calibration curves and daily calibration checks were maintained on the laboratory computer for reference.

Early on, it was noticed that there was a constant offset between the network conductivity probes and the handheld. Recalibration did not fix this problem. Since the offset was constant and data were to be normalized, it was decided to check the calibration each time and to try to get all probes to read the same value, albeit different than the actual conductivity of the solution being measured. The measured difference was typically less than 10%, but was always less than 15%.

Water meters were calibrated after the network was built, and if any modification was made using a bucket and stopwatch method. Calibration curves and calibration checks were maintained on the laboratory computer for reference.

Regardless of the network set-up, each set of experiments was run in an identical manner. Three sets of steady state measurements were performed for each configuration (i.e. flow rate). The first run would also include a transient step where the system would first be filled with ambient water. Next pure tracer would be added to the system until steady state was reached. Finally, ambient water would be added to the system until steady state was reached. At least 10 minutes of data at steady state was gathered for the three experimental result runs.

Ambient water is tap water from the city of Albuquerque, with a conductivity near 500 μS/cm. Tracer water is ambient water with NaCl added to obtain a conductivity between 1,700-2,000 μS/cm.

All conductivity probes and water meters are connected to a data logger, which is connected to a desktop PC. The PC provides real time data, as well as storing for further analysis. Pressure is monitored via a manometer at the inlet end of the network; relative pressure readings are recorded for each run.

4.3 3x3 Network Studies

Since the new experimental set-up allowed for more data collection potential, the two scenarios are re-run to validate data obtained in 2005. **Figures 43 and 44** summarize the data from the original and new experiments. It can be seen that the EPANET program oversimplifies the mixing scenario. All points are considered to be at a normalized value of 0.56 in EPANET, with experimental normalized values ranging from 0.27 to 0.82.

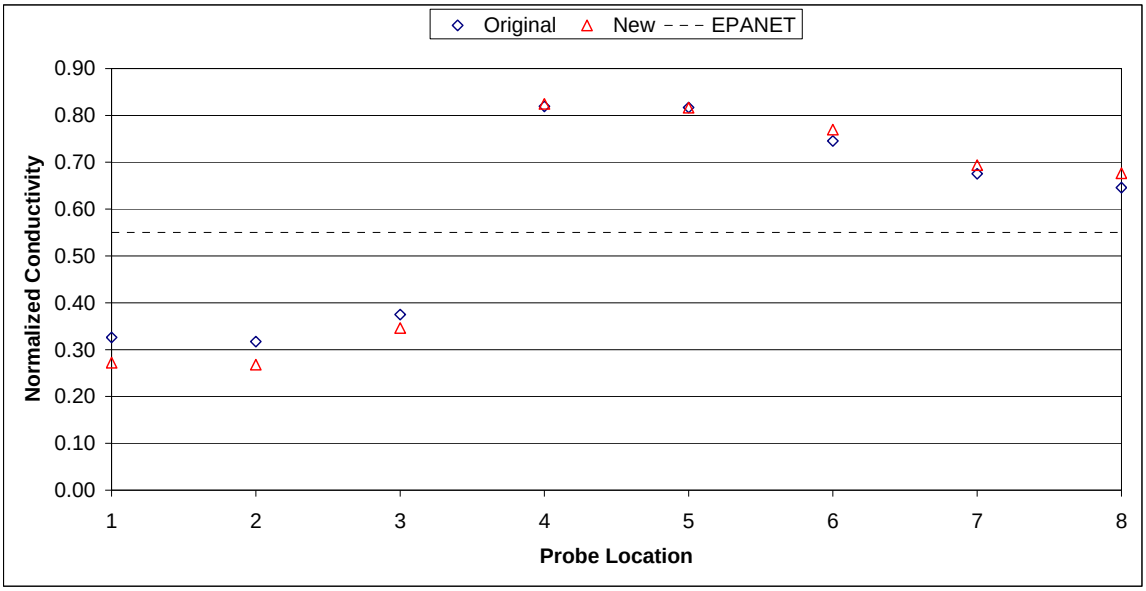

Figure 43. 3x3 Network Comparison of Ho (2006) and Current Data – Scenario 1.

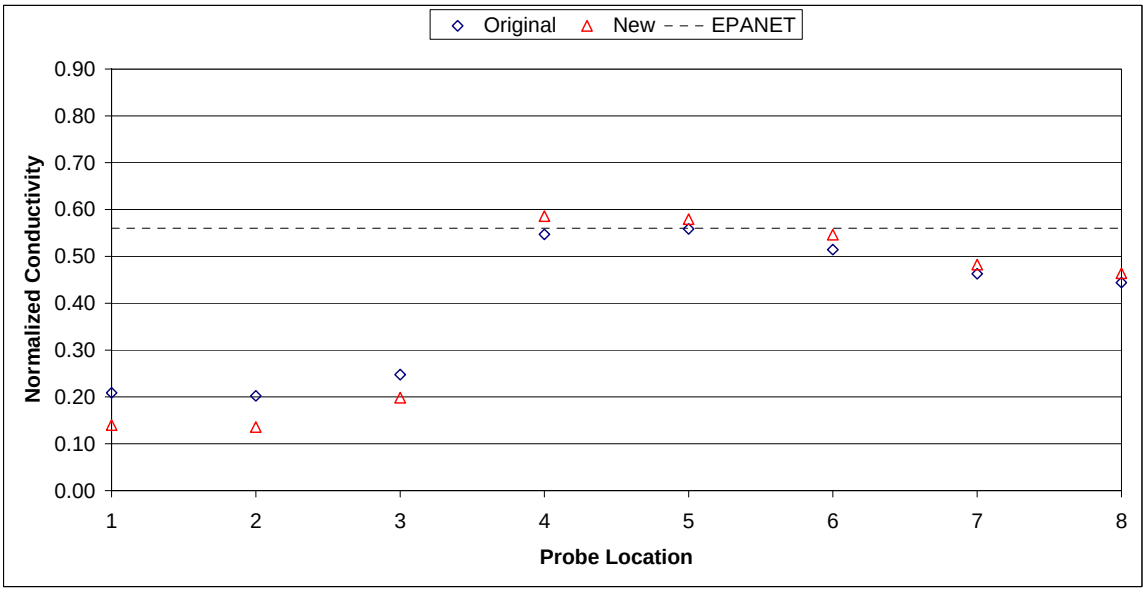

Figure 44. 3x3 Network Comparison of Ho (2006) and Current Data – Scenario 2.

Comparison to EPANET-BAM model.

Figure 45 and **Figure 46** below display one set of 3x3 network experimental results predicted results from EPANET-BAM simulated with the scaling factor, s, for all cross junctions set to be the same specified value. Compared to the complete-mixing assumptions, EPANET-BAM shows good agreement with the experimental data.

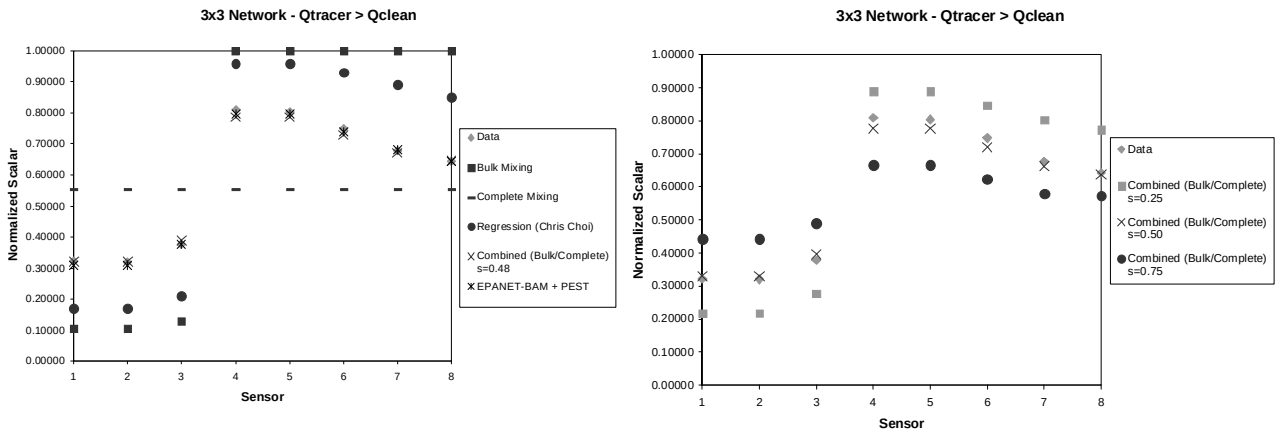

Figure 45. Comparison of 3x3 network, Scenario 1 between data and EPANET-BAM. The scaling factor, s, for all cross junctions set to be the same specified value.

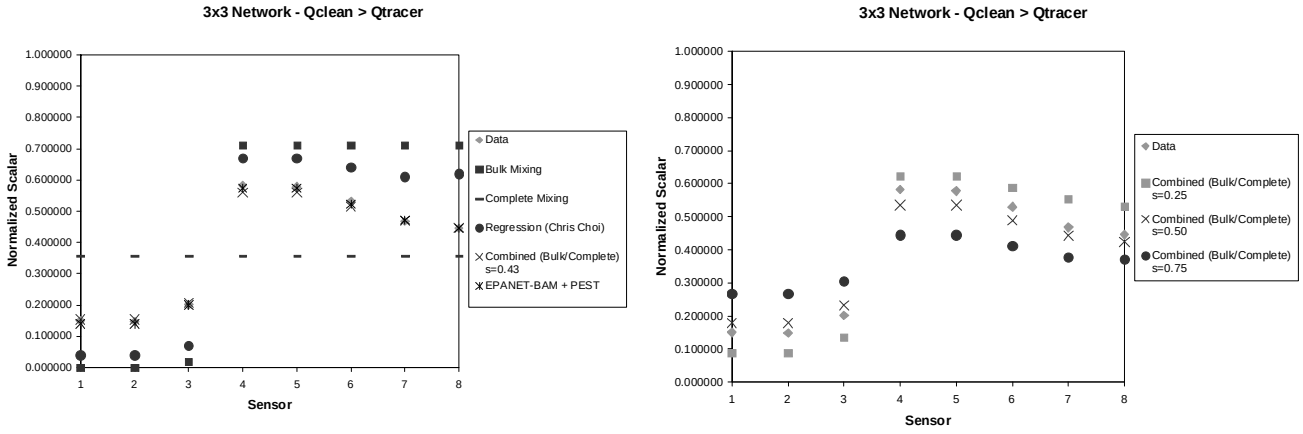

Figure 46. Comparison of 3x3 network, Scenario 2 between data and EPANET-BAM. The scaling factor, s, for all cross junctions set to be the same specified value.

4.4 Effect of Network Outlet Locations

The 3x3 Network experiments were repeated with different outlet locations in order to check for sensitivities of solute mixing within segments. A total of four modifications on the exit locations are conducted and show in **Figure 47**.

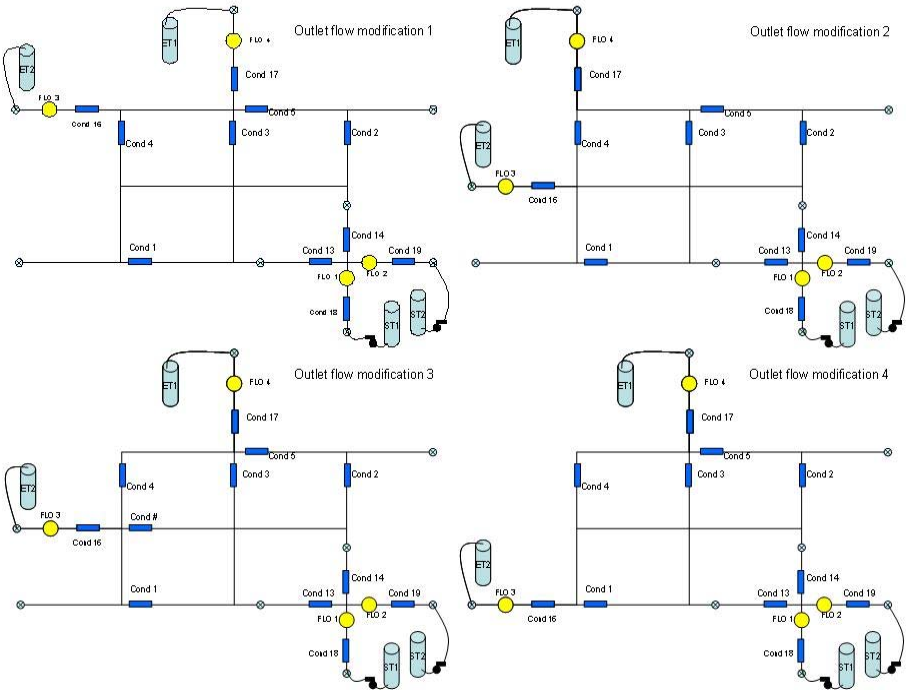

Figure 47. 3x3 Experiment Flow Diagram with Outlet Modifications.

The experimental runs are listed in **Table 3.2**. For each modification, both scenarios are run and the concentrations collected at points schematically shown in Figure 3.2.

Table 6. Summary of 3x3 Network Effluent Location Modifications – Run Conditions

	Flow Rates (gpm)				Re, Average Run Conditions			
Scenario Description	$Q_{A,IN}$	$Q_{T,IN}$	$Q_{A,OUT}$	$Q_{T,OUT}$	A-in	T-in	A-Out	T-out
Modification 1, Scenario 1	0.94	1.17	1.09	1.01	6700	8300	7700	7100
Modification 1, Scenario 2	1.56	0.86	1.45	0.95	11000	6100	10300	6700
Modification 2, Scenario 1	0.92	1.21	1.13	0.98	6500	8600	8000	6900
Modification 2, Scenario 2	1.57	0.85	1.43	0.97	11100	6000	10100	6800
Modification 3, Scenario 1	1.00	1.18	1.14	1.03	7100	8400	8000	7300
Modification 3, Scenario 2	1.61	0.82	1.44	0.98	11400	5800	10200	7000
Modification 4, Scenario 1	1.02	1.14	1.14	0.99	7200	8000	8100	7000
Modification 4, Scenario 2a	1.41	0.97	1.43	0.92	10000	6800	10100	6500
Modification 4, Scenario 2b	1.47	0.94	1.44	0.96	10400	6700	10200	6800

Comparison to EPANET model.

Figure 48 is an EPANET layout of the same 3x3 network, and the solute concentrations of the same probe locations are plotted with the experimental data in **Figure 49** (Scenario 1) and **Figure 50** (Scenario 2). It is important to note that the sampling locations are based on EPANET identifications; hence, **Figures 49 and 50** do not follow the identifications in **Figure 42**. As with previous experiments, there was poor correlation between EPANET model results and experimental results.

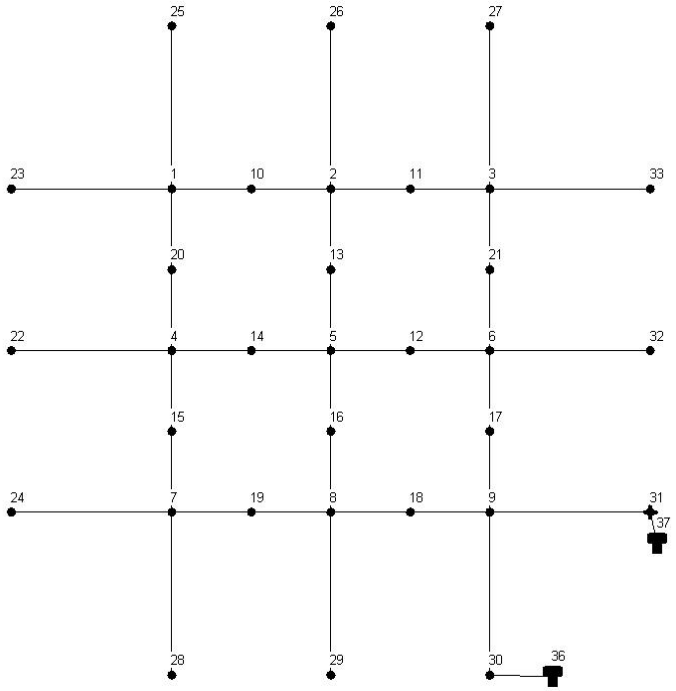

Figure 48. 3x3 EPANET Flow Network – Outlet Flow Modifications.

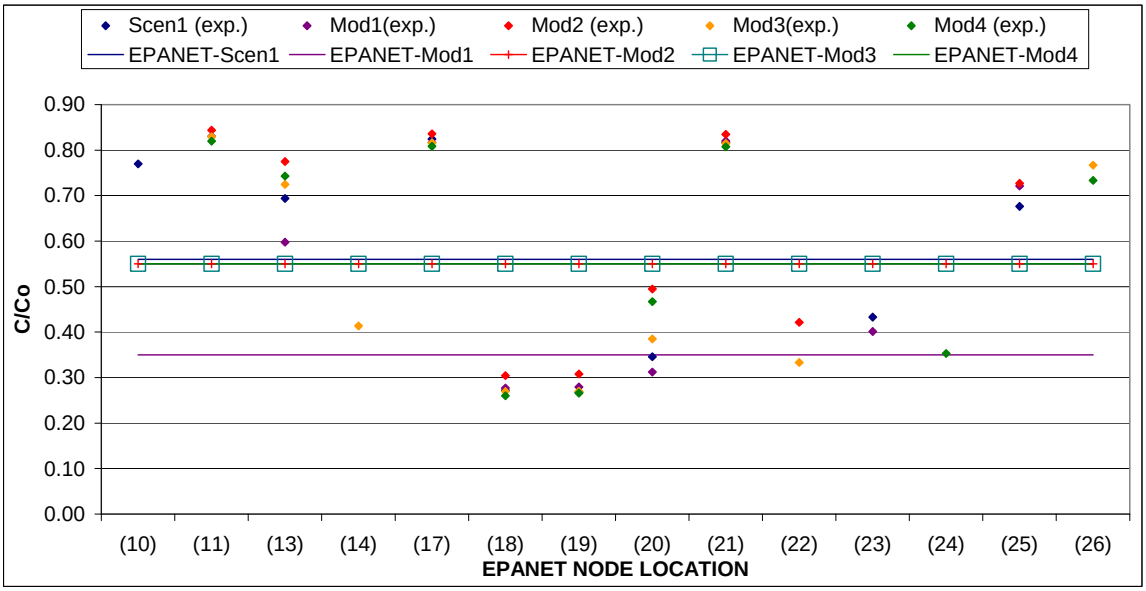

Figure 49. 3x3 Scenario 1 Network Data – Effect of Effluent Location.

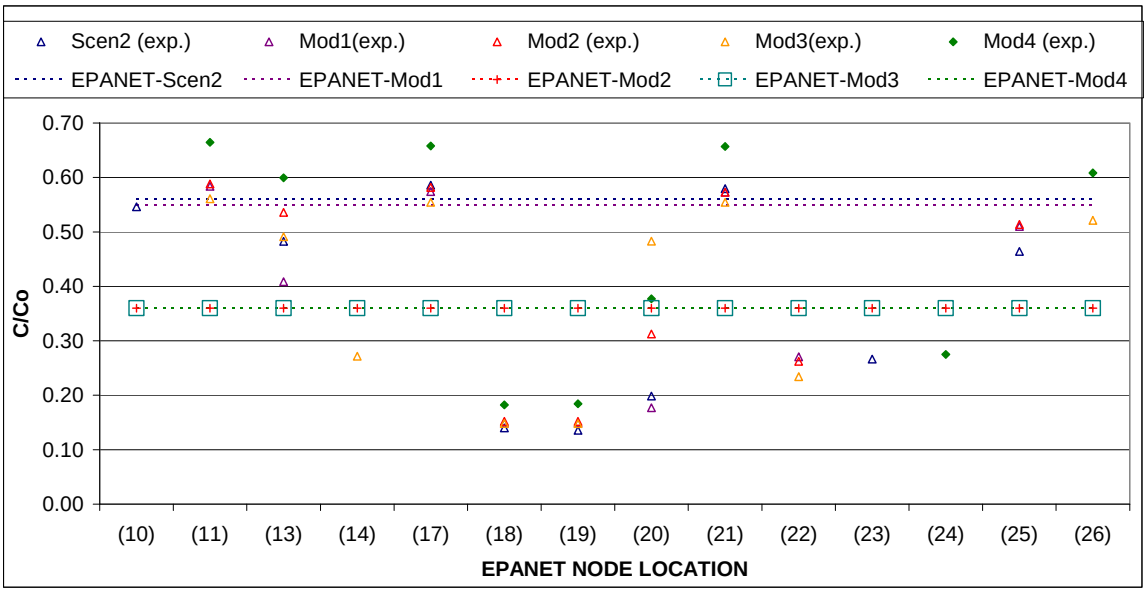

Figure 50. 3x3 Scenario 1 Network Data – Effect of Effluent Location.

Figure 51 shows averaged data for the normalized concentrations at all of outlet locations in the modifications and the original set-up. **Table 7** summarizes the effluent locations using **Figure 51** as the reference. There are some interesting features worth noting. In Mod-1, only the tracer outlet is moved closer to its inlet. This shift raises the tracer outlet concentration but does not cause a significant shift in recorded ambient outlet concentration, regardless of the scenarios. The same holds for Mod-2. In Mod-3 and Mod-4, when both tracer and ambient outlets are moved, the disparity in their concentrations widens even more. As the outlets are moved closer to the inlet junction, the tracer outlets (nodes 25 and 26) have higher normalized conductivity values and the ambient outlets (nodes 22-24) have lower normalized conductivity values.

Second, the standard deviation is larger for the scenario 1 set of data as compared to scenario 2. Not shown in Figure 51, the data points for scenario 1 exhibit higher standard deviation as outlet moves closer to inlet junction. In addition, the standard deviation increases for the scenario 1 sets as the outlets are moved closer to the inlet junction.

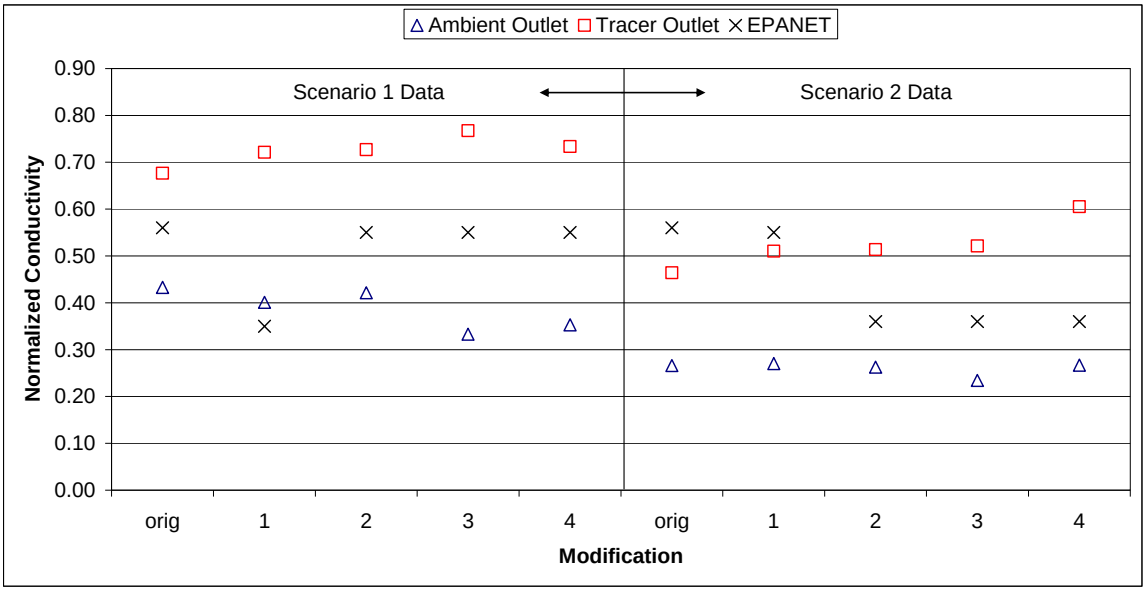

Figure 51. 3x3 Network Model Data – Effect of Effluent Location.

Table 7. EPANET 3x3 Network Outlet IDs based on Figure 48 for the Corresponding Experiments in Table 6.

	Locations	
Scenario Description	Tracer Out	Ambient Out
Scenario 1	25	23
Scenario 2	25	23
Mod 1, Scen 1	26	23
Mod 1, Scen 2	26	23
Mod 2, Scen 1	25	22
Mod 2, Scen 2	25	22
Mod 3, Scen 1	26	22
Mod 3, Scen 2	26	22
Mod 4, Scen 1	26	24
Mod 4, Scen 2	26	24

4.5 EPANET-BAM Analysis of 3x3 Network to Assess Impact of Contaminant Transport

The following example illustrates the use of EPANET-BAM and compares the results of the complete mixing model and the BAM model using a scaled replica of a laboratory network described in Ho et al. (2007). Steady-state contaminant transport through the network is simulated, and a hypothetical risk assessment is performed. Additional examples of transient transport and source detection can be found at www.sandia.gov/epanet-bam.

Problem Background

Consider a hypothetical sub-domain of a water distribution network shown in **Figure 52** below. The network consists of 12 neighborhoods. The network is supplied by two inlet pipes, *Clean Inlet* and *Contaminated Inlet*. Water leaves the network through two pipes, one leading to a *Reservoir* and the other to another *Outlet*. The boundary conditions are indicated in **Figure 52**. The neighborhood demands are negligible compared to the outflow of the network sub-domain.

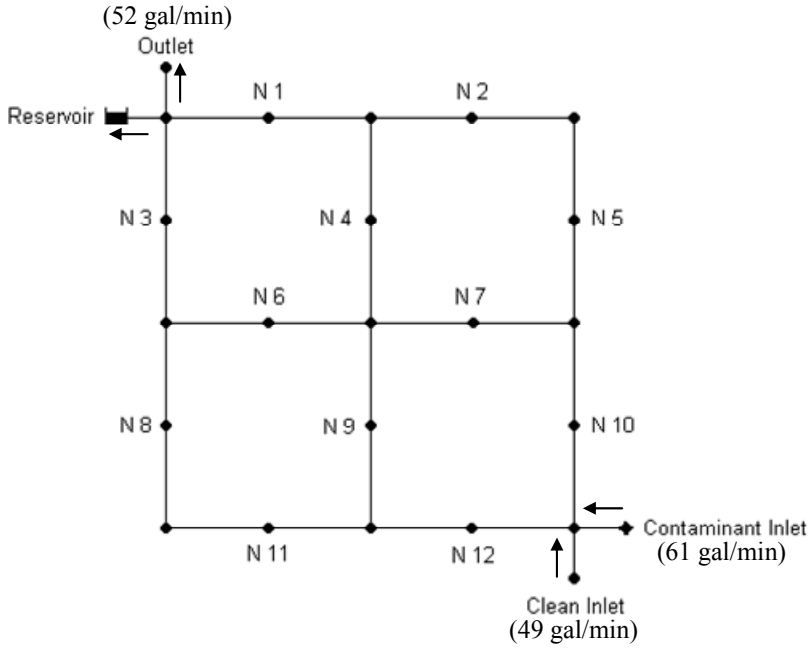

Figure 52. Example EPANET-BAM network model. Each connecting pipe is 150 ft in length and 8" in diameter. Chemical X enters through the Contaminant Inlet at a concentration of 1000 mg/L.

The objective of this example problem is to predict the concentration of Chemical X at each neighborhood after the contaminant has spread completely throughout the network, assuming (1) incomplete mixing (s = 0.5) and (2) complete mixing in the cross junctions. Because this example network is a scaled version of an actual laboratory experiment (Ho et al., 2006), results can be compared to laboratory measurements. In addition, assuming that each neighborhood is populated by 100 people, each of whom weighs 60 kg and consumes 2 L of water per day, we can predict the number of deaths that would occur in each neighborhood after one day if we assume that Chemical X has the hypothetical lethal-dose response curve shown in

.

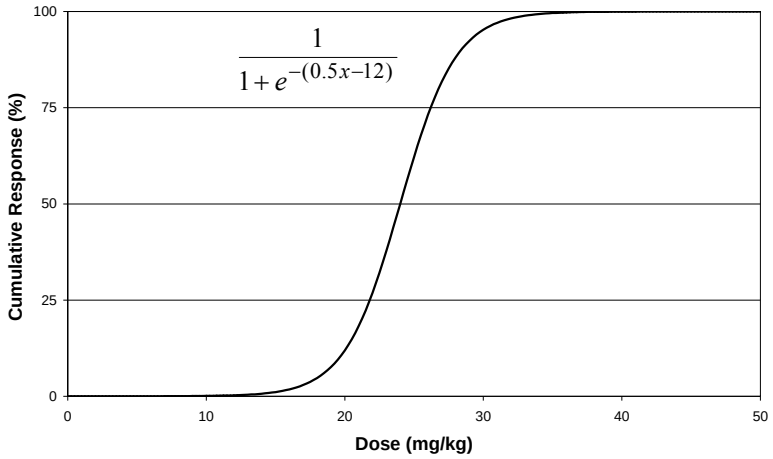

Figure 53. Hypothetical lethal-dose response curve for Chemical X.

EPANET-BAM Results

Figure 54 shows the results of EPANET-BAM assuming incomplete and complete mixing models. The assumption of complete mixing within cross junctions in this example yields uniform concentrations throughout the network. The assumption of incomplete mixing (s = 0.5) yields spatially variable concentrations throughout the network. The predicted concentrations are greater in the top-right half of the network as a result of the contaminant splitting off in that direction at each cross junction. Comparisons with the laboratory data (Ho et al., 2006) show that the results of the BAM model with incomplete mixing (s = 0.5) yield good matches with the experimental data, but the predictions assuming complete mixing do not capture the spatial variability (see **Figure 55**).

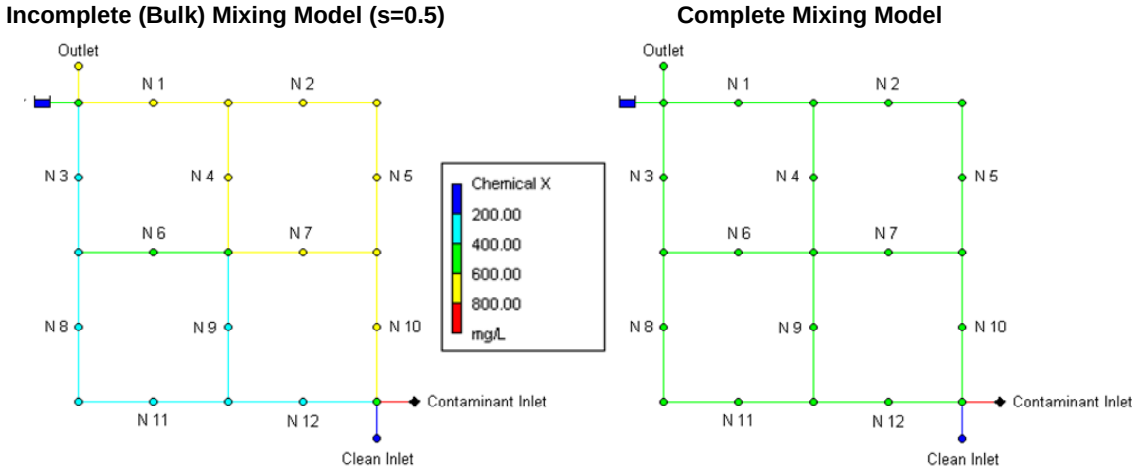

Figure 54. EPANET-BAM predictions of contaminant concentrations using incomplete (s = 0.5) and complete-mixing (s = 1) models.

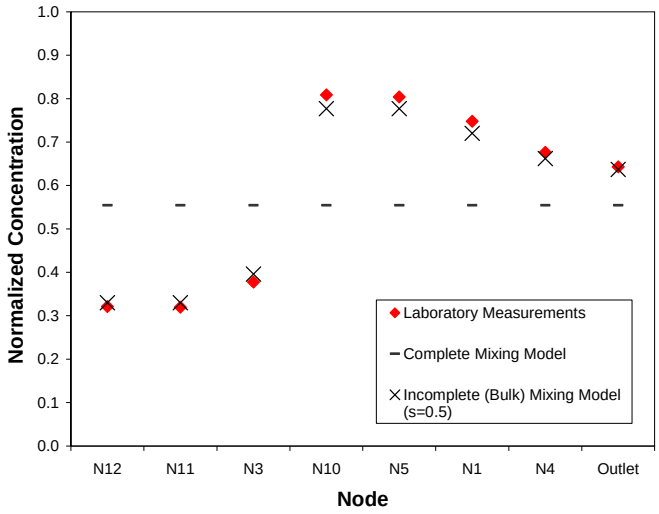

Figure 55. Comparison of EPANET-BAM predictions with experimental data (Ho et al., 2006) at selected locations where samples were taken.

The simulated concentrations are used to predict the number of deaths resulting from the consumption of contaminated water after one day assuming the hypothetical lethal-dose response curve shown in **Figure 52**. **Table 8a** and **Table 8b** show the results of the risk assessment assuming incomplete and complete mixing. Because of the higher concentrations predicted in the model assuming incomplete mixing, significantly more deaths are predicted. It should be noted, however, that the lethal-dose response curve was designed to illustrate the potential differences between the two models given the disparity in predicted concentrations. If the hypothetical lethal-dose response curve was shifted to the left, more deaths may have been predicted by the complete-mixing model (i.e., if the threshold lethal dose was less than the uniform dose predicted by the complete-mixing model but greater than the minimum dose predicted by the incomplete-mixing model).

Table 8a. Predicted deaths in each neighborhood assuming incomplete mixing (*s* = 0.5).

Neighborhood	Concentration (mg/L)	Mass of X Ingested per Person per Day (mg)	Dose (mg/kg)	Predicted Mortality (%)	**Predicted Deaths**
N1	722	1443	24.1	50.7%	**50**
N2	777	1555	25.9	72.2%	**72**
N3	388	775	12.9	0.39%	**0**
N4	666	1332	22.2	28.9%	**28**
N5	777	1555	25.9	72.2%	**72**
N6	443	886	14.8	0.98%	**0**
N7	777	1555	25.9	72.2%	**72**
N8	332	664	11.1	0.15%	**0**
N9	332	664	11.1	0.15%	**0**
N10	777	1555	25.9	72.2%	**72**
N11	332	664	11.1	0.15%	**0**
N12	332	664	11.1	0.15%	**0**
				Predicted Death Toll:	**366**

Table 8b. Predicted deaths in each neighborhood assuming complete mixing (*s* = 1).

Neighborhood	Concentration (mg/L)	Mass of X Ingested per Person per Day (mg)	Dose (mg/kg)	Predicted Mortality (%)	**Predicted Deaths**
N1	555	1109	18.5	5.97%	**5**
N2	555	1109	18.5	5.97%	**5**
N3	555	1109	18.5	5.97%	**5**
N4	555	1109	18.5	5.97%	**5**
N5	555	1109	18.5	5.97%	**5**
N6	555	1109	18.5	5.97%	**5**
N7	555	1109	18.5	5.97%	**5**
N8	555	1109	18.5	5.97%	**5**
N9	555	1109	18.5	5.97%	**5**
N10	555	1109	18.5	5.97%	**5**
N11	555	1109	18.5	5.97%	**5**
N12	555	1109	18.5	5.97%	**5**
				Predicted Death Toll:	**60**

4.6 Diamond Network Experiments

Data obtained from the 3x3 experiments seemed to indicate that there might be an optimum number of mixing points at which perfect mixing occurs. A set of six diamonds in series was built using the same equipment as the 3x3 to determine the amount of mixing points necessary to get perfect mixing as calculated in the current EPANET program.

The data from each of the experiments were difficult to interpret, as the conductivity offset may have been more noticeable. That is to say, if an ambient probe was reading high and a tracer probe reading low, the difference is artificially lower. One can see general trends, in that the standard of deviation decreases with increased mixing. All experiments had normalized outlet concentrations close to the perfect mixing results shown from EPANET. In addition, the turbulent experiments tended to approach perfect mixing slightly faster than the others. These results are shown in **Figures 11-13**.

The diamonds experiment involved a set of six diamonds in series as shown in **Figure 56**. This is followed by **Table 9** for the experimental runs for the network. Scenario 1 is Tracer flow greater than Ambient while the Ambient flow is greater than the Tracer flow is shown in Scenario 2.

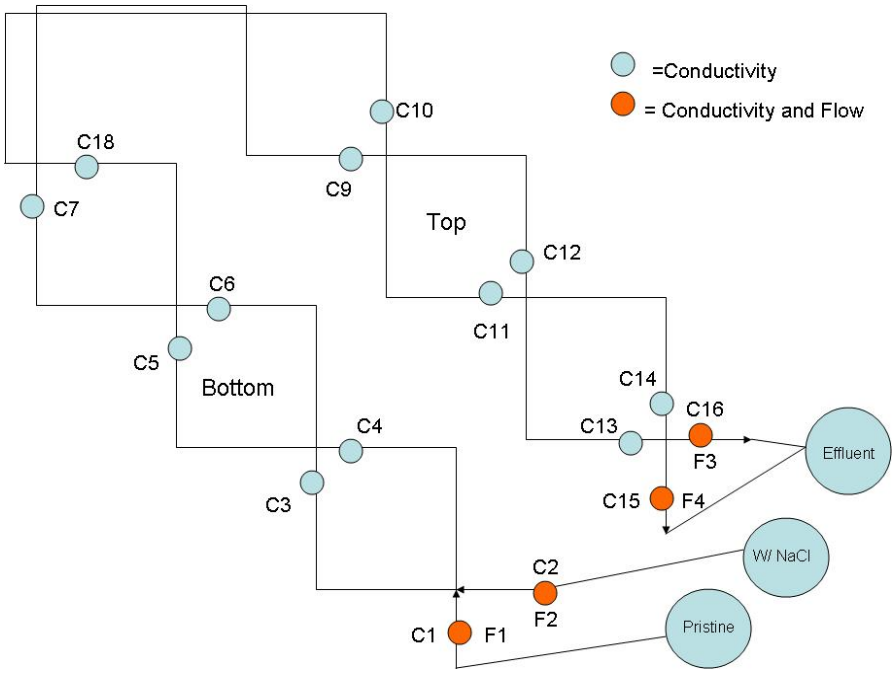

Figure 56. Diamonds Flow Diagram.

Table 9 Diamonds Data – Original Runs

	Flow Rates (gpm)			
Scenario Description	$Q_{A,IN}$	$Q_{T,IN}$	$Q_{A,OUT}$	$Q_{T,OUT}$
Diamonds, Equal (Re=2300)	0.40	0.40	0.40	0.40
Diamonds, Equal (Re=3000)	0.55	0.55	0.55	0.55
Diamonds, Equal (Re=5000)	0.70	0.70	0.70	0.70
Diamonds, Equal (Re=7000)	1.00	1.00	1.00	1.00
Diamonds, Equal (Re=10000)	1.50	1.50	1.50	1.50
Diamonds, Scen1 (lam)	0.20	0.40	0.20	0.40
Diamonds, Scen1 (lam)-equal out	0.20	0.40	0.30	0.30
Diamonds, Scen1 (trans)	0.40	0.60	0.40	0.60
Diamonds, Scen1 (trans)-equal out	0.40	0.60	0.50	0.50
Diamonds, Scen1 (turb1)	0.50	1.00	0.75	0.75
Diamonds, Scen1 (turb1)-equal out	0.50	1.00	0.75	0.75
Diamonds, Scen1 (turb1)	0.50	1.00	0.75	0.75
Diamonds, Scen1 (turb2)	0.75	1.50	1.13	1.13
Diamonds, Scen1 (Re=turb3)	1.00	2.00	1.50	1.50
Diamonds, Scen2 (lam)	0.40	0.20	0.40	0.20
Diamonds, Scen2 (lam)-equal out	0.42	0.20	0.30	0.30
Diamonds, Scen2 (trans)	1.00	0.50	0.75	0.75
Diamonds, Scen2 (trans)-equal out	0.60	0.40	0.50	0.50

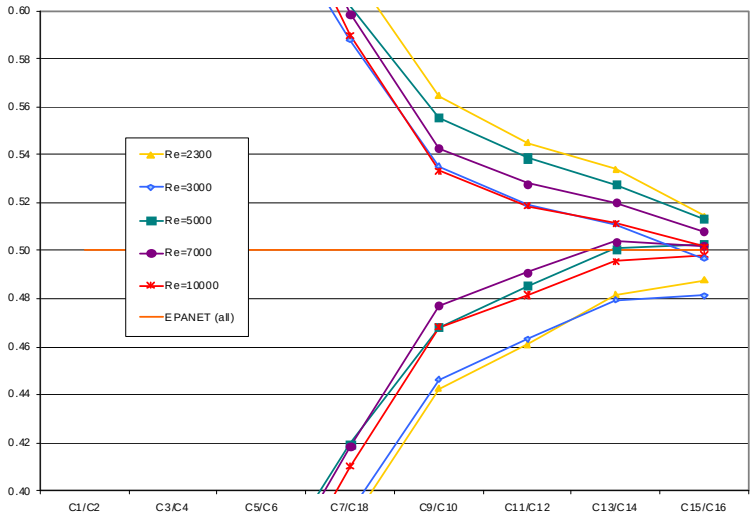

Figure 57. Comparison of equal inlet flow rate experiments (averaged data).

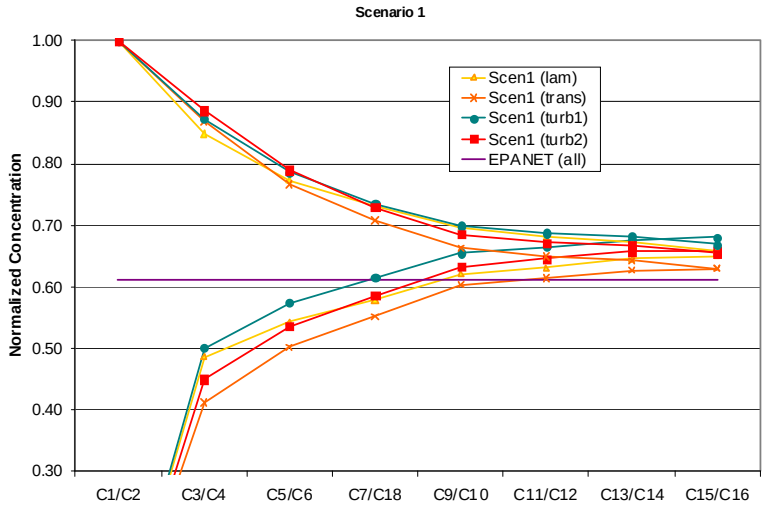

Figure 58. Normalized Concentration for Scenario 1, Diamond Network Runs.

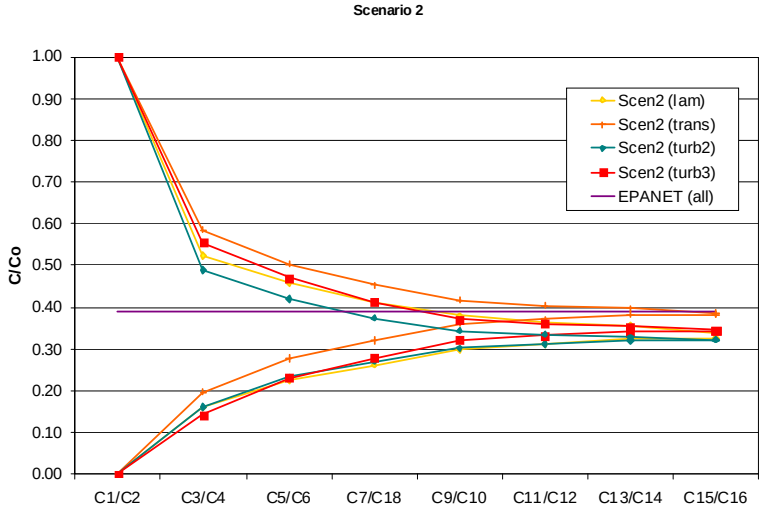

Figure 59. Normalized Concentration for Scenario 2, Diamond Network Runs.

Diamond Data Reruns

Some of the diamond network runs were repeated due to unequal outflows. These are shown with highlights in Table xx. However, the re-runs yielded no new information, and the results were almost exactly what was found with uneven outflows.

Comparison to EPANET-BAM model.

Figure 13 below shows the 'Diamond Network' as depicted in EPANET. The numbered junctions represent concentration sensors, whose readings are compared to the predictions of the various mixing models in **Figure 14**.

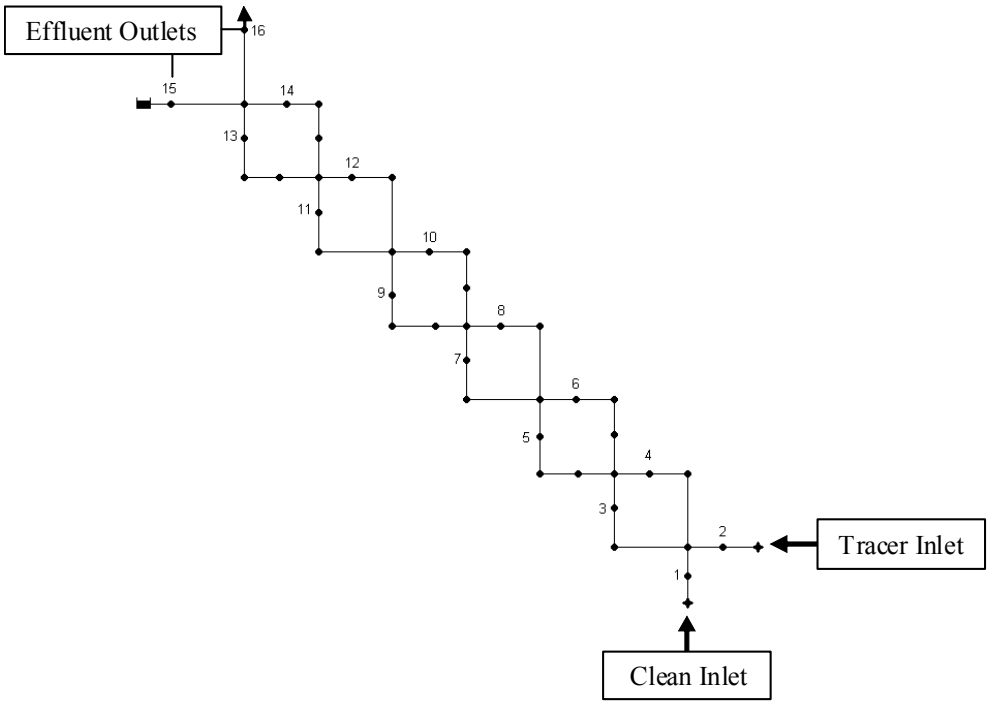

Figure 60 – EPANET diagram of the diamond experiments.

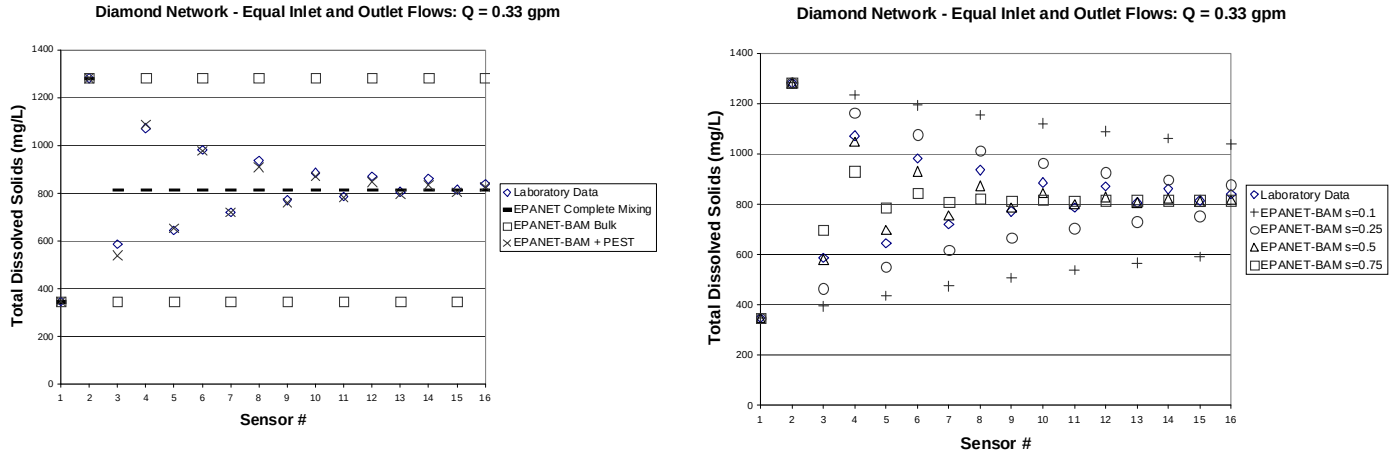

Figure 61 – EPANET and EPANET-BAM results compared to data.

4.7 Summary

This chapter is devoted to experimental and EPANET-BAM studies of pipe networks. Overall, results for the multi-joint experiments have been consistent with single-joint data when the outlet concentrations are modeled with EPANET-BAM. The validation results for single-joint data are presented in Chapter 3.

- Network results for 3x3 network, diamond network are presented in details here. Sensitivities of the incomplete mixing relative to the outlet location, Reynolds numbers are investigated for the 3x3 network. None of the variant flow scenarios approach complete-mixing limit, and EPANET-BAM improves the predictability of solute distribution.

- Diamond network results show approximately three divergent-convergent cycles to transition from incomplete to complete solute mixing.

- A risk assessment example was provided that illustrated the potential differences between network models that assume complete versus incomplete mixing. Spatial variability in the concentrations was not predicted by the complete mixing model, and subsequent risk assessments resulted in significant differences. Because pipe conditions and junction configurations that impact mixing can be highly uncertain in water distribution networks, we recommend conducting simulations using both complete ($s = 1$) and incomplete ($s = 0$) mixing models to provide bounding scenarios for risk assessments.

5. COMBINED NETWORK-TANK EXPERIMENTS

Based on extended experience with single-joint, tank, and network pipeline experiments, this research concludes with combined pipeline-tank experiments that assist our understanding of contaminant transport in a real distribution system. An illustrative example of how modeling is used for tracking the source of contaminant is the *Salmonella* outbreak in Gideon, Missouri in December, 1993 (Clark et al., 1996). The causal analysis carried out by the EPA had relied on limited assay samples and anecdotal descriptions over an extended response time. EPANET was also used to simulate transport of contaminated water in an analysis for the Gideon outbreak (Chandrasekaran, 2006).

The last phase of this project focuses on configurations that are challenging but realistic. This chapter describes two aspects of this work: dynamic mixing in storage tank and dynamic mixing in combined network-tank system. Characterization of dynamic mixing in a single storage tank is required before combining itself with a pipeline network. The contaminant evolution in a combined network-tank system is also studied and summarized in this chapter.

5.1 Storage tank Characterization

Unlike solute mixing in a single joint and pipeline networks, experimental and theoretical studies that involve mixing in storage tanks have been developed and well documented (Mays, 2000; Grayman et al., 1999). Mixing considerations in storage tanks have been important in the designs of water distribution systems because the potential variability in water quality. Poor mixing that does not allow sufficient disinfection of water will result in non-compliance and health threats. There have been different equations to describe mixing times based on geometries of the tank and the momentum of inlet fluid, which has been summarized nicely by Grayman in 1999.

Table 10. Mixing time for storage tanks

Investigators	Formula	Constant
Fossett & Prosser	$\frac{KD^2}{M^{0.5}}$	$K = 8$
Van de Vusse	$\frac{KD^2}{M^{0.5}}$	$K = 9$
Okita & Oyama	$\frac{KH^{0.5}D^{1.5}}{M^{0.5}}$	$K = 4.9$ for Reynold > 5,000
Fox & Gex	$\frac{KH^{0.5}D}{\mathrm{Re}^{0.17}M^{0.67}g^{0.17}}$	K depends on units

D = tank diameter
M = inlet momentum = velocity x flow
H = water level
Re = Reynolds number

g = gravitational constant

Furthermore, based on dimensional analysis, one can scale up storage tanks (with no density difference between inlet jet and tank) to any size based on model tank results (Roberts, 2005).

One way of obtaining mixing time in a storage tank is by coefficient of variation (COV), defined as the standard deviation of the concentrations in the tank divided by their mean value. Such time is recorded when COV falls reaches 10%.

A tank of 100-gallon by volume is used in this study for characterization to check for consistency with the correlations. Mixing data in different relative inlet and outlet flows are recorded to understand the internal mixing characteristics. This is tested against the tank model within EPANET.

5.1.1 Experimental Set-up

The basic set-up of this experiment consists of two connected water tanks, as shown in **Figure 62**. The first tank is used for holding and distributing the saline water that pumps into the second tank which is used for the dynamic mixing. The two tanks are 100-gallon polyurethane tanks that are separated 8' from each other. A Dayton 4TU19 pump is used to pump water from the saline tank through a flow meter, a conductivity probe and a series of regulating valves into the main mixing tank.

Figure 62 - Two-tank fill drain cycle set-up.

As schematically shown in **Figure 63**, inside of the mixing tank, there are three hanging conductivity probes that are attached and wired into the data logger. This is similar to the set up described previously by Grayman (1999). Additionally, there are three hanging handheld

conductivity probes that are each situated right next to a data logger probe making a pair of probes. The bottom pair of probes hangs 1 ½" from the bottom of the tank, the next pair hangs 7" from the bottom of the tank and the highest probe hangs 13" from the bottom of the tank.

The two lowest handheld probes are Hach SensION 5 handheld probes and the highest probe is the Orion Model 150 handheld probe. All of the data logger probes are Orion CDE1201 electrodes. After the water mixes in the mixing tank, it leaves via an outlet pipe that again passes through a flow meter, a conductivity probe and a series of regulating valves. This outlet flow is also powered by a Dayton 4TU19 pump. The mixed outlet water is pumped directly into the drain. All of the Flow meters are hooked into the data logger along with the In-line conductivity probes. The Datalogger collects data directly into the computer. The data logger is a Campbell Scientific CR23x Micrologger.

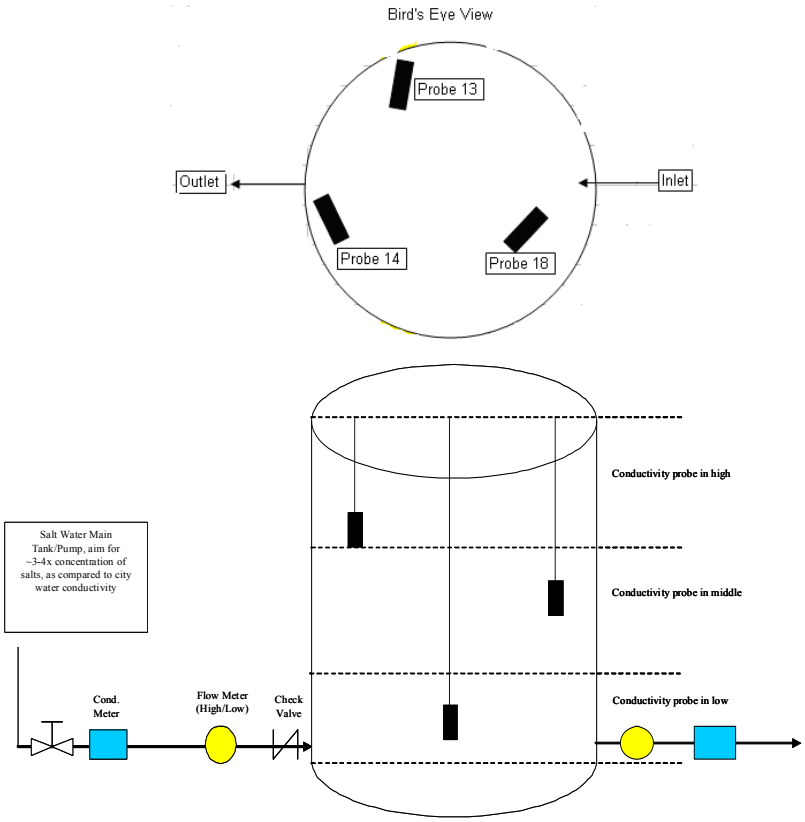

Figure 63 - 100-gallon storage tank configuration. A 12 mm pipe diameter is used for both inlet and outlet pipes.

At the start of the each experiment, both handheld and data-logger conductivity probes are calibrated against a standard solution (1500 µs). The tracer tank is then spiked with NaCl until it reaches between 1750µs and 1800 µs. The mixing tank is filled to its initial level according to the experimental conditions and spiked with NaCl until it reaches ~800µs. It was found during earlier experimentations that higher initial salt concentrations are less subject to data drift and noise.

5.1.2 Storage Tank Dynamic Mixing Scenarios

Six sets of experiments labeled A through F are conducted for dynamic mixing in single tank. These are conditions that will likely be encountered in the network, and the goal is to understand whether well-mixed conditions are met with different fill-drain cycles.

The first set (set A) is specific to assessing the minimal characteristic mixing time for well-mixed condition as provided in tank mixing guideline. The remainder five sets the concentration evolution of the probes in the tank. In cases B and C, where influent is greater than the effluent flow, the data are recorded as soon as the tank fills to 900mm. In cases E and F, the tank initially fills to 900mm before data are recorded.

Experiments:

A. Influent only – Measure concentration in the tank as a function of time.

Experiment	**1**	**2**	**3**	**4**
Influent FR (L/min)	2	6	2	6
Initial Height (mm)	200	200	600	600
Final Height (mm)	900	900	900	900

B. Effluent ~ 10% of Influent

Experiment	**1**	**2**	**3**	**4**
Influent FR (L/min)	2	6	2	6
Effluent FR (L/min)	0.2	0.6	0.2	0.6
Initial Height (mm)	200	200	600	600
Final Height (mm)	900	900	900	900

C. Effluent = ~ 50% of Influent

Experiment	**1**	**2**	**3**	**4**
Influent FR (L/min)	2	6	2	6
Effluent FR (L/min)	1	3	1	3
Initial Height (mm)	200	200	600	600
Final Height (mm)	900	900	900	900

D. Effluent = Influent

Experiment	**1**	**2**	**3**	**4**	**5**	**6**
Influent FR (L/min)	2	6	2	6	2	6
Effluent FR (L/min)	2	6	2	6	2	6
Initial Height (mm)	200	200	600	600	900	900

E. Influent = 50% Effluent

Experiment	**1**	**2**	**3**	**4**
Influent FR (L/min)	1	3	1	3
Effluent FR (L/min)	2	6	2	6
Initial Height (mm)	900	900	900	900
Final Height (mm)	200	200	600	600

F. Influent = 10% Effluent

Experiment	1	2	3	4
Influent FR (L/min)	0.2	0.6	0.2	0.6
Effluent FR (L/min)	2	6	2	6
Initial Height (mm)	900	900	900	900
Final Height (mm)	200	200	600	600

5.1.3. Dynamic Characteristics

One estimates the contact time (CT) in a tank during delivery by its hydraulic detention time multiplied by a factor. In a poorly mixed set-up, like a clearwell that have no baffles, the factor can be as low as 0.1. In a perfectly mixed storage tank, the CT is equivalent to the detention time, or the factor is 1.0 [Renner, 1990]. The accuracy of CT is important because it takes time for chlorine to achieve certain disinfection goal mandated by the EPA guideline. For example, *Giardia* removal must be 99.9% effective and one calculates the time it takes for chlorine (of certain residual concentration in the network) to effectively remove the required amount. The range is 10% for a low mixing clearwell to 30% for a single pipe inlet to 100% for a plug-flow system. While the scenarios for this study are mere characterization and do not attempt to reach a contact time, the guidelines illustrate the wide range variability in CT in storage tank and the importance of experimental validation.

Figure 64 shows the conductivity response as a function of time for the three probes in Experiment 1. The different response curves reflect relative inlet to outlet flows. Probe 13 is located at the bottom of the tank near inlet pipe; probe 14 is located in the middle while probe 18 is located near the top of the tank. Probe 18 responded partially in experiments where the level of fluid did not reach the probe until later in the filling experiments. During the draining experiments, the probe did not react to varying concentration either.

Figure 65 to Figure 67 show the results for sets 2 through 4 of the tank characterization experiments. The data show transient evolutions of salt solution mixing in the tank. In all three probes, the slopes are higher during filling experiments than draining experiments, indicating better mixing when the inlet flow is higher than the outlet flow. The only difference between set 1 and set 3 and between set 2 and set 4 is in the initial tank level, and this impacts the time-to-fill/time-to-drain. The dynamics in the data show more dampened slope in set 3 compared to set 1, indicating poorer mixing due to higher initial/final tank level. Similarly, the data between set 2 and set 4 show poorer mixing with higher initial tank level. Differences in probe readings are small despite different locations in the tank. Not shown, the data from sets 5 and 6 have no change in the salt concentration, indicating poor mixing.

Using the formula defined by **Table 10**, the mixing times can be calculated for this experiment, which is shown in Table y. The correlations show mixing times well beyond our experimental window with no outlet flow.

Table 11 Mixing times calculated based on different formula given in Table 10.

Inlet flow (L/min)	2	6	1	3	0.2	0.6
M (m^4/min/min)	1.01E-05	9.06E-05	2.52E-06	2.27E-05	1.01E-07	9.06E-07
Mixing time in minutes @ H= 900(mm), Okita & Oyama	857.97	285.99	1715.94	571.98	8579.68	2859.89
Mixing time in minutes @ H= 600(mm), Okita & Oyama	700.53	233.51	1401.06	467.02	7005.28	2335.09
Mixing time in minutes @ H= 200(mm), Okita & Oyama	404.45	134.82	808.90	269.63	4044.50	1348.17
Mixing time (Van de Vusse)	1434.61	478.20	2869.21	956.40	14346.06	4782.02
Mixing time (Fossett & Prosser)	1275.21	425.07	2550.41	850.14	12752.05	4250.68

While our experimental results indicate the salt concentrations in the tank not reaching the tracer tank values during the experiments, by linear extrapolation of the slopes, the time to arrive at tracer concentration in all of our filling experiments (i.e. inflow>outflow) is much shorter than the values calculated in Table y.

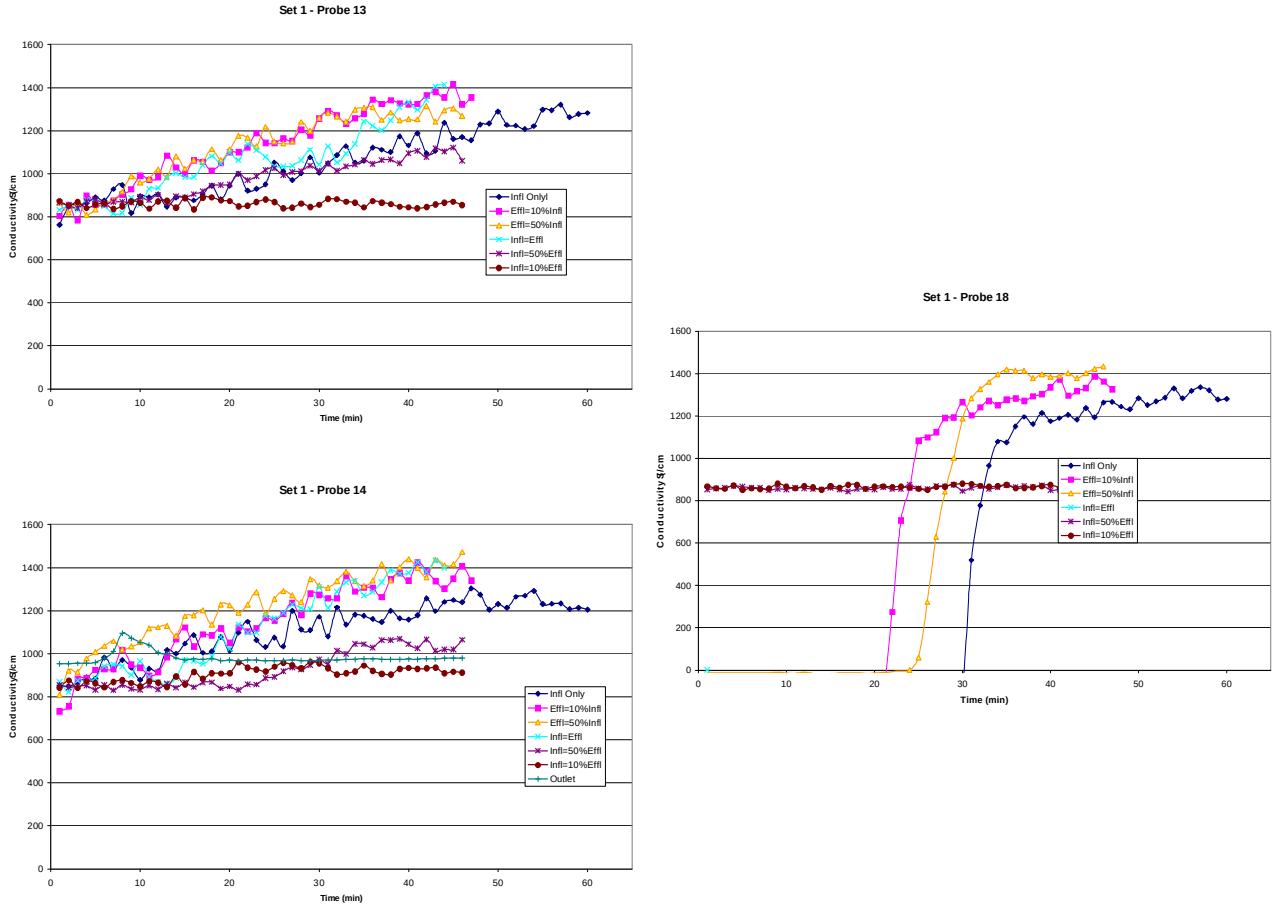

Figure 64 – Set 1 experiments showing the conductivity response of all three probes in the storage tank.

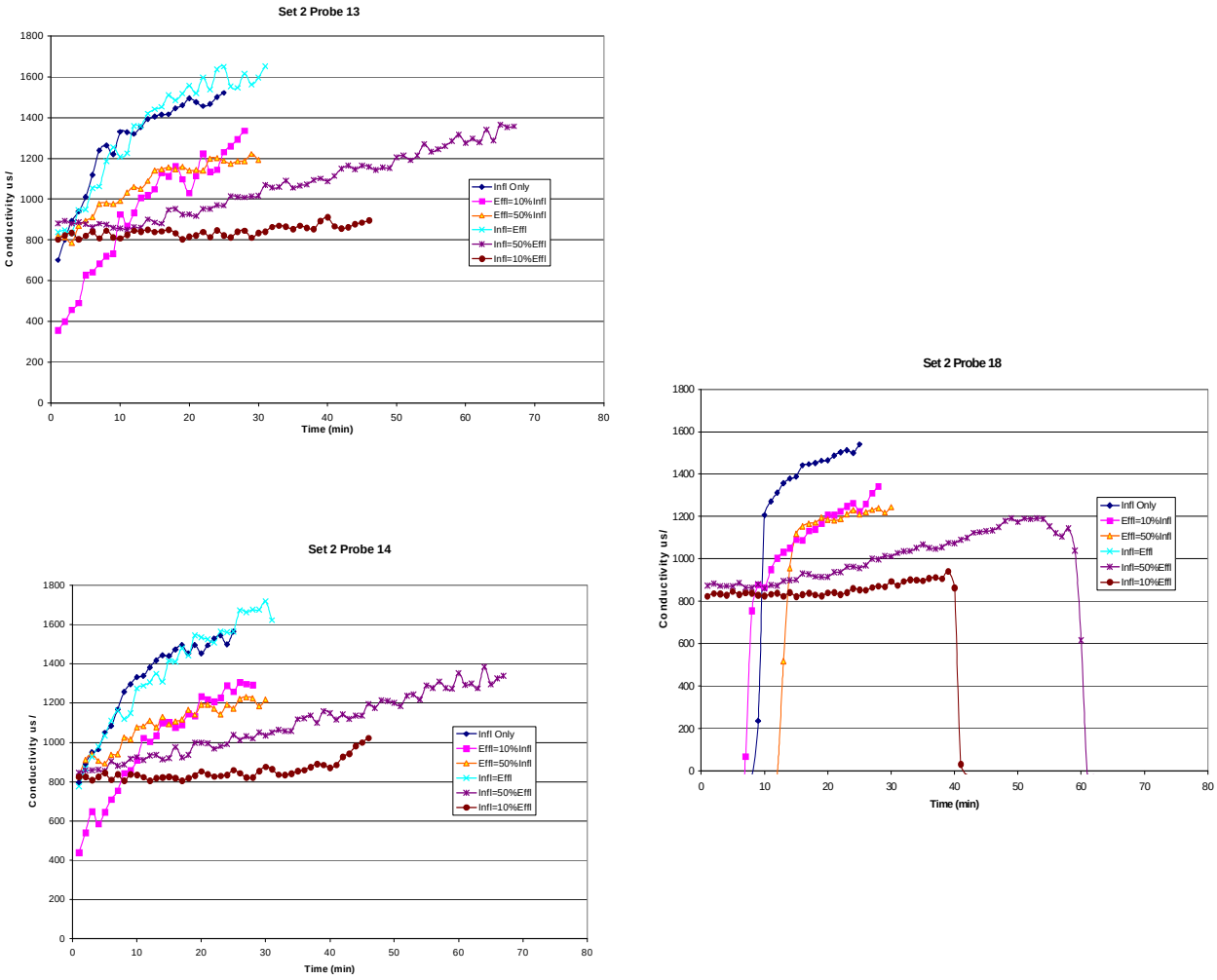

Figure 65 – Set 2 experiments showing the conductivity response of all three probes in the storage tank. Specifically, case B was calibrated against blanks that registered 400 µs

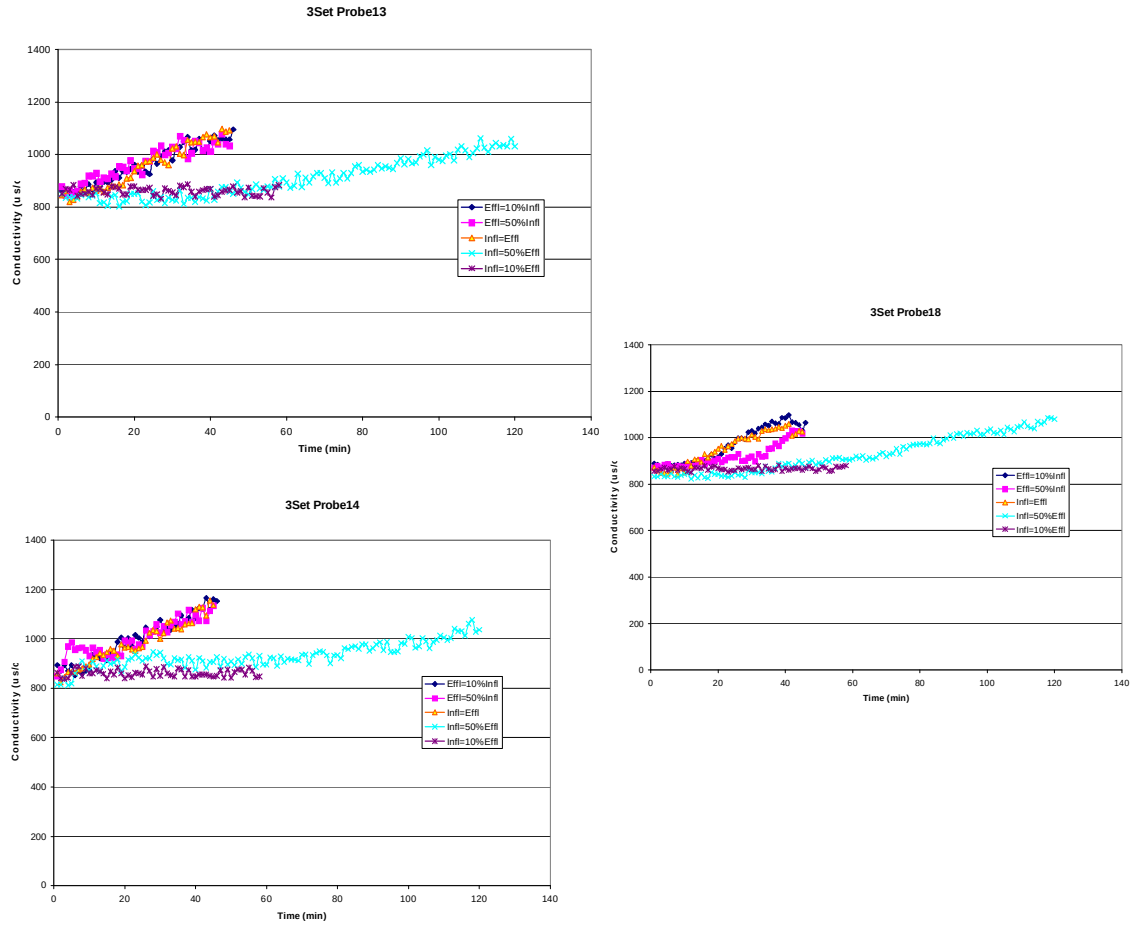

Figure 66 – Set 3 experiments showing the conductivity response of all three probes in the storage tank.

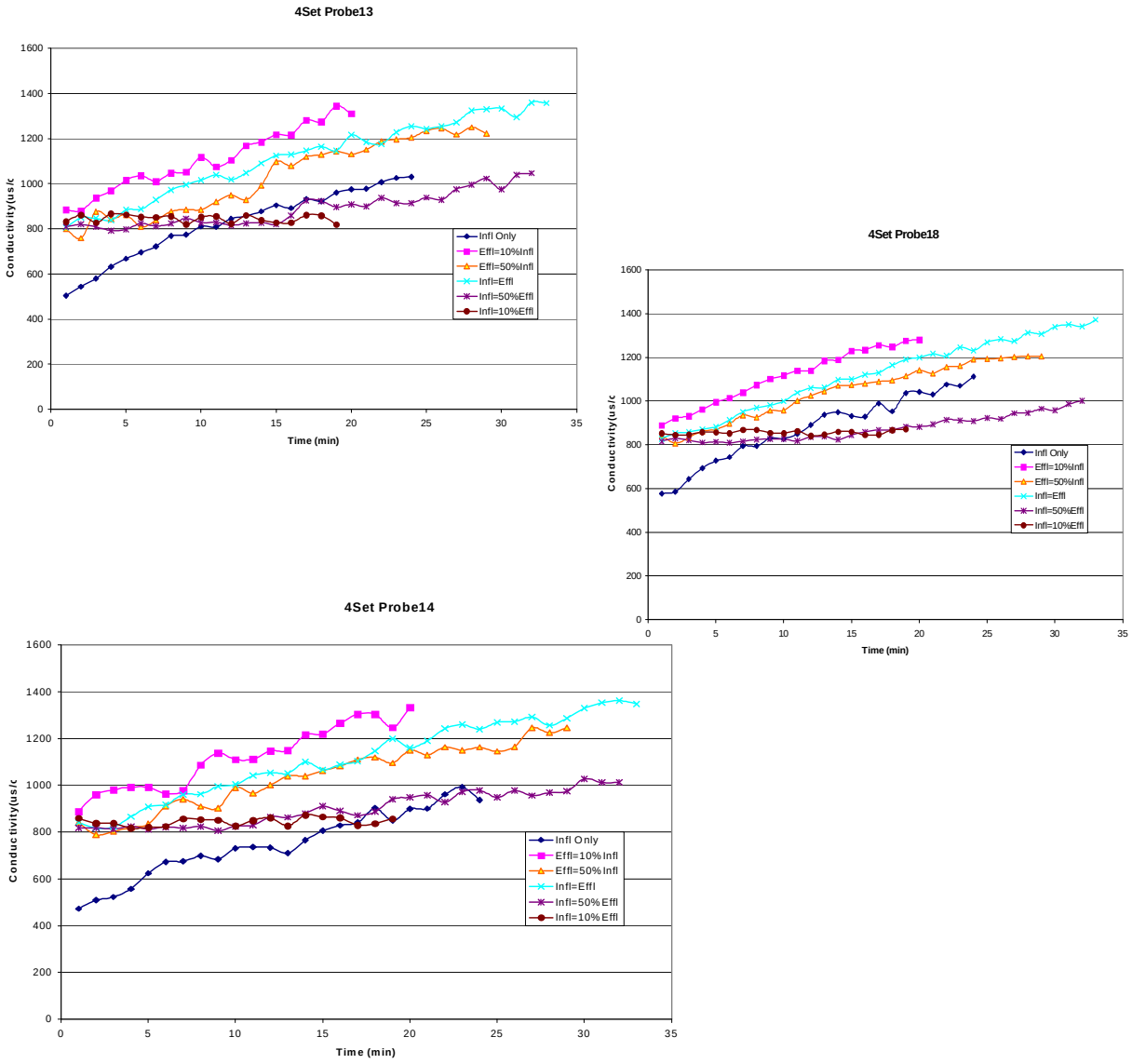

Figure 67 – Set 4 experiments showing the conductivity response of all three probes in the storage tank.

5.1.4. Extent of mixing

The time required to reach 1.5X initial concentration as a function of ratio of inlet to outlet flows was plotted for sets 1 and 2 and 1.25x initial concentration for sets 3 and 4 in Figure x. This indicates a drastic increase in time for draining experiments. The dynamic response of mixing in the model experiment has revealed mixing rates over a specific time period help us understand the behavior in a combined network set-up.

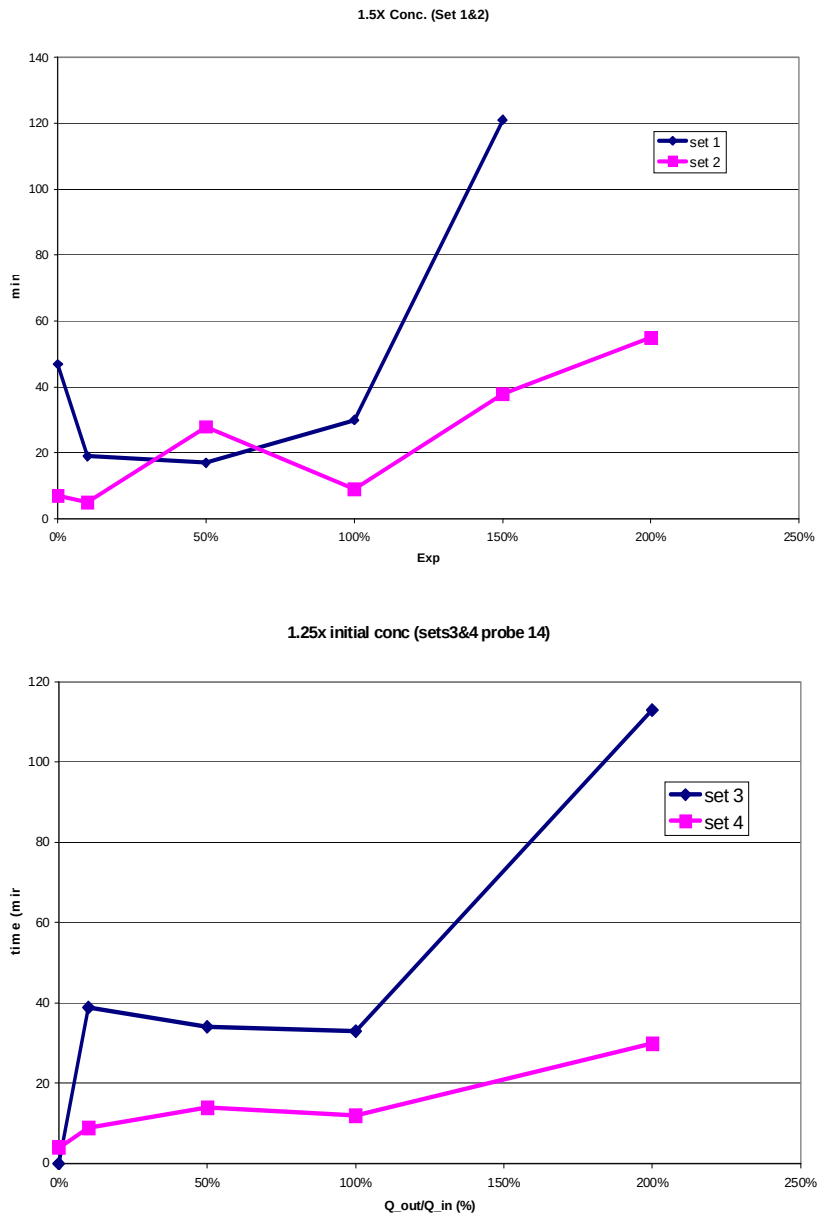

Figure 68 – Time required to reach 1.5 and 1.25 times the initial concentrations in storage tank experiments as a function of Qin/Qout (%).

The coefficients of variance are calculated for tank experiments with no outlet flow (case A) and plotted in **Figure 69**. Data for set 3are not available. Qualitatively, the coefficients do decrease as a function of time; however, the values remain fairly low throughout the experimental periods, indicating little stratification in the tank. This is consistent with the previous plots showing little variations amongst all three probes.

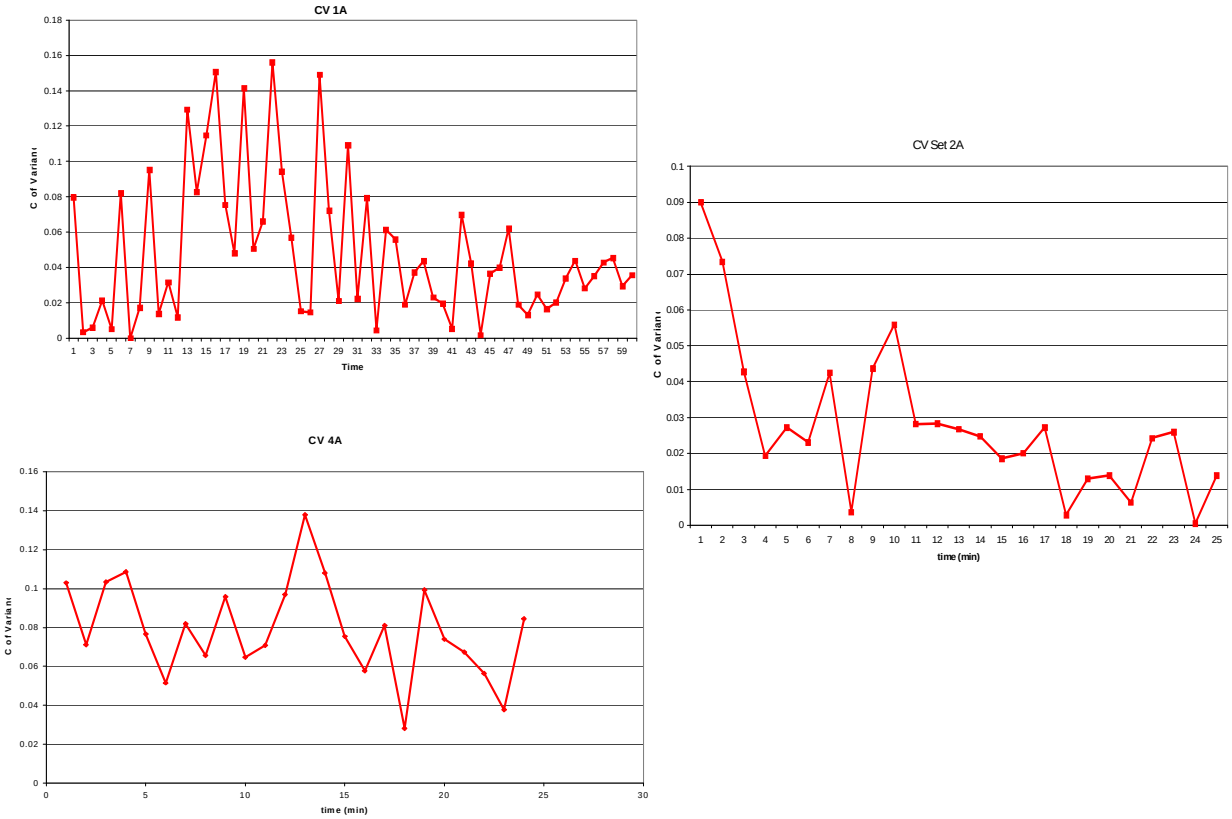

Figure 69 – Coefficient of Variance for Tank filling experiments A. Set 3 results are not available.

5.1.5. Comparison to EPANET

The storage tank experiment is also modeled in EPANET to check for the type of mixing model that best represents the one used in the experiment. We have found that in some cases the 2-component mixing with the ratio near 0.7 to be the best mechanism and in others well-mixed representation best fit the experimental observations. Figure x shows some of the EPANET-experiment validation data. They are plotted against other models or different 2-compartment constants. Unlike solute mixing in the pipe network, the different theoretical models that exist in the software adequately provide mixing mechanisms in storage tanks.

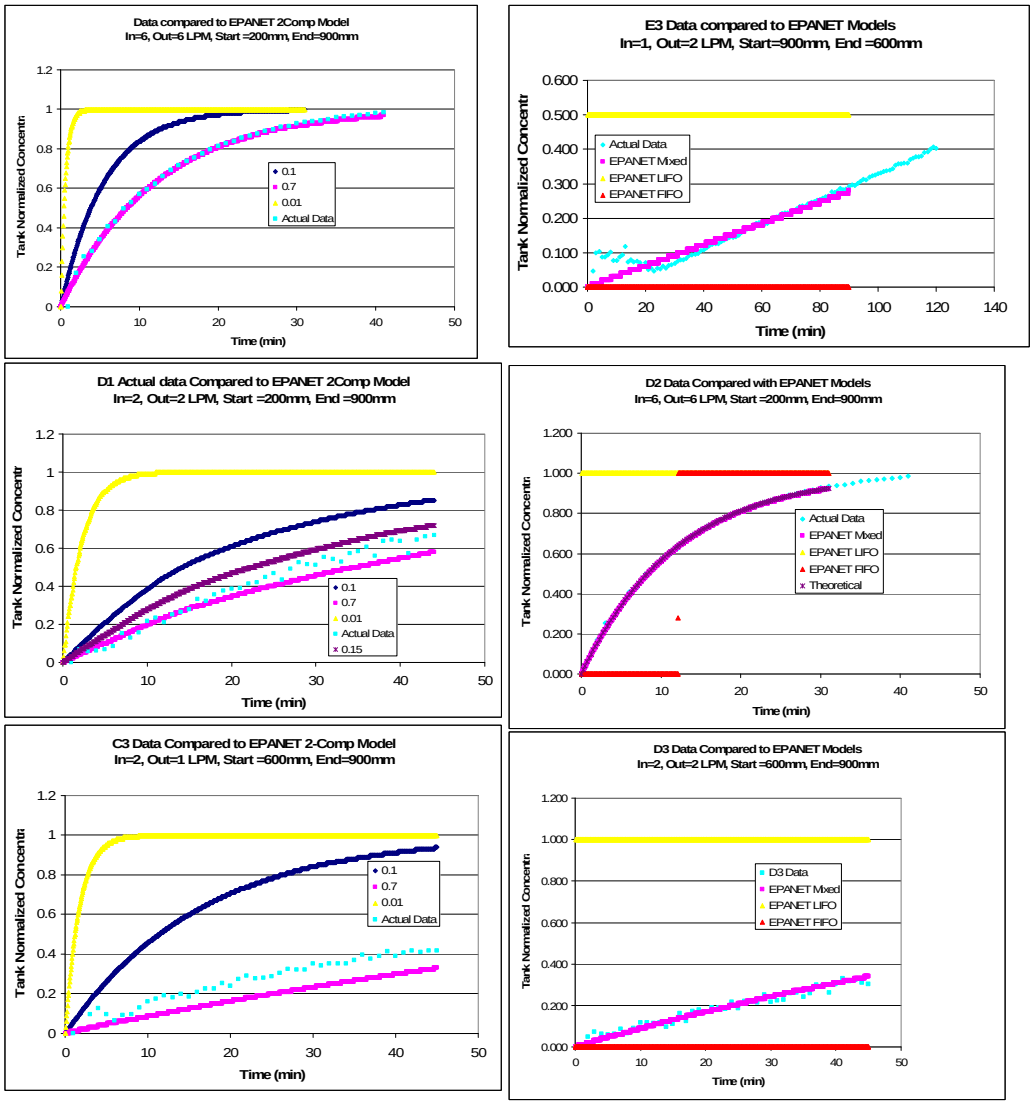

Figure 70 – Selected comparison of storage tank dynamic mixing data to EPANET tank mixing models.

5.2 Coupled Storage Tank – Network Study

The last set of experiments for this project involves coupling of a single storage tank with a 3x3 pipeline network, qualitatively represented in **Figure 71**.

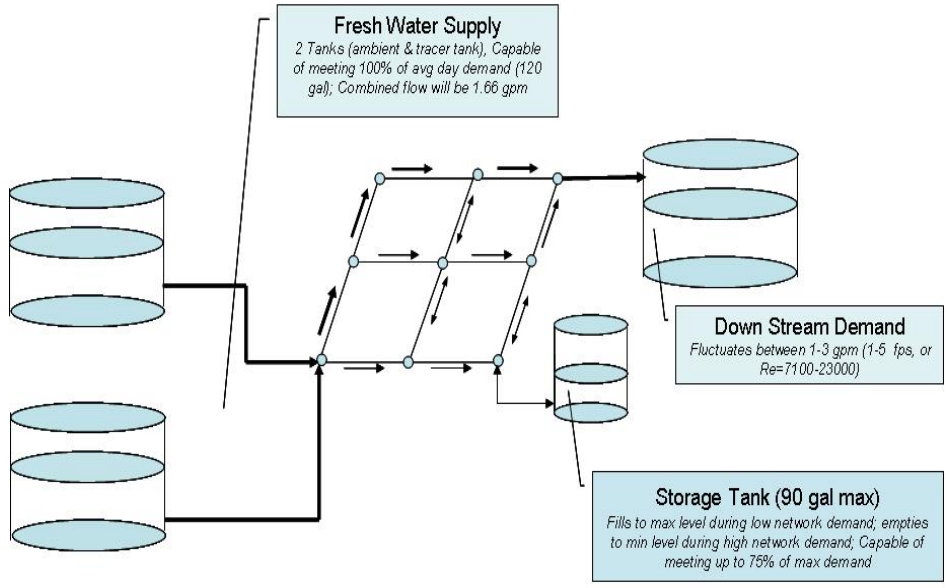

Figure 71 – Coupled storage tank with a 3x3 pipeline network.

The feed flows are calculated by scaling back a typical municipality supply and by the capacities of holding tanks. **Table 12** summarizes the scaling applied to this set of experiments, showing consistency in velocities between the laboratory scale and full scale distribution systems.

Table 12 - Full Scale & Lab Scale Flow Comparison

	Lab Scale			Full Scale			ratio
Mean Velocity (ft/s)	2.05	3.43	4.9	2.05	3.43	4.9	1
Pipe diameter (in)	0.5	0.5	0.5	10	10	10	20
Flowrate (gpm)	1.25	2.10	3.00	502	840	1200	400
Time (s)	0.020	0.012	0.009	0.407	0.243	0.170	20
Mean Velocity (m/s)	0.625	1.046	1.494	0.625	1.046	1.494	1
Reynold's number	8882	14861	21230	8882	14861	21230	1

5.2.1 Experimental Set-up

The instrumentation diagram for **Figure 71** is illustrated in **Figure 72**. Photographs of the experimental set up are also given in **Figure 73**. The 3x3 network and tank experimental set ups have been described in previous sections of this report and will not be repeated in this section.

Flow meters and conductivity probes are installed in every segment of the network. In addition,

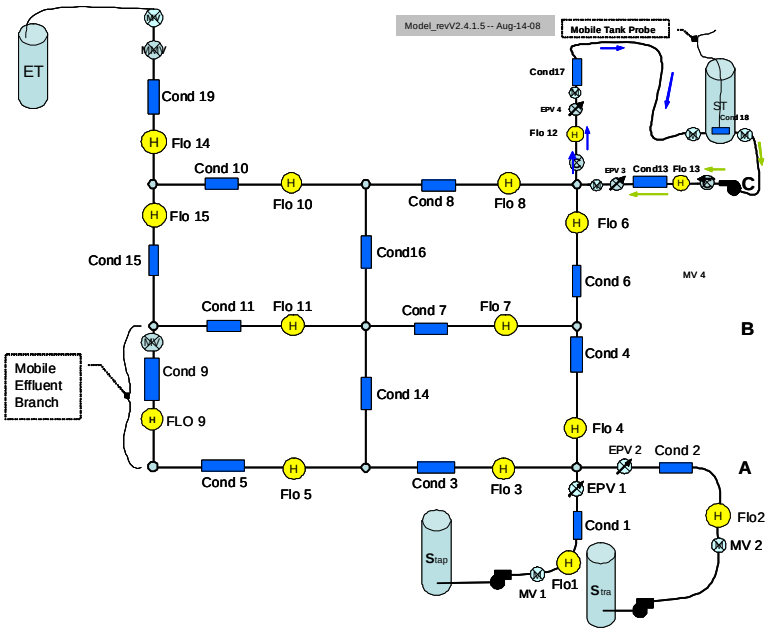

Figure 72. Combined Network-Tank Dynamic Experiment Set-up.

Figure 73 – Combined tank-network experiment. The supply tanks are shown on the top image in the foreground. The storage tank is shown on the right and elevated. The discharge tanks are shown in the bottom image behind the network.

5.2.2 Diurnal Demand and Supply Implementation

A sequence of valve opening and closing actions is orchestrated to mimic diurnal demand pattern. **Figure 74** shows the desired flow fluctuations designed for the experiments. Given a constant supply of water, the cycles of demand and storage tank fill/drain work in opposite directions. The experimental design has been scaled back to a 70-minute cycle to represent a full-day period. Based on **Figure 74**, the initial demand is low from midnight to early AM, then it peaks during the full morning period. This is followed by another decline until the evening period, where demand rises again.

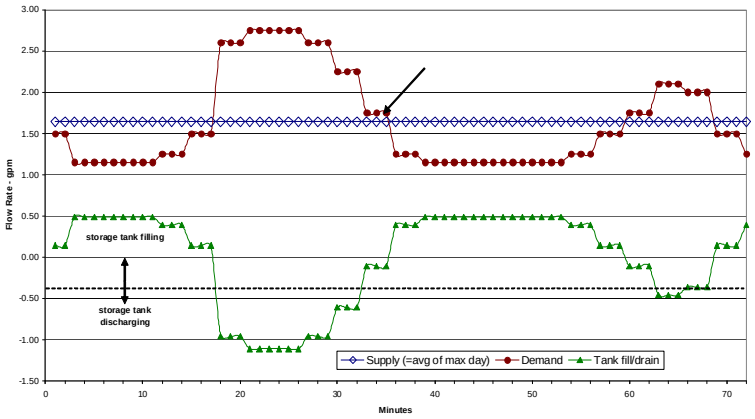

Figure 74 – Design flow over an entire scaled day (70 minutes).

The actual flow data collected during the experiments follow the design curves closely as shown in **Figure 75**. The two supply tanks: tracer and ambient maintain constant flow while the inlet and outlet flow rates of the storage tank reflect the opposite cycle relative to demand curve. This is accomplished by manually adjusting the valves to match that of demand curves.

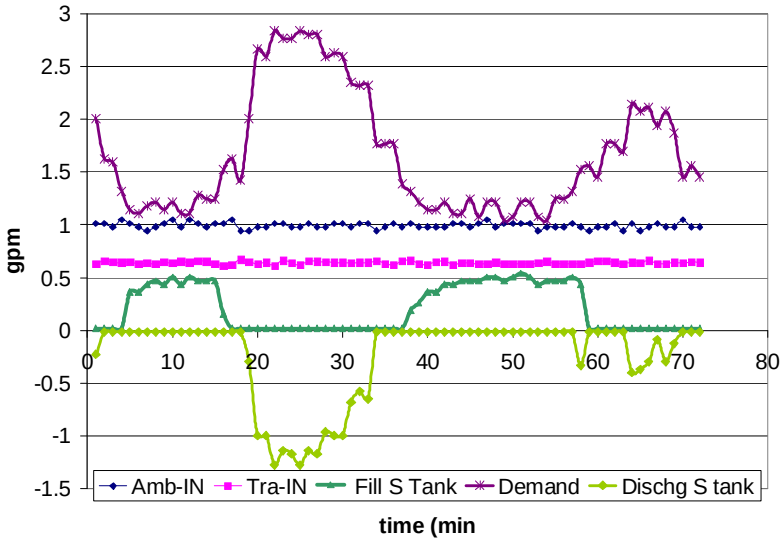

Figure 75 – Experimental flow data during an entire scaled day.

Tank – Network Experiments Summary

- Same 3 x 3 as designed previously.
- Same tank design as used previously with modifications for a pump and additional valves around the storage tank.
- One "day" is a 72-minute period
- Supply Tank(s) are on for duration of each experiment – (combined) flow is ~1.66 gpm
- Demand fluctuates as shown in chart below
- Storage tank will fill & drain as shown in chart below – try to approximate this. I would like to do a low & high level on the tank itself (more later)

5.2.3 Dynamic Mixing Scenarios

Three scenarios had been created for the combined network-storage tank experiments; nevertheless, only the two sets were completed due to funding shortfall. The three scenarios are briefly described in this section. Data for Set 1 and Set 2 are analyzed in the following section using EPANET-BAM.

Experiment Set 1 – Two well supply, contamination (tracer) in one supply
The set up for this experiment is identical to **Figures 71** and **72**. The objective for this study is to check for sensitivity of mixing as a function of relative supply flow at two tank levels.

- $Q_{Tracer} < Q_{Ambient}$
- $Q_{Tracer} > Q_{Ambient}$

Experiment	Q_{Tracer}	$Q_{Ambient}$	Tank Level	Demand
ES1-A	0.66 gpm	1.0 gpm	25 gal	1.15-3 gpm
ES1-B	0.66 gpm	1.0 gpm	50 gal	1.15-3 gpm
ES1-C	1.0 gpm	0.66 gpm	25 gal	1.15-3 gpm
ES1-D	1.0 gpm	0.66 gpm	50 gal	1.15-3 gpm

Experiment Set 2 – Single well supply, contamination (tracer) in storage tank
This set of experiment tests the dynamic mixing when tracer is introduced in the storage tank. The same volume of a "contaminant" as in the first set is now added to the storage tank when it is low and when it is high.

Experiment	Q_{supply}	Tank Level	Demand
ES2-A	1.66 gpm	25 gal	1.15-3 gpm
ES2-B	1.66 gpm	50 gal	1.15-3 gpm

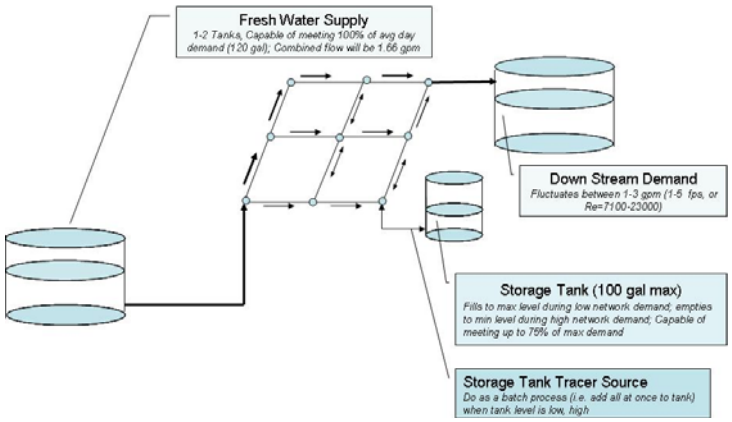

Figure 76 – Modified network-storage tank set up for Experiment Set 2. The tracer source originates from the storage tank rather than the supply tank.

<u>Experiment Set 3 – Single well supply, contamination (tracer) inside network</u>

This set of experiments were designed and included in the report for completion, but they were not run due to funding and time constraints. **Figure 77** shows the design of new tracer input locations

Experiment	Q_{supply}	Tracer Location	Tank Level	Demand
ES3-A	1.66 gpm	a	25 gal	1.15-3 gpm
ES3-B	1.66 gpm	e	25 gal	1.15-3 gpm
ES3-C	1.66 gpm	a	50 gal	1.15-3 gpm
ES3-D	1.66 gpm	e	50 gal	1.15-3 gpm

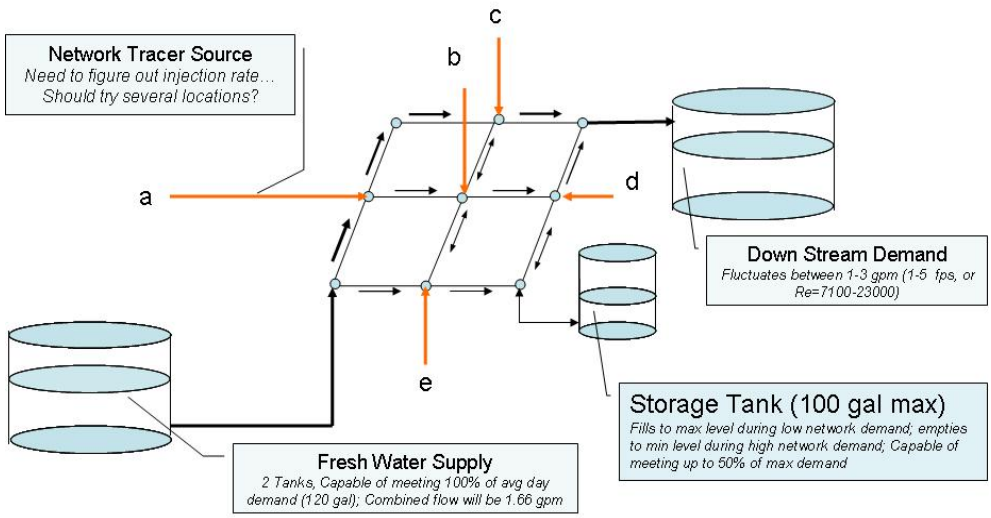

Figure 77 – Modified network-storage tank set up for Experiment Set 3.

5.2.4. Comparison to EPA-BAM model

Due to shortage of time, the only comparison of experimental data versus EPANET-BAM model is carried out in the first run of Set 1 experiments. A diagram of the EPANET model is shown in **Figure 78**. The conductivity reading, normalized between 0 and 1 are plotted in Figure x. Along with the experimental reading, there are three simulated EPANET-BAM mixing parameters. It is interesting to note that EPANET-BAM with mixing parameter of 0.5 match the dynamic mixing data very well. This will have to be confirmed with the other data collected during the other runs. The results will be published later in another document.

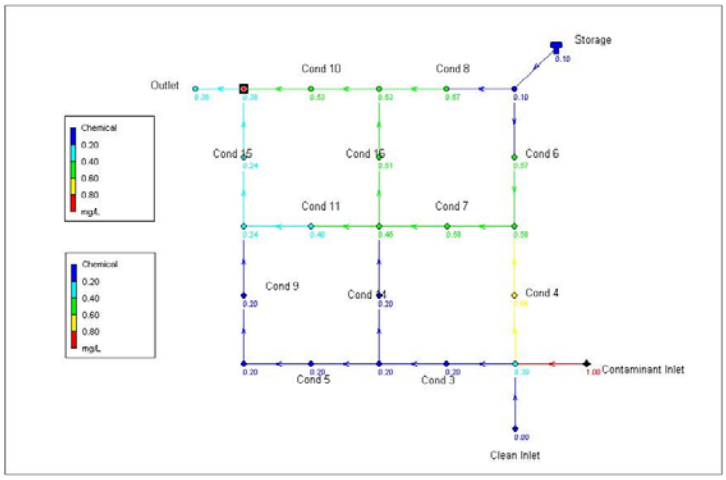

Figure 78 – EPANET-BAM model for the combined network-tank experiments.

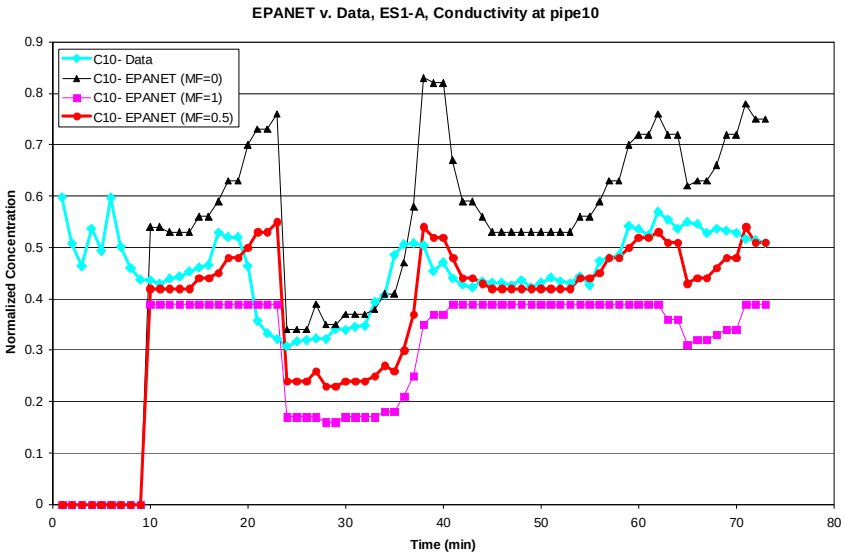

Figure 79 – Comparison of Experimental data and EPANET-BAM model at node C10 (refer to Figure 72 for keys).

5.2.5. Discussion

Despite the shortened schedule for the coupled 3x3 network and storage tank experiments, the methodology and results yielded valuable hands-on expertise and insight for dynamic mixing in a distribution network.

- The dynamic experiments differ from steady-state experiments since temporal variations are to be monitored and recorded. The single-tank characterization shows better mixing when the tank is filling as opposed to draining. The mixing time for our storage tank is shorter than those described by the literature.

- The expertise gained from individual unit testing made the combined network-tank experiments easier to set up and monitor. We have scaled a network-tank demand and supply flow that is comparable to a daily diurnal cycle. The preliminary results of EPANET-BAM of the combined network still show consistent improvement with EPA-BAM with a scaling factor of 0.5.

6. SUMMARY AND FUTURE DIRECTIONS

This report describes the accomplishments of the concluding year of a three-year LDRD project. Experimental and computational work completed within this project clearly shows that incomplete mixing occurs within pipe joint geometries used in municipal water distribution systems. These results are in contrast to the complete mixing scenarios used within common distribution network simulators (e.g., EPANET). In particular, solute mixing within the cross-joint is considerably different from that predicted by models of complete mixing.

Joint experimental and computational analyses built a critical knowledge base and expertise in contaminant transport within water distribution networks. Experimentally, the data from single joint, idealized networks, storage tanks, and combined tank-network consistently revealed incomplete solute mixing that persists spatially and temporally with complex interfacial instability. The quantifiable observations impact the way one analyzes the contamination threats that have both spatial and temporal components. The integrated simulation component of this project enhanced the numerical techniques applied to solving turbulence equations at the interface as well as macroscopic momentum balance in the bulk. The wealth of information regarding solute mixing from sensitivities with respect to geometries, Reynolds numbers, and network configurations serves as an important dataset for model validation, for risk mitigation, for distribution network improvement, and for design of future distribution systems.

Several outstanding issues regarding accurate application of these results in modeling the spread of a contaminant within existing distribution networks must still be addressed:

1) The prevalence of different joint geometries within the network. Solute transport through a large number of cross-joints will create a much different contamination event than transport through double-T joints where the T's are separated by 20-40 pipe diameters. Unfortunately, network designs are not necessarily consistent with the "as built" results and it may be impossible to accurately determine how many cross and double-T joints exist in a network. Additionally, distribution network modeling packages may change the joint geometry from that entered by "snapping" two pipes together in a geometry different than that of the actual joint design.
2) Location of the different joint geometries. Uncertainty in the as built conditions of the distribution network means that the locations of the different pipe joints are also unknown. A small number cross-joints within a network composed of double-T joints may not significantly impact the contamination event if they are spread randomly throughout the network. However, if they are concentrated in a certain portion of the network that is near the contaminant source, the resulting concentration distribution will be significantly different.
3) The considerable effect on solute mixing of small variations of the interior geometry of the joint. CFD modeling completed as part of this project demonstrated the large effect of solute mixing that small ridges in the pipe diameter can have on solute mixing. Interior details of the joint geometry are available from the manufacturer and these records need to be maintained to accurately predict mixing behavior.
4) Incomplete solute mixing coupling with chemical decomposition throughout the network presents some interesting challenges for mitigating risks of contamination. The techniques employed here are well extendable to understanding reactive solute transport.

The solution to these issues is better record keeping of as built conditions within networks. With the advent of electronic record keeping within GIS-enabled databases, record keeping of as built conditions will continue to improve.

Our critical water supplies will face challenges from climate change, agricultural practice, and increased reuse. This study is synergistic with our laboratories interests in securing our critical infrastructure, critical resources, and advancing science and technologies.

7. REFERENCES

AGARD, 1998, "A Selection of Test Cases for the Validation of Large-Eddy Simulations of Turbulent Flows," Advisory Group for Aerospace Research & Development, AGARD Advisory Report 345 (AGARD-AR-345), NATO.

Ashgriz, N., W. Brocklehurst, and D. Talley, 2001, "Mixing Mechanisms is a Pair of Impinging Jets," *J. Propulsion and Power*, 17:736-749.

Austin, R.G., van Bloemen Waanders, B., McKenna, S., and Choi, C.Y. (2008) "Mixing at Cross Junctions in Water Distribution Systems. II: Experimental Study." *J. Water Resources, Planning, and Management*, 134(3), 295-302.

Berry, J., W.E. Hart, C.A. Phillips, J.G. Uber, and J.-P. Watson, 2006, Sensor Placement in Municipal Water Networks with Temporal Integer Programming Models, *Journal of Water Resources Planning and Management*, 132 (4), pp. 218-224.

Blazek, J., 2001, Computational Fluid Dynamics: Principles and Applications, Elsevier Science.

Breidenthal, R., (1981). "Structure in turbulent mixing layers and wakes using a chemical reaction," J. Fluid Mech., vol. 109, pp. 1–24.

Bristow, E.C. and K. Brumbelow, 2006, Delay Between Sensing and Response in Water Contamination Events, *Journal of Infrastructure Systems*, 12 (2), pp. 87-95.

Chandrasekaran, Latha, "Predicting Disease Incidence due to Contaminant Intrusion in a Water Distribution System," Master Thesis, Environmental Engineering, University of Cincinnati, 2006.

Clark, J. W., Viessman, W., and Hammer, M. J. (1977). Water Supply and Pollution Control, 3rd Edition, Harper & Row, Publishers, New York.

Clark, R.M. et al., "Tracking *Salmonella* serovar *typhimurium* outbreak in Gideon, Missouri: role of contaminant propagation modeling," Journal Water SRT – Aqua Volume 45, **4**, 171-183, 1996.

Clark, R.M. et al., "A waterborne *Salmonella typhimurium* outbreak in Gideon, Missouri: results from a field investigation," International Journal of Environmental Health Research **6**, 187-193, 1996.

Fowler, .A.G., and P. Jones 1991, "Simulation of Water Quality in Water Distribution Systems," Proceedings Water Quality Modeling in Distribution Systems, Feb, 1991.

Fluent, Inc., 2005a, FLUENT 6.2 User's Guide, Fluent, Inc., Lebanon, NH, January 2005.

Fluent, Inc., 2005b, "Modeling Turbulence," Chapter 11 of FLUENT 6.2 User's Guide, Fluent, Inc., Lebanon, NH, January 11, 2005.

Fluent, Inc., 2006, FLUENT 6.3 User's Guide, Fluent, Inc., Lebanon, NH, September 2006.

Grayman, W.M., et al, "Water quality modeling of distribution system storage facilities," AWWA Research Foundation Publication, 1999.

Ho, C.K., L. O'Rear, J.L. Wright, and S.A. McKenna, 2006, "Contaminant Mixing at Pipe Joints: Comparison between Experiments and Computational Fluid Dynamics Models." 8th Annual Water Distribution System Analysis Symposium, Cincinnati, Ohio, USA. Aug. 27-30, 2006.

Ho, C.K. (2008) "Solute Mixing Models for Water Distribution Pipe Networks." *J. Hydraulic Engineering*, in press.

Ho, C.K. and Khalsa, S.S. (2008) "Improved Contaminant Mixing Models for Water Quality Modeling in Water Distribution Networks." *Singapore Internal Water Week Water Convention*, Singapore, June 23-27, 2008.

Ho, C.K. and Khalsa, S.S. (2008) "EPANET-BAM: water Quality Modeling with Incomplete Mixing in Pipe Junctions." 10th Annual Water Distribution System Analysis Symposium, Mpumalanga, South Africa. Aug. 17-20.

Ho, C.K., Choi, C. Y., and McKenna, S. A. (2007) "Evaluation of Complete and Incomplete Mixing Models in Water Distribution Pipe Network Simulations." In *Proceedings of the 2007 World Environmental and Water Resources Congress*, Tampa, FL, May 15-19, 2007.

Islam, M. R. and Chaudhry, M. H. (1998). "Modeling of constituent transport in unsteady flows in pipe networks." *J. of Hydraulic Engineering*, v.124, no.11, p.1115-1123.

Khalsa, S.S. and Ho, C.K. (2007) EPANET-BAM v.1.0, © Sandia National Laboratories, 2007. Free software distributed under GNU Lesser General Public License as published by the Free Software Foundation, *www.sandia.gov/EPANET-BAM*.

Khanal, N., S.G. Buchberger and S.A. McKenna, 2006, Distribution System Contamination Events: Exposure, Influence and Sensitivity, *Journal of Water Resources Planning and Management*, 132 (4), pp. 283-292.

Kim, S-E., 2004, "Large Eddy Simulation Using Unstructured Meshes and Dynamic Subgrid-Scale Turbulence Models," AIAA Paper 2004-2548, 34th AIAA Fluid Dynamics Conf and Exhibit, June 28-July 1, Portland, OR.

Kim, S.-E., and L.S. Mohan, 2005, "Prediction of Unsteady Loading on a Circular Cylinder in High Reynolds Number Flows Using Large Eddy Simulation," OMAE Paper 2005-67044, 24th International Conference on Offshore Mechanics and Artic Engineering, June 12-16, Halkidiki, Greece.

Kim, S.-E., 2006, "Large Eddy Simulation of Turbulent Flow Past a Circular Cylinder in Subcritical Regime" AIAA Paper 2006-1418, 44th Aerospace Sciences Meeting and tExhibit, January 9-12, 2006, Reno, Nevada.

Kim, S.-E., and H. Nakamura, 2006, "Large Eddy Simulation of Turbulent Heat Transfer Around a Circular Cylinder in Crossflow," 13th International Heat Transfer Conference, Sydney, Australia, August 13-18.

Kok, J. B. W., and van der Wal, S. (1996). "Mixing in T-junctions." Applied Mathematical Modelling, vol.20, no.3, pp.232-43.

Laird, C.D., L.T. Biegler and B. G. van Bloemen Waanders, 2006 Mixed-Integer Approach for Obtaining Unique Solutions in Source Inversion of Water Networks, *Journal of Water Resources Planning and Management*, 132 (4), pp. 242-251.

Lesieur, M. and O. Metais, 1996, "New trends in large-eddy simulations of turbulence," ARFM, 28:45-82.

Mays, L.W., "Water distribution systems handbook," McGraw-Hill, New York, 2000.

McKenna, S.A., Orear, L., and Wright, J. (2007). "Experimental Determination of Solute Mixing in Pipe Joints." in Proceedings of the ASCE 2007 World Environmental and Water Resources Congress, Tampa, FL, May 15-19, 2007.

McKenna, S.A., T. O'Hern, and J. Hartenberger, 2008, "Detailed Investigation of Solute Mixing in Pipe Joints Through High Speed Photography," 10th Annual Water Distribution System Analysis Symposium, Mpumalanga, South Africa. Aug. 17-20.

Moin P., and K. Mahesh, 1998, "Direct Numerical Simulation: A Tool in Turbulence Research," Annual Reviews in Fluid Mechanics, 30:539-578.

O'Rear, L., G. Hammond, S.A. McKenna, P. Molina, R. Johnson, T. O'Hern, and B.G. van Bloemen Waanders, 2005, "Physical Modeling of Scaled Water Distribution Systems Networks," SAND2005-6776, Sandia National Laboratories, Albuquerque, NM.

Piomelli, U. and E. Balaras, 2002, "Wall-Layer Models for Large Eddy Simulations," ARFM, 34:349-374.

Plesniak, M. W. and Cusano, D.M. (2005). "Scalar mixing in a confined rectangular jet in crossflow." J. Fluid Mech., vol. 524, pp. 1-45.

Pope, S.B., 2000, Turbulent Flows, Cambridge University Press, Cambridge.

Renner, R.C. et al., "Procedure for assessing capability of disinfection systems," Interim Handbook: Optimizating Water Treatment Plant Performance using the Composite Correction Program Approach, US EPA Technology Transfer handbook, 1990.

Roberts, P.J., X. Tian and F. Sotiropoulos, "Physical modeling of mixing in water storage tanks," AWWA Research Foundation Publication, 2005.

Romero-Gomez, P., C. Y. Choi, B. G. van Bloemen Waanders, and S. A. McKenna, 2006, "Transport Phenomena at Intersections of Pressurized Pipe Systems," 8th Annual Water Distribution System Analysis Symposium, Cincinnati, Ohio, USA. Aug. 27-30.

Rossman, L., (2000). "EPANET 2 User's Manual." United States Environmental Protection Agency (EPA), EPA/600/R-00/057, Cincinnati, OH. www.epa.gov/nrmrl/wswrd/epanet.html

Sagaut, P., 2004, Large Eddy Simulation for Incompressible Flows – An Introduction, Second Edition, Springer.

Smagorinski, J., 1963, "General Circulation Experiments with the Primitive Equations. I. The Basic Experiment," *Month. Wea. Rev.*, 91:99-164.

Takahashi, S. and Shina, K. (2001). "Turbulence mixing and temperature fluctuation of hot and cold fluids in tee pipes." 8th International Symposium on Flow Modeling and Turbulence Measurement. Advances in Fluid Modeling and Turbulence Measurements, Tokyo, Japan, Dec. 4-6, 2001, pp.635-42.

Tennekes H. and J.L. Lumley, 1972, A First Course in Turbulence, The MIT Press.

van Bloemen Waanders, B, and G. Hammond, J. Shadid, S. Collis, R. Murray, 2005, "A Comparison of Navier Stokes and Network Models To Predict Chemical Transport in Municipal Water Distribution Systems," World Water & Environmental Resources Congress, Anchorage, AL, May 15-19, 2005.

Wang, S. J. and Mujumdar, A. S. (2005). "A numerical study of flow and mixing characteristics of three dimensional confined turbulent opposing jets: unequal jets." Chemical Engineering and Processing, Vol. 44, 1068-1074.

Watson, J.-P., H.J. Greenberg and W.E. Hart, 2004, A Multiple Objective Analysis of Sensor Placement Optimization in Water Networks, in Proceedings of: ASCE World Water & Environmental Resources Congress, Salt Lake City, UT.

Webb, S.W., and J.T. Cook, 2006, "LES Data-Model Comparisons for Flow Over a Tube Bundle Including Heat Transfer," 13th International Heat Transfer Conference, Sydney, Australia, August 13-18.

Webb, S.W., and B. van Bloemen Waanders, 2006, "High Fidelity Computational Fluid Dynamics for Mixing in Water Distribution Systems," 8th Annual Water Distribution System Analysis Symposium, Cincinnati, Ohio, USA. Aug. 27-30.

Webb, S.W., 2007, High-Fidelity Simulation of the Influence of Local Geometry on Mixing in Crosses in Water Distribution Systems, in**:** Proceedings of ASCE World Water & Environmental Resources Congress, Tampa, FL.

Wolf, F., 1999, Calculation of information and complexity in time series: Analysis of the water budget of forested catchments, Department of Ecological Modeling, University of Bayreuth, Germany, http://www.dr-frank-wolf.de/diss/calcen.htm (accessed April 28th, 2008)

DISTRIBUTION

1 Joe Chwirka
CDM
6000 Uptown Blvd. NE Suite 200
Albuquerque, NM 87110

2 Walter M. Grayman Consulting Engineers
321 Ritchie Avenue
Cincinnati, OH 45215

3 Kim Foxx
EPA
Cincinnati, OH 45215

Lewis Rossman
EPA
Cincinnati, OH 45215

4 Regan Murray
EPA
Cincinnati, OH 45215

		Name of Person	**Org. Number**
1	MS0735	John Merson	6310
1	MS0735	Rush Rabinett	6320
1	MS0735	Pat Brady	6316
1	MS0735	Larry Costin	6311
1	MS0735	Mark Rigali	6316
1	MS0735	Ray Finley	6313
1	MS0735	David Hart	6313
1	MS0735	Vince Tidwell	6313
1	MS0735	Tom Lowry	6313
1	MS0735	Susan Altman	6316
1	MS1108	Mike Hightower	6332
1	MS0734	Wayne Einfeld	6327
1	MS0735	Dan Rader	1514
1	MS0735	Randy Schunk	1514
1	MS0735	Rekha Rao	1515
1	MS0735	David Noble	1515
1	MS0735	Bill Hart	1411
1	MS0899	Technical Library	9536 (electronic copy)

For LDRD reports, add:

1	MS0123	D. Chavez, LDRD Office	1011


Sandia National Laboratories